Theoretical Studies in Solar Cell Physics

Alfredo Sanchez Garcia

UiA University of Agder

Doctoral Dissertations at
the University of Agder 390

Alfredo Sanchez Garcia

Theoretical Studies in Solar Cell Physics

Doctoral Dissertation for the Degree *Philosophiae Doctor (PhD)* at
the Faculty, Specialisation in Engineering Sciences

University of Agder
Faculty
2022

Doctoral Dissertations at the University of Agder 390
ISSN: 1504-9272
ISBN: 978-82-8427-103-3

Printed by 07 Media
Oslo

Abstract

In this thesis, we develop analytical models with the purpose of expanding knowledge and gaining understanding of some of the internal mechanisms that limit the efficiency of single-junction solar cells. We focus on three distinct topics: fundamental energy losses, the temperature sensitivity of single-junction solar cells and the effect of the series resistance on the maximum power point. The thesis is divided in two parts. The first part reviews basic solar cell physics topics and introduces some more advanced concepts to provide the reader with the necessary background to understand the attached papers. The latter constitute the second part of the thesis.

A new set of analytical expressions for the fundamental energy losses of single-junction solar cells is derived. These make use of Lambert's W function and an analytical model for maximum power point, which constitutes an improvement upon the existing expressions found in the scientific literature. In the new expression for the thermalization loss, the fermionic nature of electrons and holes is included, which results in the need of a second thermalization to the conduction band edge. From here, we conclude that the overall thermalization process occurs step-wise. The employment of Lambert's W function allows for an analytical expression that combines the emission, Carnot and Boltzmann energy losses.

The temperature sensitivity of single-junction solar cells is investigated. We use Lambert's W function and an analytical model for maximum-power point as starting point to develop analytical expressions for the temperature coefficients of the maximum power point voltage, current and power. A new expression for the temperature coefficient of the fill factor is also derived. The new model for the temperature coefficients uses solar cell parameters that can be extracted from $I - V$ characteristics as inputs. The expressions are tested against experimental data obtained from multi-crystalline silicon cells. We conclude that the derived model describes with low discrepancy the temperature sensitivity of the investigated parameters.

We investigate the so-called recombination parameter γ by developing a model in which we relate γ to the carriers mobilities and lifetimes. This is possible by assuming that all non-radiative recombination occurs in the neutral region of the cell. In our attempt to relate γ to impurities in semiconductor crystals, we encounter problems regarding the definition of γ and its dependency with the open-circuit voltage. Solutions to these prob-

lems are suggested. Particularly, for low-level injection, we derive analytical expressions for γ that are note voltage dependent and fully determine γ from the characteristics of the defect. From numerical experiments, we conclude that the parameter γ alone may not be suitable for impurity identification but, still be useful in conjunction with other characterization techniques for defect characterization.

Finally, we derive analytical expressions for the maximum power point that include the effect of the series resistance. The properties of Lambert's W function allow for this. Discrepancies below 0.1% for typical values of the series resistance are obtained when comparing the new expressions to a numerical single-diode model. We test the experimental applicability of our expressions and compare them to existing models found in the scientific literature. For this, we use of 18 multi-crystalline silicon cells, from which we extract $I - V$ characteristics at multiple temperature. We showed that our model achieves the same level of accuracy as the previously existing ones, predicting experimental maximum power of the cells with discrepancies below 0.2%. Compare with the previously existing models, our model improves in the simplicity of the expressions.

Sammendrag

I denne avhandlingen har det blitt utarbeidet analytiske modeller med mål om å øke kunnskapen om noen av de interne mekanismene som begrenser effektiviteten til solceller. Det settes søkelys på tre ulike emner: fundamentale energitap, temperatursensitiviteten til solceller og effekten av seriemotstand på det såkalte *maximum power point* (MPP). Denne avhandlingen består av to deler. Den første delen beskriver grunnleggende solcellefysikk, og introduserer leseren for mer avanserte konsepter. Denne bakgrunnsinformasjonen trengs for å forstå de vedlagte artiklene. Artiklene utgjør den andre delen av avhandlingen.

Nye analytiske uttrykk, som beskriver de fundamentale energitapene i solceller, er utledet. Uttrykkene er basert på en tidligere kjent analytisk modell for spenningen ved MPP. Det nye uttrykket for termaliseringstap tar hensyn til elektronenes fermioniske natur. Dette resulterer i et behov for en ekstra termalisering. Ved å bruke Lamberts W funksjon, er et nytt uttrykk, som kombinerer strålings-, Carnot- og Boltzmanntap, utledet.

Temperatursensitiviteten til solceller er også utforsket. Vi bruker Lamberts W funksjon og en analytisk modell for spenningen ved MPP til å utlede analytiske uttrykk for temperaturkoeffisientene til spenningen, strømmen og effekten ved MPP. Et nytt uttrykk for temperaturkoeffisienten til fyllfaktoren er utledet. Den nye modellen for temperaturkoeffisientene bruker solcelleparametre som kan leses fra en IV-karakteristikk. Uttrykkene er testet med eksperimentelle data fra multikrystallinske silisiumceller. Vi konkluderer med at modellen beskriver temperatursensitiviteten til de utforskede parameterne med lite avvik.

Videre utforsker vi rekombinasjonsparameteren γ ved å utvikle en modell som kobler sammen γ med ladningsbærermobilitet og levetider. Dette er mulig hvis man antar at all ikke-strålingsrekombinasjon foregår i den nøytrale regionen av en $p-n$ overgang. Vi forsøker å koble γ til urenheter, noe som viser seg å være problematisk, blant annet på grunn av hvordan γ defineres, og på grunn av at γ er spenningsavhengig. Vi forslår så mulige løsninger for disse problemene. Blant disse finner vi at ved lavinjeksjon kan γ bestemmes helt fra egenskapene til urenheten. Fra numeriske beregninger blir det konkludert med at γ alene ikke kan brukes til å identifisere urenheter, men den kan være nyttig i samspill med andre defektkarakteriseringsteknikker.

Til slutt utleder vi et analytisk uttrykk for spenningen ved MPP som tar hensyn til virkningen til seriemotstand. Modellen er sammenlignet med en numerisk én-diodemodell, og avvik under 0.1% er oppnådd for typiske verdier for seriemotstanden. Modellen er også testet med eksperimentelle data fra multikrystallinske silisiumceller, og sammenlignet med eldre modeller funnet i den vitenskapelige litteraturen. Resultatene viser at modellen vår er like nøyaktig som de alternative modellene, og kan forutse effekten ved MPP med avvik under 0.2%. Sammenlignet med de eldre modellene, består vår modell av kortere og enklere matematiske uttrykk.

Acknowledgments

A lot of people deserve recognition for their support during my time as a PhD student.

First, I would like to thank my supervisor, Rune Strandberg, for exceptional supervision during the PhD period. Thank you for the supervision sessions in front of a whiteboard and for teaching me to let things "mature". I would also like to thank my co-supervisor, Tor Oskar Sætre, for being encouraging and supportive.

Thanks to everyone at the Energy Materials group for providing the perfect working environment for the PhD period. Special gratitude goes to Sissel Tind Kristensen for lots of conversations on temperature coefficients and for teaching me the experimental insights of solar cells. Thanks to Basant and Oscar for all our hallway chats. I wish you both good luck in the last stages of your PhD's.

I want to thank Emilio for all the pizza boxes full of equations and for being the best roommate one could have. Thank you to my friends Shaun, Saeed, Reyn, Philipp, Lorenzo, Charly, Bernhard, Rolf, Arild, Sinziana, Gulshan, Luismi, Eleni, Saga, Mareike and the list goes on. Every single one of you has contributed to making these past three years unforgettable.

I want to also thank my friends and family back home. To my parents, Alfredo and Inma, and my sister, Laura, for the FaceTime calls and your love and support; and to my friends for always reminding me to be humble.

Last but certainly not least, thank you to my partner, Sandra. Thank you for your patience and understanding of the long working nights. Thank you for always being there and for your infinite love. I could not have made it without you.

Alfredo Sanchez Garcia
Trondheim, Norway
2022

Publications

Paper A: **Garcia, A.S.** and Strandberg, R., 2019, June. Analytical expressions for radiative losses in solar cells. In 2019 IEEE 46th Photovoltaic Specialists Conference (PVSC) (pp. 1774-1779). IEEE.

Paper B: **Garcia, A.S.**, Kristensen, S.T., Christiansen, S.N. and Strandberg, R., 2020, June. Temperature Coefficients of Solar Cell Parameters at Maximum Power Point. In 2020 47th IEEE Photovoltaic Specialists Conference (PVSC) (pp. 1232-1237). IEEE.

Paper C: **Garcia, A. S.**, Kristensen, S. T., and Strandberg, R., 2022. Analytical Modeling of the Temperature Sensitivity of the Maximum Power Point of Solar Cells. IEEE Journal of Photovoltaics.

Paper D: **Garcia, A.S.**; Strandberg, R. Analytical Modeling of the Maximum Power Point with Series Resistance. Appl. Sci. 2021, 11, 10952.

Paper E: **Garcia, A.S.**, Kristensen, S.T. and Strandberg, R., 2021, June. Assessment of a New Analytical Expression for the Maximum-Power Point Voltage with Series Resistance. In 2021 IEEE 48th Photovoltaic Specialists Conference (PVSC) (pp. 0961-0965). IEEE.

Paper F: **Garcia, A.S.**, Kristensen, S.T. and Strandberg, R., 2022. The Recombination Parameter γ: Modeling and Comments. *To be submitted*

The following papers were published but are not included in the thesis.

- Kristensen, S.T., **Garcia, A.S.**, Nie, S., Hameiri, Z. and Strandberg, R., 2020, June. Improved Temperature Coefficient Modeling through the Recombination Parameter γ. In 2020 47th IEEE Photovoltaic Specialists Conference (PVSC) (pp. 0083-0087). IEEE.

Contents

List of Figures

Chapter 1

Introduction

In the past centuries, the world's energy needs have mostly been met with fossil fuels, whose conversion to useful energy results in greenhouse gas emissions to the atmosphere. These processes have resulted in the Earth warming up around 1°C above pre-industrial levels [1]. As the world's population is expected to increase by two billion people over the next 20 years, the total energy usage is expected to increase by nearly 50% by 2050 [2]. A transition to green and renewable sources of energy is therefore necessary to bring down greenhouse gas emissions and stop climate change.

Solar photovoltaic (PV) energy is expexted to play a huge role in the so-called green transition and become a key piece in the future energy market. This is due to its great reduction in costs during the past decade [3]. Particularly, the cost of electricity from PV energy fell 82% between 2010 and 2019. These cost improvements were driven mainly by a 90% reduction in module prices, together with decreasing system costs [3]. This resulted from both technological improvements and increased market competition mainly facilitated by China [4]. Even in 2020, despite the impact of the global pandemic and the disruptions caused by the spread of the COVID-19 virus, solar PV had another record-breaking year, with new installations reaching an estimated 139 GW_{DC}, bringing the global total to an estimated 760 GW_{DC} [4].

1.1 Motivation

As of the time of writing of this thesis, the conventional single junction solar cell, commonly made of crystalline silicon, completely dominates the market, though higher efficiency types of cells have been theorized and are in pursuit of practical implementation [5]. Because modern silicon cells are approaching their efficiency limit [6, 7], a deeper understanding of the mechanism that hinder achieving this limiting efficiency is necessary.

Our goal for this PhD project has been to develop analytical models that describe some of the underlying processes occurring within single-junction solar cells that directly

affect their efficiency. The motivation for most of these models comes from Ref. [8], where Khanna et al. made use of a not very well-known function, called Lambert's W, to obtain an analytical expression for the maximum power point voltage.

The work of this thesis can be divided in three main blocks: (i) fundamental energy losses, (ii) temperature sensitivity and (iii) the effect of the series resistance.

Within the first block, we aim to derive analytical expressions that describe the energy losses intrinsic to single-junction solar cells. Hirst and Ekin-Daukes previously derived in Ref. [9] a set of equations with the same goal. However, as Khanna's expression for the maximum power point voltage had not yet been derived, the authors in Ref. [9] made use of some approximations to obtain their results. These approximations can be avoided by making use of Lambert's W function.

In the second block, we focus on the temperature sensitivity of solar cells, which is often described with the so-called temperature coefficients (TC). These are parameters that describe, with a single value, how solar cell parameters change with the temperature. Among all the solar cell parameters, the open-circuit voltage, i.e., the maximum voltage obtainable by a solar cell, is the parameter whose temperature sensitivity has been studied the most [10]. The temperature sensitivity of the maximum power point, however, has not been explored from an analytical perspective. As the efficiency of solar cells is affected by temperature variations, gaining deeper understanding on the TCs can only be beneficial.

Still within the second block, we focus on studying the TC of the open-circuit voltage through the so-called recombination parameter γ. This parameter was introduced by Green in Ref. [10], where it was said to account for the temperature sensitivity of the mechanisms determining the open-circuit voltage. Later in Ref. [11], a link between γ and material properties was shown through the so-called *external radiative efficiency*. There are still some questions regarding γ. For example, what is the physical meaning of γ, or can γ be used to uniquely identify defects in solar cells?

In the final block of this thesis, we focus on the effect of series resistance on the maximum power point. Particularly, we note that accounting for the effect of the series resistance in the modeling of the maximum power point results in a set of transcendental equations that do not have analytical, or closed-form, solution. Singal derived in Ref. [12] a set of approximate solutions that, although accurate, are not simple to use. Singal's model did not make use of Lambert's W function. Can this function be used to simplify Singal's model?

1.2 Research questions

The motivation for the thesis work can be summed up in finding answers to the following research questions:

1. **How can we use Lambert's W to obtain analytical expressions that describe the fundamental energy losses without requiring approximations?**

2. **How can we use Khanna's model to derive analytical expressions that describe the temperature sensitivity of the maximum power point?**

3. **What is the physical meaning of the recombination parameter γ?**

4. **How can we use Lambert's W function to derive expressions for the maximum power point that account for the effect of the series resistance and are both accurate and of simplicity comparable to Khanna's model?**

1.3 Outline

This PhD project has resulted into six publications that are included in the appendices of this thesis. These papers have been either published or submitted for publication in peer-reviewed international conference proceedings and journals. The goal of this part of the thesis is to provide the reader with the necessary background within solar cell physics to understand the attached papers. We divide the thesis in five chapters, including the present one.

In **chapter 2**, we introduce fundamental concepts in solar cell physics, starting first with a review of solar radiation models followed by a brief discussion on how electrons behave in semiconductor crystals. This leads to the introduction of the concepts of generation and recombination of electron-hole pairs, finally allowing for the introduction of the detailed balance theory and Shockley's diode equation. The knowledge of Shockley's diode equation allows in **chapter 3** for the introduction of Khanna's model for the maximum power point previously mentioned in this chapter. This is accompanied by a short introduction to Lambert's W function and its properties. We then introduce the fundamental energy losses intrinsic to single-junction solar cells, which are the natural next step after the results from the detailed balance theory presented in chapter 2. This is followed by a discussion of the temperature sensitivity of solar cells. Here, we define the concept of temperature coefficient and introduce Green's [13] and Dupré's [11] models for the TC of the open-circuit voltage. This allows us to briefly introduce the recombination parameter γ. Finally, we account for the effect of the series resistance in Shockley's diode equation by introducing the reader to Banwell's closed-form expression for the current [14] and Singal's model for the maximum power point [12]. In **chapter 4**, we present and summarize the findings of the attached papers and, finally, in **chapter 5**, we conclude the thesis work.

Chapter 2

Fundamentals of Solar Cell Physics

Solar cells are devices capable of converting solar radiation into electricity [15]. These devices are made of semiconductors, materials that are capable of using the so-called photovoltaic effect to convert sunlight into electricity. The main operation can be summed up as follows: when a solar cell is illuminated, the electrons within the semiconductor may absorb the incoming photons, allowing them to be promoted from an energy state called the *valence* band (VB) to a higher energy state, the *conduction* band (CB). The difference between these two energy states is called bandgap (E_g). After the excitation, it is possible to extract the electrons to an electric circuit. The photovoltaic effect was discovered by Edmond Becquerel in 1839 [16].

The goal of this chapter is to introduce the reader to the limiting efficiency of single junction solar cells and characteristic solar cell parameters. In order to do so, we will first review fundamental concepts such as the nature of solar radiation and generation and recombination of charge carriers. This will lead to the theory of detailed balance, which will allow us to compute the limiting efficiency of single junction solar cells and formulate the diode equation.

2.1 Solar radiation and the effect of the atmosphere

The Sun can be modeled as a blackbody radiating at $T_\mathrm{sun} = 6000$ K. The flux of photons emitted from a blackbody at a temperature T within the energy interval $[E, E + \mathrm{d}E]$ and chemical potential μ is given by the generalized Planck's law of thermal radiation [17, 18],

$$\dot{n}(E, T, \mu, F_\mathrm{s})\mathrm{d}E = \frac{2F_s}{c^2h^3}\frac{E^2\ \mathrm{d}E}{\exp\left(\frac{E-\mu}{kT}\right) - 1}, \tag{2.1}$$

Here h, c and k are Planck's constant, the speed of light in vacuum and Boltzmann's constant, respectively. F_s is a geometrical factor related to the solid angle with which the blackbody radiates. Thermal radiation, such as sunlight, cannot produce work [17]. The

photon flux emitted from, e.g., the Sun may therefore be given by $\dot{n}(E, T_{\text{sun}}, \mu = 0, F_{\text{s}})$, and the total power density, P, of the sunlight is then obtained by integrating the energy flux, $E \cdot \dot{n}(E, T_{\text{sun}}, 0, F_{\text{s}})$, over all possible energies, i.e.,

$$P = \int_0^\infty E \cdot \dot{n}(E, T_{\text{sun}}, 0, F_{\text{s}}) \mathrm{d}E = F_{\text{s}} \frac{2\pi^5 k^4}{15c^2h^3} T_{\text{sun}}^4 \tag{2.2}$$

$$= F_{\text{s}} \sigma T_{\text{sun}}^4 \tag{2.3}$$

which corresponds to Stefan-Boltzmann's law [19]. In order to model the actual conditions under which a solar cell will operate, standardized spectra based on empirical data are available. Among the most commonly utilized, we encounter the AM0 and AM1.5 spectra. "AM" stands for "air mass", and AM1.5 implies that the spectrum is based on solar radiation that has traveled through air corresponding to 1.5 times the thickness of the Earth's atmosphere. Solar cells are commonly characterized and optimized under standard test conditions (STC), defined as a global standard solar spectrum AM1.5G corresponding to an irradiance of 1000 W/m^2 [10, 20]. In Fig. 2.1, we compare the three spectrum models described in this section. Here, we plot the spectral irradiance as a function of the wavelength, λ. In black, we represent a blackbody radiating at a temperature $T = 6000$ K while AM0 and AM1.5G are represented in blue and orange, respectively.

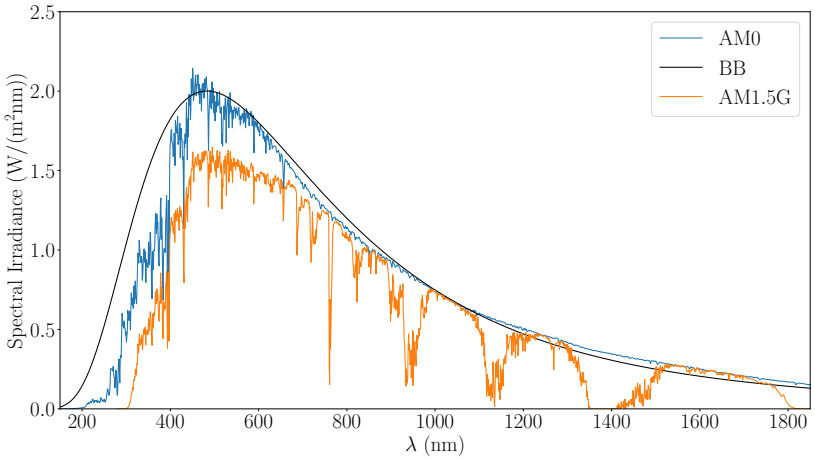

Figure 2.1: Comparison of three spectra. In black, the Sun is assumed to be a blackbody radiating at $T_{\text{sun}} = 6000$ K. The AM0 and AM1.5G spectra are represented in blue and orange, respectively. The latter data can be obtained from the National Renewable Energy Laboratory (NREL).

2.1.1 Optical étendue

The geometrical factor F_{s} introduced in Eq. (2.1) is related to the solid angle in which a blackbody radiates through the so-called *optical étendue*, a concept often used in geomet-

rical optics to describe light propagating through a medium. An infinitesimal element of étendue, $\mathrm{d}\mathcal{E}$, is defined by [21]

$$\mathrm{d}\mathcal{E} = n^2 \cos\theta \mathrm{d}S\mathrm{d}\Omega, \tag{2.4}$$

i.e., the solid angle, Ω, angled an angle θ with respect to the normal of the surface of a medium with area S and refractive index n. In Fig. 2.2, we display a visual representation of a differential element of étendue. As Eq. (2.1) describes the emitted photon flux per unit area, the correct interpretation of F_s would be optical étendue density per unit refraction index. We refer to it as a "geometrical factor" for simplification.

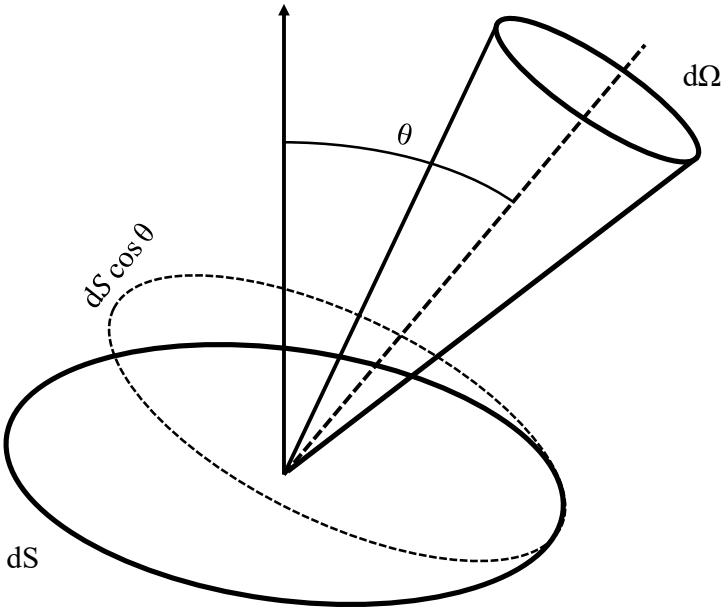

Figure 2.2: Étendue of a differential surface element.

2.2 Charge carriers in semiconductors

In semiconductor physics, the absence of an electron (e) within a semiconductor's energy band is called hole (h). Holes are treated as positively charged particles which are mobile. The electron and hole populations (n and p, respectively) within a semiconductor are described by Fermi-Dirac (F-D) statistics [22, 23]. In thermal equilibrium, there is no net particle flow and F-D statistics describe the most stable energy configuration for electrons and holes. The potential energy of electrons is described by its Fermi energy, E_F, which equals, at absolute zero, to the energy until which energy states are filled. If the semiconductor is exposed to light, the electron and hole population will no longer be in equilibrium with the surroundings resulting in particle flow. The Fermi level may then

split into two *quasi*-Fermi levels. In Fig. 2.3 we show a schematic band representation of a semiconductor being disturbed from equilibrium by exposure to light.

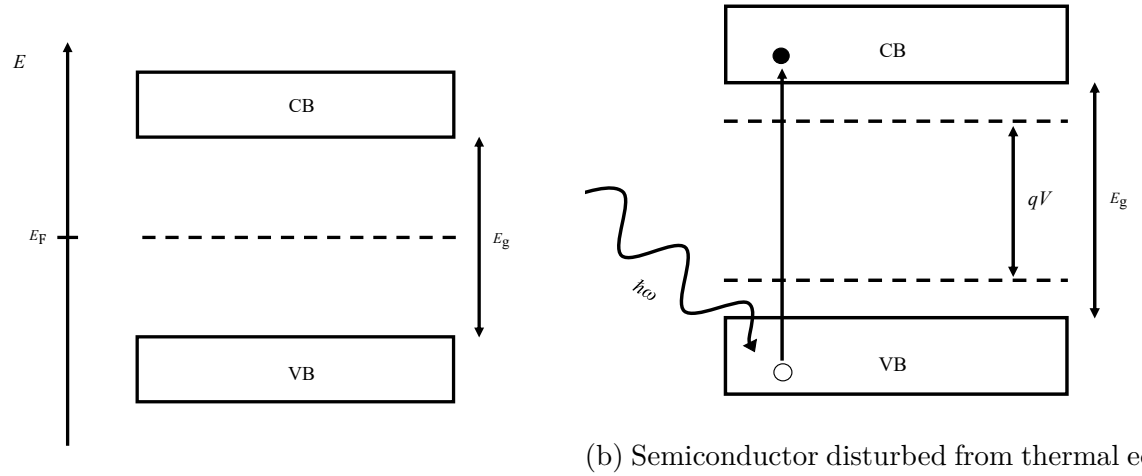

(a) Semiconductor in thermal equilibrium.

(b) Semiconductor disturbed from thermal equilibrium by exposure to light.

Figure 2.3: Schematic band structures of a semiconductor in equilibrium (a) and disrupted from equilibrium (b). If the disturbance is not too big, the semiconductor will evolve into a state of quasi-thermal equilibrium, resulting into particle flow. The Fermi level may then split into two quasi-Fermi levels. The difference between the quasi-Fermi energies equals the chemical potential, μ, of the cell which is proportional to the voltage V, that a solar cell will produce. The disturbance is represented by incoming light with energy equals to $\hbar\omega$. The particle flow is represented by an electron (black circle) being excited to the CB, leaving a hole (white circle) in the VB.

2.3 Photogeneration

Photogeneration refers to the process in which an electron within a semiconductor is promoted from the VB to the CB by means of photon absorption. The excitation leaves a hole in the VB and, therefore, this process is usually referred to as the generation of an electron-hole $(e-h)$ pair.

We denote the $e-h$ pair generation rate for a given energy and per unit volume by $g_{e-h}(E)$. The rate $g_{e-h}(E)$ is related to the incoming photon flux from the Sun through $g_{e-h}(E) = a(E)\dot{n}(E, T_{\text{sun}}, 0, F_{\text{abs}})$, where $a(E)$ is the absorptivity of the material for a given energy. Here, we have introduced the geometrical factor F_{abs}, which arises from integrating over the solid angles of absorption, Ω_{abs}, with respect to the normal of the cell. To calculate F_{abs}, let us assume a solar cell that absorbs radiation through a disk subtended an angle θ_{X} from the cell's surface normal. Defining θ' as the polar angle, F_{abs} will be given by

$$F_{\text{abs}} = \int_{\Omega_{\text{abs}}} \cos\theta' \mathrm{d}\Omega = \int_0^{2\pi} \int_0^{\theta_{\text{X}}} \cos\theta' \sin\theta' \mathrm{d}\theta' \mathrm{d}\phi = \pi \sin^2\theta_{\text{X}}. \tag{2.5}$$

The angle θ_{X} is related to the semi-angle to which the Sun subtends through $\sin\theta_{\mathrm{X}} = \sqrt{X}\sin\theta_{\mathrm{sun}}$, with $\theta_{\mathrm{sun}} = 0.267°$ and X being the Sun *concentration factor*. Let us define $X_{\mathrm{max}} = {}^{1}/_{\sin^2\theta_{\mathrm{sun}}}$ as the maximum Sun concentration factor. The total generation rate per unit volume, G, is obtained by integrating g_{e-h} over all possible energies, i.e.,

$$G = \int_0^\infty a(E)\dot{n}(E, T_{\mathrm{sun}}, 0, F_{\mathrm{abs}})\mathrm{d}E = \frac{X}{X_{\mathrm{max}}}\frac{2\pi}{c^2h^3}\int_0^\infty \frac{a(E)E^2\ \mathrm{d}E}{\exp\left(\frac{E}{kT_{\mathrm{sun}}}\right) - 1}. \tag{2.6}$$

Note In principle, the surroundings of a solar cell will also contribute to $e-h$ pair generation if the solar cell and the surroundings are in radiative exchange. However, this contribution is negligible compared to the contribution of the sunlight and therefore, it is not worth including it in Eq. (2.6).

2.4 Recombination

Recombination refers to the loss of mobile charge carriers due to electrons decaying to a lower energy state and, therefore, occupying a hole. We say that an electron *recombines* with a hole. The recombination process may occur from spontaneous band-to-band transitions or through impurities (*Shockley-Read-Hall* recombination). The released energy may then be radiated to the surroundings (*radiative* recombination) or as kinetic energy to another carrier (*Auger* recombination). In this section, we review the three most important recombination process that occur within solar cells; Shockley-Read-Hall, radiative and Auger recombination. While the former two are necessary to understand essential parts of this thesis, Auger recombination is briefly described for completeness.

2.4.1 Radiative recombination

Radiative recombination results from the spontaneous decay of an electron from the CB to the VB, thereby emitting a photon to the surroundings. As this recombination process results into radiative emission, the radiative recombination rate at a given energy and angle, $U_{\mathrm{rad}}(E, \theta)$, can be related to the emitted photon flux of a biased blackbody through $U_{\mathrm{rad}}(E, \theta) = a(E) \cdot \dot{n}(E, T, \mu, F_{\mathrm{emi}}(\theta))$, where F_{emi} is geometrical factor related to the solid angle with which the cell radiates. If the cell emits energy within a whole hemisphere, then F_{emi} will equal π. In $\dot{n}(E, T, \mu, F_{\mathrm{emi}}(\theta))$, T is the temperature of the solar cell, which is typically set to 300 K and $\mu = qV$ is the splitting of the quasi-Fermi levels for electrons in the CB and holes in the VB (Fig. 2.3b). The total radiative recombination rate, R, i.e., the number of photons emitted per second and unit area is obtained by integrating

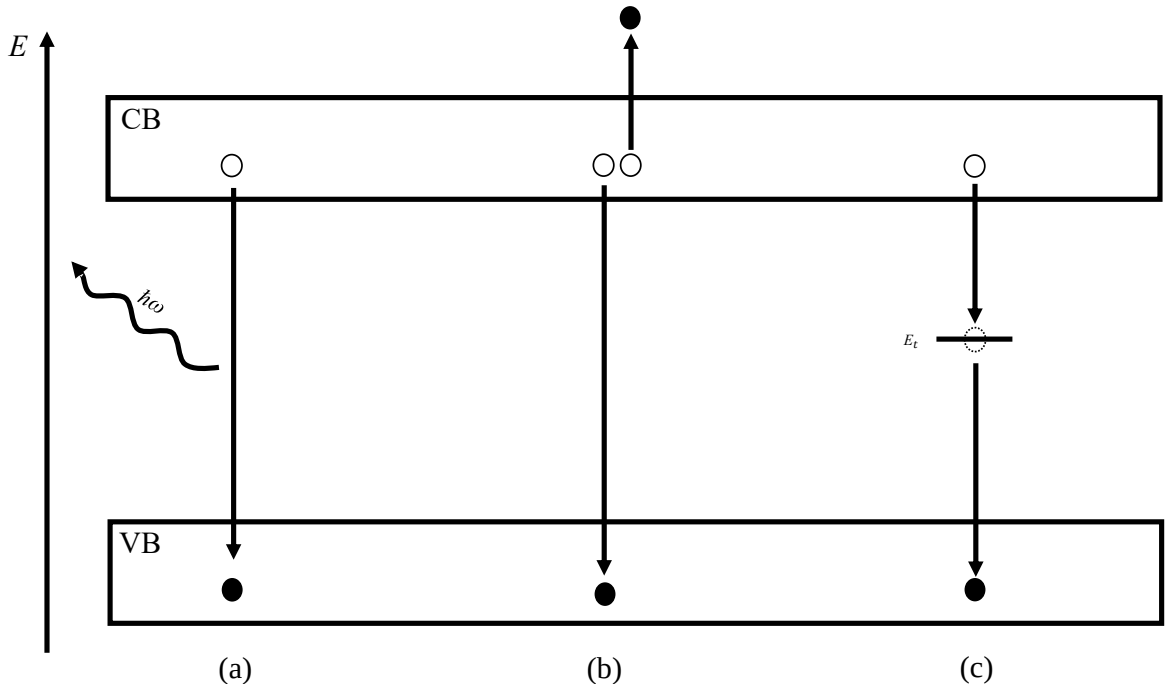

Figure 2.4: Band diagram of the three most common recombination mechanisms: (a) radiative, (b) Auger and (c) SRH recombination. Electrons and holes are represented by black and white circles, respectively. The emitted photons are represented by their energy $\hbar\omega$ and the trap states in (c) by their energy levels, E_{t}.

$U_{\mathrm{rad}}(E,\theta)$ over all possible energies and angles, i.e.,

$$R = \int_0^\infty \int_{\Omega_{\mathrm{emi}}} U_{\mathrm{rad}}(E,\theta')\cos\theta' \mathrm{d}\Omega \mathrm{d}E = \frac{2n\pi}{h^3c^2}\int_{E_{\mathrm{g}}}^\infty \frac{a(E)E^2}{\exp\left[\frac{E-\mu}{kT}\right]-1}\mathrm{d}E, \tag{2.7}$$

where we have assumed that the absorptivity of the cell is 0 for any energy lower than the bandgap, E_{g}. In Fig. 2.4.a, we display the band structure of a solar cell where an electron (black circle) spontaneously decays to the VB, thereby leaving a hole (white circle) in the CB and emitting a photon with energy $\hbar\omega$.

2.4.2 Shockley-Read-Hall recombination

Shockley-Read-Hall (SRH) recombination [24, 25] is the most important recombination process occurring in real semiconductors. Impurities within the material introduce available energy states, usually referred to as *traps*, within the bandgap. Trap states create very efficient two-step band-to-band recombination processes by acting as available energy states to which an electron within the CB may spontaneously decay [15]. The trapped electron will then decay to the VB and fill a hole. The net SRH recombination rate, U_{SRH}, is given by [24, 25]

$$U_{\mathrm{SRH}} = \frac{np - n_{\mathrm{i}}^2}{\tau_{n0}(p+p_{\mathrm{t}}) + \tau_{p0}(n+n_{\mathrm{t}})}, \tag{2.8}$$

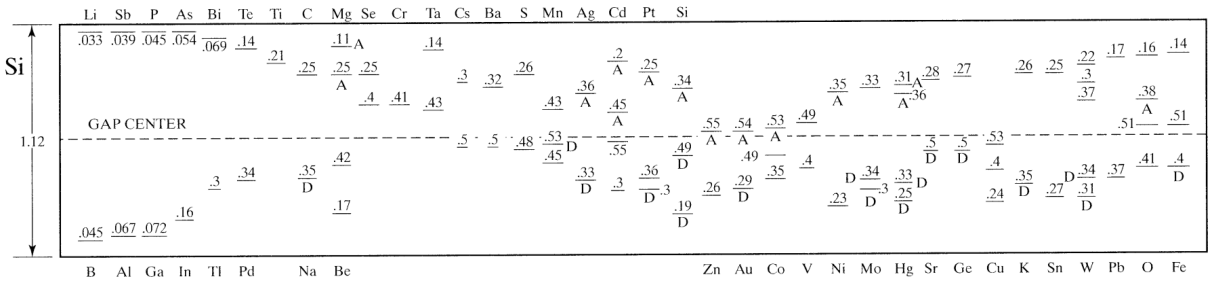

Figure 2.5: Trap energy levels for the most commonly found impurities within the silicon bandgap. The figure is obtained from Ref. [26] where it was reformatted from its original publication in Ref. [27].

where n_i is the intrinsic carrier density and is given by

$$n_\mathrm{i}^2 = N_\mathrm{v} N_\mathrm{c} \exp\left(-\frac{E_\mathrm{g}}{kT}\right), \tag{2.9}$$

with N_x (x = c,v) being the effective conduction and valence band density of states and given by

$$N_x = 2\left(\frac{m_x^* k}{2\pi\hbar^2}\right)^{\frac{3}{2}} T^{\frac{3}{2}}, \tag{2.10}$$

where m_x^* denotes the effective mass of the conduction (valence) band and $\hbar$ is the reduced Planck constant.

The electron and hole population in Eq. (2.8) are given by $n = n_0 + \Delta n$ and $p = p_0 + \Delta p$, where n_0 and p_0 are the electron and hole density at thermal equilibrium and Δn and Δp are the excess carrier densities. The parameters n_t and p_t are the electron and hole densities when their quasi-Fermi level matches the trap energy level, E_t, and are given by

$$p_t = N_\mathrm{v} \exp\left[\frac{-E_\mathrm{t}}{kT}\right], \tag{2.11}$$

$$n_t = N_\mathrm{c} \exp\left[\frac{E_\mathrm{t} - E_\mathrm{g}}{kT}\right]. \tag{2.12}$$

The *capture time* parameters τ_{j0} ($j = n, p$), which depend on the type and density of traps, are given by

$$\tau_{j0} = \frac{1}{N_t v_j \sigma_j}, \tag{2.13}$$

where N_t is the density of traps, v_j is the carrier thermal velocity and σ_j is the capture cross section of the carriers. A schematic representation of SRH recombination is presented in Fig. 2.4.c. Here, we display how an electron in the CB may spontaneously decay to a trap state with energy E_t. From here, the electron will decay to the VB and fill a hole. In Fig. 2.5, we show the trap energy states for the most commonly found impurities in silicon solar cells.

2.4.3 Auger recombination

In the Auger recombination process, the excess energy resulting from an $e-h$ pair recombining is absorbed by a third carrier, an electron in the CB or a hole in VB. The excited carrier then thermalizes to its original energy through phonon emission. [28]. This process can also be visualized as two electrons in the CB colliding and giving the excess kinetic energy to a hole, or, alternatively, two holes in the VB colliding and giving the excess energy to an electron [29]. The Auger recombination rate, U_{Aug}, is therefore proportional to the densities of the three involved carriers, i.e.,

$$U_{\text{Aug}} = A_n(n^2p - n_0^2p_0) + A_p(np^2 - n_0p_0^2) \tag{2.14}$$

where A_n and A_p are Auger coefficients of electrons and holes, respectively. Since this process is a three-particle interaction, it is normally only significant in non-equilibrium conditions with highly doped semiconductors. Auger recombination is schematically represented in Fig. 2.4.b. Here, an electron and a hole recombining give an energy excess to another electron. The latter is excited to an even higher energy level, from which it will thermalize to the edge of the CB.

2.5 Detailed balance theory

The theory of detailed balance was proposed by William Shockley and Hans J. Queisser (SQ) in 1961 [30]. In their work, the authors showed that single junction solar cells have a limiting efficiency of 40.8% under concentrated light. In this section, we review briefly the theory of detailed balance.

The core of the SQ model is to omit all mechanisms of energy loss that are not physically unavoidable. This can be done by assuming the following:

i Only radiative recombination occurs within the cell,

ii carriers have infinite mobility,

iii all photons with energy larger than the bandgap are absorbed,

iv one absorbed photon generates one $e-h$ pair and,

v a perfect mirror is placed in the back of the cell to ensure that the cell will only radiate in a hemisphere.

Assumptions (i) and (iv) are achieved by assuming a not-highly doped impurity-free semiconductor, so that neither SRH nor Auger recombination are present. Assuming carriers with infinite mobility implies that all generated $e-h$ pairs are extracted to an

electric. This also implies zero series resistance with the metal contacts. Assumption (iii) is achieved by setting unit absorptivity, i.e., $a(E) = 1$ for $E \geq E_{\mathrm{g}}$ and zero otherwise, in Eq. (2.6) and (2.7). Finally, assumption (v) is achieved by setting $F_{\mathrm{emi}} = \pi$.

If a solar cell fulfills these five assumptions, it is said to be at the *radiative limit* and the number of electrons that can be extracted from the cell equals the difference between the number of absorbed and emitted photons. From Eqs. (2.6) and (2.7), since the number of extracted electrons is proportional to the current, the total current density produced by a solar cell is given by

$$J = qG - qR = q\int_{E_{\mathrm{g}}}^{\infty} \dot{n}(E, T_{\mathrm{sun}}, 0, F_{\mathrm{abs}})\mathrm{d}E - q\int_{E_{\mathrm{g}}}^{\infty} \dot{n}(E, T_{\mathrm{c}}, qV, F_{\mathrm{emi}})\mathrm{d}E, \tag{2.15}$$

where q is the electron charge.

The power density, P, obtainable from a solar cell is given by the product $P = VJ$, where J is given by Eq. (2.15). The recombination term in the detailed balance equation increases with increasing voltage. For a sufficiently high voltage, the recombination term in Eq. (2.15) will cancel the generation term, resulting in zero current, and therefore zero power. This is the *open-circuit* voltage, V_{oc}. In order to calculate the maximum efficiency of a solar cell, one needs to find the voltage that maximizes the output power. This is known as the *maximum power point* voltage, V_{mpp}. The maximum power point current, J_{mpp}, is obtained by evaluating Eq. (2.15) at $V = V_{\mathrm{mpp}}$. Consequently, the maximum power density from the cell is given by the product $P_{\mathrm{mpp}} = V_{\mathrm{mpp}}J_{\mathrm{mpp}}$ and, the limiting efficiency, η_{max}, will therefore be given by

$$\eta_{\mathrm{max}} = \frac{P_{\mathrm{mpp}}}{P_{\mathrm{in}}} = \frac{V_{\mathrm{mpp}}J_{\mathrm{mpp}}}{X/X_{\mathrm{max}} \cdot \sigma T_{\mathrm{sun}}^4}. \tag{2.16}$$

In Fig. 2.6, we display the limiting efficiency of an ideal solar cell as a function of the energy gap, E_{g}. The displayed plots correspond to concentrated ($X = 46050$) and unconcentrated ($X = 1$) light. The maximum efficiencies are 40.8% and 30.9%, respectively, and are known as the SQ limits.

2.5.1 The diode equation

The last term in Eq. (2.15) corresponds to the photon flux emitted due to radiative recombination. In the regime of useful bandgaps, which corresponds to $E_{\mathrm{g}} \geq 0.5$ eV, it holds that $E - qV >> kT_{\mathrm{c}}$, which implies that the Bose-Einstein (B-E) distribution appearing in the generalized Planck law is well-approximated by a Boltzmann distribution [31]. As a consequence, the exponential in the denominator of Eq. (2.1) is much larger than one,

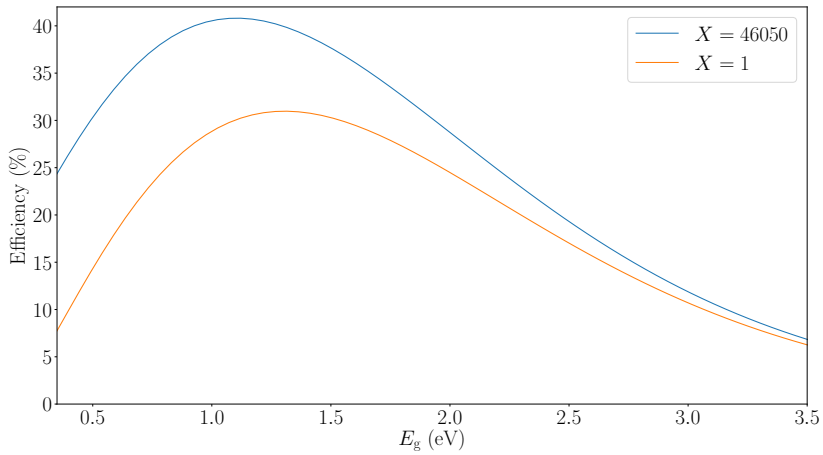

Figure 2.6: Limiting efficiency of a solar cell as a function of the energy gap. The Sun is here modeled as blackbody radiating at $T_{\text{sun}} = 6000$ K.

and the current produced by radiative recombination can be expressed as

$$\begin{aligned} q\int_{E_g}^{\infty} \dot{n}(E, T_c, qV, F_{\text{emi}})\mathrm{d}E = & \frac{2qF_{\text{emi}}}{c^2h^3}\int_{E_g}^{\infty} \frac{E^2\mathrm{d}E}{\exp\left(\frac{E-qV}{kT_c}\right)-1} \\ \approx & \frac{2qF_{\text{emi}}}{c^2h^3}\int_{E_g}^{\infty} \frac{E^2\mathrm{d}E}{\exp\left[\frac{E-qV}{kT_c}\right]} \\ = & \left[\frac{2qF_{\text{emi}}}{c^2h^3}\int_{E_g}^{\infty} E^2\exp\left[-\frac{E}{kT_c}\right]\mathrm{d}E\right]\exp\left[\frac{qV}{kT_c}\right] \\ = & J_0\exp\left[\frac{qV}{kT_c}\right], \end{aligned} \tag{2.17}$$

where J_0 is the *thermal recombination* current [32]. Eq. (2.17) is known as the *Boltzmann approximation* [29]. The first term on the RHS of Eq. (2.15) corresponds to the current associated to the photogeneration of $e-h$ pairs and is therefore often referred to as the photogeneration, or just generation, current, J_{ph}. Using Boltzmann's approximation, Eq. (2.15) becomes

$$J = J_{\text{ph}} - J_0\exp\left[\frac{qV}{kT_c}\right], \tag{2.18}$$

which describes the current that will be delivered to the electric circuit to which the solar cell is coupled. From Eq. (2.18), the *short-circuit* current, J_{sc}, i.e., the current through a solar cell at zero voltage, can be expressed as $J_{\text{sc}} = J_{\text{ph}} - J_0$. By inserting this identity into Eq. (2.18), we arrive at

$$J = J_{\text{sc}} - J_0\left(\exp\left[\frac{qV}{kT_c}\right]-1\right), \tag{2.19}$$

which corresponds to the so-called *diode* equation, the characteristic equation of solar

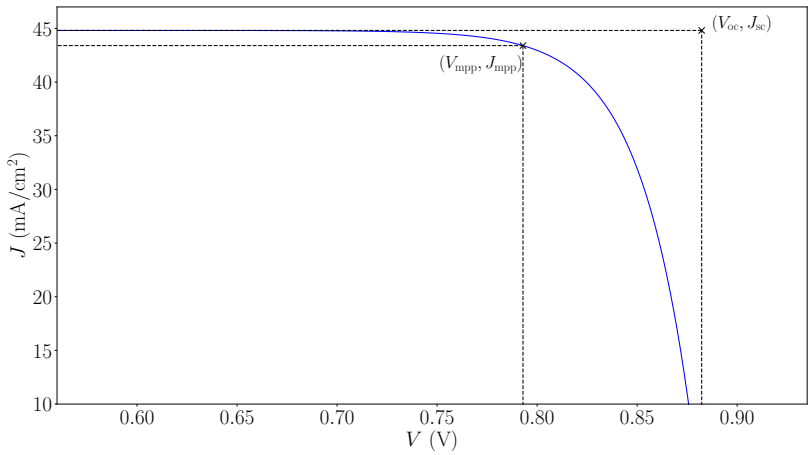

Figure 2.7: Example of a $J - V$ characteristic corresponding to a semiconductor with bandgap $E_g = 1.125$ eV at $T_c = 300$ K under an AM 1.5G spectrum.

cells [33, 34]. The beauty of the theory of detailed balance is that from a particle balance, namely "photons in, electrons out", we are able to show that a solar cell device will behave as an ideal diode. Shockley had previously derived the diode equation for $p-n$ junction in his "The Theory of $p-n$ Junctions in Semiconductors and $p-n$ Junction Transistors" in 1949 [33].

2.5.2 Solar cell parameters

Solar cells can be characterized by constructing their current-voltage ($J-V$) curve. An example of a $J-V$ curve is presented in Fig 2.7. The curve is obtained from Eq. (2.19) and corresponds to a semiconductor with bandgap $E_g = 1.125$ eV at $T_c = 300$ K under an AM 1.5G spectrum.

A $J-V$ curve is characterized by four points; V_{oc}, J_{sc}, V_{mpp} and J_{mpp}. From Eq. (2.19), an expression for V_{oc} can be found by setting $J = 0$. We obtain

$$V_{oc} = kT_c \log\left[\frac{J_{sc}}{J_0} - 1\right] \approx kT_c \log\left[\frac{J_{sc}}{J_0}\right], \tag{2.20}$$

where we have approximated $J_{sc} = J_{ph} - J_0 \approx J_{ph}$, as this is the case for most solar cells. Another important solar cell characterization parameter is the fill factor (FF), which measures the quality of a solar cell by comparing the maximum obtainable power, P_{mpp}, to the product of the open-circuit voltage and the short-circuit current.

$$\text{FF} = \frac{V_{mpp} J_{mpp}}{V_{oc} J_{sc}}. \tag{2.21}$$

Finally, it is worth mentioning that in real cells that the output power of real solar

cells is usually negatively affected by voltage and current drops due to series and shunt resistance effects, respectively. These are not included in the ideal diode equation and will be further explored in the next chapter.

Chapter 3

Advanced Topics in Photovoltaics

Now that we have introduced the basics of solar cell physics, we can explore more advanced concepts that are necessary to understand the attached papers. In this chapter, we introduce Lambert's W function as the mathematical function that allows for an analytical expression of the maximum power point voltage. Next, we present the thermodynamic efficiency limit and the fundamental energy losses of single-junction solar cells. The discussion follows with a review on the temperature sensitivity of solar cells. Particularly, we explore the concept of *temperature coefficient* and Green's [10] and Dupré's [11] models for the temperature coefficient of V_{oc}. Finally, the effect of the series resistance on the maximum power point is discussed.

3.1 Lambert's W function and the maximum power point

In Chapter 2, we introduced the concept of the *maximum power point* (MPP), in the context of calculating limiting efficiencies. The MPP is the point (V, J) of a $J-V$ characteristic that maximizes the power P, given by the product $P = VJ$. In section 2.5.2, we also introduced analytical expressions for V_{oc}, J_{sc} and FF, but we did not do so for V_{mpp}, nor J_{mpp}. The reason for this is that, traditionally, the MPP has been calculated numerically from the diode equation, as only approximate expression for V_{mpp} were in use. It was not until recently that Khanna noticed that Lambert's W function, defined by $z = \mathrm{W}(ze^z)$ [35], allows for an exact analytical expression of V_{mpp} and, consequently J_{mpp} and $P_{\mathrm{mpp}} = V_{\mathrm{mpp}}J_{\mathrm{mpp}}$ [8]. In this section, we introduce the reader to Lambert's W function, the properties of the W function that were most relevant for the research done for this thesis and how Khanna made use of it in Ref. [8] to derive an expression for V_{mpp}.

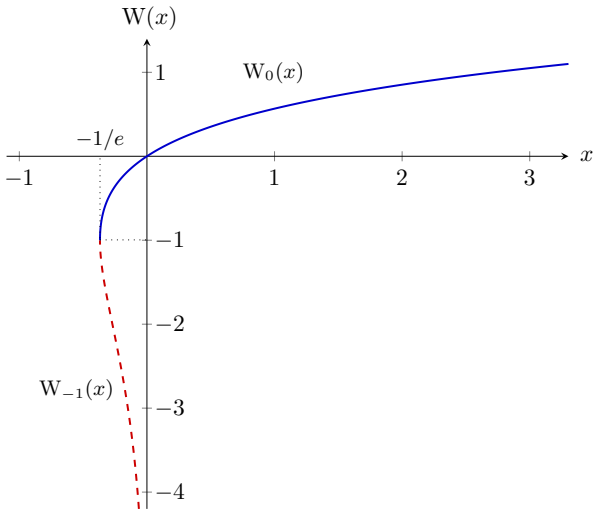

Figure 3.1: The two real branches of the W function, $\mathrm{W}_0(x)$ (blue) and $\mathrm{W}_{-1}(x)$ (red).

3.1.1 Properties of Lambert's W function

Lambert's W function is a multi-valued function defined by the inverse of $f(x) = xe^x$, where $x \in \mathcal{C}$. For an integer k, it holds that

$$x = \mathrm{W}_k(xe^x), \tag{3.1}$$

where W_k is the k-th branch of the W function. Only two values of k result in functions defined within the field of the real numbers: $\mathrm{W}_{-1}(x)$, defined for $-1/e \leq x < 0$, and $\mathrm{W}_0(x)$, defined for $x \geq -1/e$. The latter is known as the *principal branch* of Lambert's W. In Fig. 3.1, we display the two real branches of the W function, $\mathrm{W}_0(x)$, in blue continuous lines, and $\mathrm{W}_{-1}(x)$ in red dashed lines.

In photovoltaics, we deal with real-valued positive-defined quantities and therefore, unless otherwise stated, we will always use the principal branch, W_0. We will refer to it as just Lambert's W function, W. In the following, we derive some of the properties of Lambert's W function, as these are used in the attached papers.

Identities Define first $x = \mathrm{W}(y)$. Eq. (3.1) then reads $\mathrm{W}(y) = \mathrm{W}\left[\mathrm{W}(y)e^{\mathrm{W}(y)}\right]$. Applying the inverse of W function, i.e., the function $\mathrm{W}^{-1}(x)$, such that, $y = \mathrm{W}^{-1}(\mathrm{W}(y))$, to both sides of the equality yields $y = \mathrm{W}(y)e^{\mathrm{W}(y)}$ and therefore

$$e^{\mathrm{W}(y)} = \frac{y}{\mathrm{W}(y)}. \tag{3.2}$$

Calculus The derivative of Lambert's W function can be found from Eq. (3.1) by

implicit differentiation. Letting $z := xe^x$, we have

$$\begin{aligned} 1 = \frac{\mathrm{d}}{\mathrm{d}x}\mathrm{W}(z) = \frac{\mathrm{dW}}{\mathrm{d}z}\frac{\mathrm{d}z}{\mathrm{d}x} &= \frac{\mathrm{dW}}{\mathrm{d}z}(e^x + xe^x) \\ &= e^x \frac{\mathrm{dW}}{\mathrm{d}z}(1+x). \end{aligned} \tag{3.3}$$

From $z = xe^x$ and Eq. (3.1), note that $e^x = z/x = z/\mathrm{W}(z)$. The derivative of W is then given by

$$\frac{\mathrm{d}}{\mathrm{d}z}\mathrm{W}(z) = \frac{1}{e^x(1+x)} = \frac{1}{z}\frac{x}{1+x} = \frac{1}{z}\frac{\mathrm{W}(z)}{1+\mathrm{W}(z)}. \tag{3.4}$$

The indefinite integral of $\mathrm{W}(x)$ can be obtained by making the substitution $x = we^w$. A differential element, $\mathrm{d}x$, is then given by $\mathrm{d}x = (e^w + we^w)\mathrm{d}w$. Therefore

$$\begin{aligned} \int \mathrm{W}(x)\mathrm{d}x &= \int \mathrm{W}(we^w)(e^w + we^w)\mathrm{d}w \\ &= \int w(e^w + we^w)\mathrm{d}w. \end{aligned} \tag{3.5}$$

Partial integrating Eq. (3.5) and making use of the identity in Eq. (3.2) yields

$$\int \mathrm{W}(x)\mathrm{d}x = x\left(\mathrm{W}(x) - 1 + \frac{1}{\mathrm{W}(x)}\right) + C. \tag{3.6}$$

Expansions For small x,the Taylor expansion of the principal branch of Lambert's W function is given by

$$\mathrm{W}_0(x) = \sum_{n=1}^{\infty} \frac{(-n)^{n-1}}{n!}x^n = x - x^2 + \frac{3}{2}x^3 - \ldots, \tag{3.7}$$

which converges as long as $x \leq \frac{1}{e}$. On the other hand, for large x, W_0 is well approximated by the asymptotic expansion

$$\mathrm{W}_0(x) \approx \log x - \log\log x + \frac{\log\log x}{\log x} - \ldots \tag{3.8}$$

3.1.2 Khanna's model for the maximum power point

The total power density, P, is given by the product $P = VJ$ [29]. At the maximum power point, the function $P(V)$ has a maximum and, therefore, it holds that

$$0 = \frac{\mathrm{d}}{\mathrm{d}V}P = \frac{\mathrm{d}}{\mathrm{d}V}VJ(V) = J + V\frac{\mathrm{d}}{\mathrm{d}V}J, \tag{3.9}$$

where $J(V)$ is given by the diode equation. Inserting Eq. (2.19) into Eq. (3.9) yields.

$$\begin{aligned} 0 = \left[J + V\frac{\mathrm{d}}{\mathrm{d}V}J\right]_{V=V_{\mathrm{mpp}}} &= J_{\mathrm{sc}} - J_0 \exp\left[\frac{qV}{kT_{\mathrm{c}}}\right] + V\frac{-qJ_0}{kT_{\mathrm{c}}}\exp\left[\frac{qV}{kT_{\mathrm{c}}}\right]\Bigg|_{V=V_{\mathrm{mpp}}} \\ &= J_{\mathrm{sc}} - J_0\left(1 + \frac{qV_{\mathrm{mpp}}}{kT_{\mathrm{c}}}\right)\exp\left[\frac{qV_{\mathrm{mpp}}}{kT_{\mathrm{c}}}\right] \\ &= \frac{J_{\mathrm{sc}}}{J_0} - \left(1 + \frac{qV_{\mathrm{mpp}}}{kT_{\mathrm{c}}}\right)\exp\left[\frac{qV_{\mathrm{mpp}}}{kT_{\mathrm{c}}}\right], \end{aligned} \tag{3.10}$$

where we have approximated the photogeneration current, J_{ph} by J_{sc}. Here, we note that the quotient ${}^{J_{\mathrm{sc}}}/_{J_0}$ can be written as $\exp\left({}^{qV_{\mathrm{oc}}}/_{kT_{\mathrm{c}}}\right)$ by means of Eq. (2.20). This allows to write the last equality in Eq. (3.10) as

$$\exp\left(\frac{qV_{\mathrm{oc}}}{kT_{\mathrm{c}}}\right) = \left(1 + \frac{qV_{\mathrm{mpp}}}{kT_{\mathrm{c}}}\right)\exp\left[\frac{qV_{\mathrm{mpp}}}{kT_{\mathrm{c}}}\right]. \tag{3.11}$$

Taking now the log at both of the equality and solving for V_{mpp} yields

$$V_{\mathrm{mpp}} = V_{\mathrm{oc}} - \frac{kT_{\mathrm{c}}}{q}\log\left[1 + \frac{qV_{\mathrm{mpp}}}{kT_{\mathrm{c}}}\right], \tag{3.12}$$

which is an implicit equation in V_{mpp}. Traditionally, one would solve Eq. (3.12) numerically to obtain values of V_{mpp}.

Lambert's W function Khanna et al. noticed that by multiplying Eq. (3.11) by Euler's number, e, we obtain

$$\exp\left(1 + \frac{qV_{\mathrm{oc}}}{kT_{\mathrm{c}}}\right) = \left(1 + \frac{qV_{\mathrm{mpp}}}{kT_{\mathrm{c}}}\right)\exp\left[1 + \frac{qV_{\mathrm{mpp}}}{kT_{\mathrm{c}}}\right]. \tag{3.13}$$

The right-hand side of Eq. (3.13) is of the form ze^z, with $z = 1 + {}^{qV_{\mathrm{mpp}}}/_{kT_{\mathrm{c}}}$, and can therefore be inverted by means of Lambert's W function. By applying W to both sides of the equality and solving for V_{mpp}, one obtains [8, 36]

$$V_{\mathrm{mpp}} = \frac{kT_{\mathrm{c}}}{q}\left(\mathrm{W}\left[\exp\left(1 + \frac{qV_{\mathrm{oc}}}{kT_{\mathrm{c}}}\right)\right] - 1\right). \tag{3.14}$$

An expression for the maximum power point current, J_{mpp}, can be obtained by evaluating Eq. (3.14) into Eq. (2.19) and, an expression for the maximum power, P_{mpp}, is obtained from the product $P_{\mathrm{mpp}} = V_{\mathrm{mpp}}J_{\mathrm{mpp}}$. This yields [8, 36]

$$J_{\mathrm{mpp}} = J_{\mathrm{sc}}\left(1 - \frac{1}{\mathrm{W}\left[\exp\left(1 + \frac{qV_{\mathrm{oc}}}{kT_{\mathrm{c}}}\right)\right]}\right), \tag{3.15}$$

$$P_{\mathrm{mpp}} = J_{\mathrm{sc}} \frac{kT_{\mathrm{c}}}{q} \left(\mathrm{W}\left[\exp\left(1 + \frac{qV_{\mathrm{oc}}}{kT_{\mathrm{c}}}\right)\right] - 2 + \frac{1}{\mathrm{W}\left[\exp\left(1 + \frac{qV_{\mathrm{oc}}}{kT_{\mathrm{c}}}\right)\right]} \right). \tag{3.16}$$

In his work, Khanna also derived an expression for the FF by inserting Eqs. (3.14) and (3.15) into (2.21). Denoting by z_{oc} the argument of Lambert's W function in Eq. (3.14), one obtain

$$\begin{aligned} \mathrm{FF} = \frac{kT_{\mathrm{c}}}{qV_{\mathrm{oc}}} \left(\mathrm{W}\left[z_{\mathrm{oc}}\right] - 2 + \frac{1}{\mathrm{W}\left[z_{\mathrm{oc}}\right]} \right) &= \frac{kT_{\mathrm{c}}}{qV_{\mathrm{oc}}} \frac{\mathrm{W}[z_{\mathrm{oc}}]^2 - 2\mathrm{W}[z_{\mathrm{oc}}] + 1}{W[z_{\mathrm{oc}}]} \\ &= \frac{kT_{\mathrm{c}}}{qV_{\mathrm{oc}}} \frac{(\mathrm{W}[z_{\mathrm{oc}}] - 1)^2 e^{\mathrm{W}[z_{\mathrm{oc}}]}}{z_{\mathrm{oc}}}. \end{aligned} \tag{3.17}$$

Eq. (3.17) differs from Khanna's expression in Ref. [8] in that $z_{\mathrm{oc}} - 1$ in the denominator of the last term is approximated by z_{oc}. This is result of having made $J_{\mathrm{ph}} \approx J_{\mathrm{sc}}$ in Eq. (3.10).

3.2 Fundamental energy losses in solar cells

In chapter 2, we introduced the SQ efficiency limit of 40.8% for single-junction solar cells. This implies that, under concentrated light, an ideal solar cell is only capable of converting around 40% of the incoming solar radiation into useful energy. The natural question that follows is, what happens to the remaining 60%? In this section, we aim to find an answer to this question. For this, we will first introduce the thermodynamic efficiency limit of solar cells. Once that we have set the upper efficiency bound, we will introduce the fundamental energy losses of solar cells.

3.2.1 Thermodynamics of energy conversion

At its core, a solar cell can be reduced to a heat engine, i.e., a system that converts energy, the incoming sunlight, into work, the chemical potential of the cell $\mu = qV$, and heat, emitted to the surroundings in form of radiative recombination. The efficiency of such an engine is limited by the efficiency of a Carnot cycle [37],

$$\eta_{\mathrm{Carnot}} = 1 - \frac{T_0}{T_{\mathrm{H}}}, \tag{3.18}$$

where T_0 and T_{H} are the temperatures of the cold and hot reservoirs, respectively. Making $T_{\mathrm{H}} = 6000$ K and $T_0 = 300$ K yields a maximum efficiency of 95%. Carnot's efficiency is calculated as the ratio of the extracted work to the incoming heat flux. A slightly more realistic approach to calculate the limiting efficiency of a solar cell heat engine assumes that the cell is in radiative exchange with the surroundings. The efficiency of the cell is then calculated as the ratio of the extracted work to the to the incoming heat flux *minus*

the radiated energy flux. A maximum efficiency of 93.33% is obtained assuming both the Sun and the cell to be blackbodies. This limit is called the Landsberg efficiency limit [38].

In both Landsberg and Carnot efficiency limits, entropy is conserved. This implies that the process of solar energy conversion is reversible, which is not. To account for the irreversibility of energy conversion, De Vos proposed in Ref. [39] an *endoreversible* solution to calculate the thermodynamic efficiency limit of solar cells. A schematic representation of De Vos' system is presented in Fig. 3.2. In this system, the heat imbalance between the hot reservoir at $T = T_{\text{sun}}$ and an virtual converter at temperature $T_{\text{C}} > T_0$ generates entropy. The converter is then coupled to a heat engine operating at Carnot efficiency at a temperature, T_0, equal to the temperature of the cold reservoir, T_{amb}. Assuming the hot reservoir and the converter to be blackbodies, the excess heat generated by the heat imbalance between the converter and the hot reservoir, Q_{in} in Fig. 3.2, will be given by the difference

$$Q_{\text{in}} = \phi_{\text{sun}} - \phi_{\text{C}} = \sigma(T_{\text{sun}}^4 - T_{\text{C}}^4). \tag{3.19}$$

Since the heat engine is operating at Carnot efficiency, entropy is conserved and therefore, it follows that

$$0 = \Delta S = \frac{Q_{\text{in}}}{T_{\text{C}}} - \frac{Q_{\text{out}}}{T_{\text{amb}}}. \tag{3.20}$$

The produced work, W, by the heat engine equals the energy entering the engine from the converter, Q_{in}, *minus* the emitted heat to the surroundings, Q_{out}. The efficiency of the whole device, η_{DV}, equals the produced work divided by the energy coming from the Sun, ϕ_{sun}. Therefore

$$W = \sigma\left(1 - \frac{T_{\text{amb}}}{T_{\text{C}}}\right)(T_{\text{sun}}^4 - T_{\text{C}}^4), \tag{3.21}$$

$$\eta_{\text{DV}} = \frac{\text{W}}{\phi_{\text{sun}}} = \left(1 - \frac{T_{\text{amb}}}{T_{\text{C}}}\right)\left(1 - \frac{T_{\text{C}}^4}{T_{\text{sun}}^4}\right). \tag{3.22}$$

For $T_{\text{sun}} = 6000$ K and $T_0 = 300$ K, i.e. the usual conditions at which a solar cell operates, Eq. (3.22) has a maximum at $T_{\text{C}} = 2540$ K of $\eta_{\text{DV}} = 85\%$. As a final note, it is worth noting that T_{C} is not necessarily a temperature in the usual interpretation, e.g., operating cell temperature. T_{C} can, for instance, be the temperature of electrons in a hot-carrier cell [13, 40, 41]

3.2.2 Fundamental Losses in Solar Cells

In the previous section, we showed that the thermodynamic efficiency limit of a solar cell is 85%. However, we showed in section 2.5 that the limiting efficiency of an ideal single-junction solar cell operating at the radiative limit is 40%. What happens then to the almost 45% missing? To find an answer to this question, we will review the assumptions

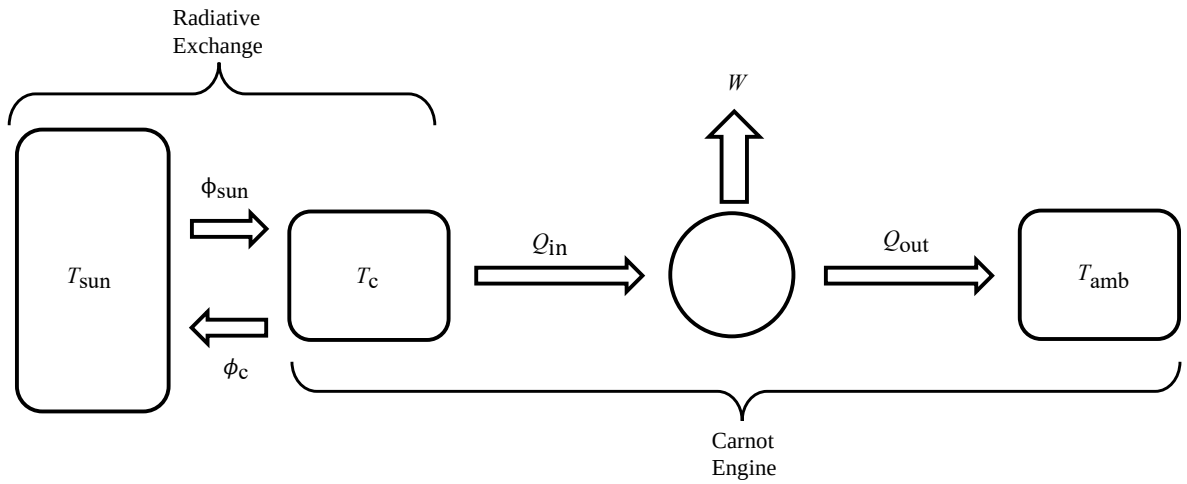

Figure 3.2: Schematic representation of a solar cell. Entropy is produced in the heat imbalance between the converter and the Sun, thus making the radiative exchange irreversible. The inner engine is operating at Carnot efficiency, which is a reversible process. The overall process of energy conversion is hence irreversible.

made to derive the SQ limit and refer to Ref. [9], where Hirst and Ekins-Daukes identified the five mechanisms of energy loss that are intrinsic to solar cells and proposed analytical expressions to calculate these losses.

The first of energy loss mechanism to study is consequence of unabsorbed photons. One of the five assumptions of the SQ model is unit absorptivity for all photons with energy larger than the bandgap and zero absorptivity otherwise. A solar cell is therefore transparent to all photons with energy $\hbar\omega < E_{\mathrm{g}}$. Referring to the notation introduced in chapter 2, the flux of photons coming from the Sun, $\dot{n}(E, T_{\mathrm{sun}}, 0, F_{abs})$, is given by Eq. (2.1). The corresponding energy flux is $E \cdot \dot{n}(E, T_{\mathrm{sun}}, 0, F_{abs})$. The energy loss due to unabsorbed photons, denoted here L_{Below}, is given then by

$$L_{\mathrm{Below}} = \int_0^{E_{\mathrm{g}}} E \cdot \dot{n}(E, T_{\mathrm{sun}}, 0, F_{\mathrm{abs}})\ \mathrm{d}E. \tag{3.23}$$

In Fig. 3.3.a, we show a schematic representation of a photon with energy lower than E_{g} going through a solar cell.

Next, if a solar cell absorbs photons with energy much larger than the bandgap, electrons will be promoted to energy levels way above the conduction band's edge. Due to strong interactions with the lattice, these excited electrons will emit the energy excess, through phonon emission, and relax to the bandgap. This process is called *thermalization*. We display in Fig. 3.3.c, a visual representation of the thermalization process. Here, an electron has been promoted to a high energy level from which relaxes to the CB by emitting the energy excess as heat. The energy loss due to this process, denoted here

L_{Therm}, is given by [9]

$$L_{\mathrm{Therm}} = \int_{E_{\mathrm{g}}}^{\infty} (E - E_{\mathrm{g}}) \cdot \dot{n}(E, T_{\mathrm{sun}}, 0, F_{\mathrm{abs}})\ \mathrm{d}E. \tag{3.24}$$

The energy losses due to thermalization of carriers and unabsorbed photons account for the remaining 45% of the total efficiency loss for single-junction solar cells.

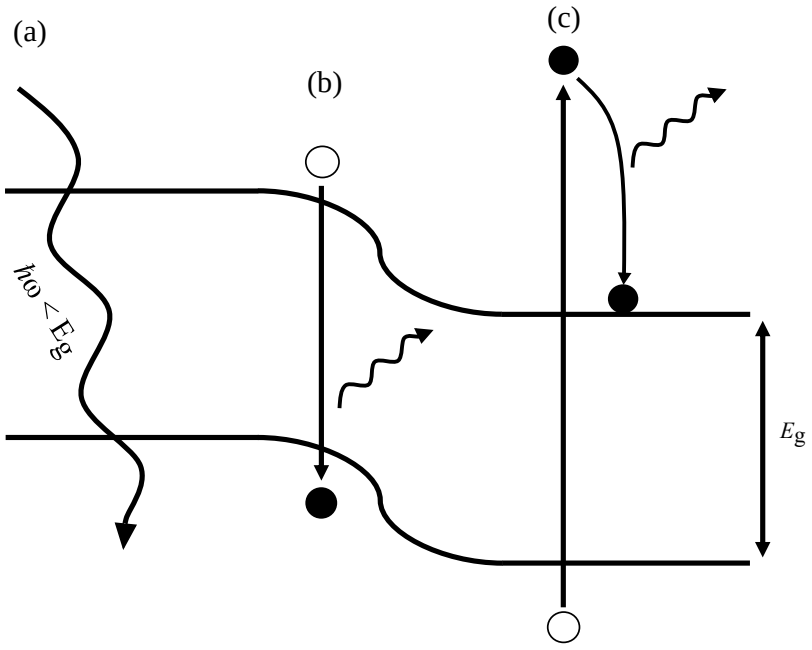

Figure 3.3: Fundamental losses in single-junction solar cell. In (a) the cell is transparent to photons with energy $\hbar\omega < E_{\mathrm{g}}$. In (b), we display radiative recombination and, in (c), we represent an electron thermalizing to the edge of the CB

The three remaining mechanism of energy loss that Hirst and Ekins-Daukes identified are intrinsic to the thermodynamic limit described in section 3.2.1. First, the energy loss consequence of the cell emitting a part of the absorbed energy, represented in Fig. 3.2 as Q_{out}. This in accordance with Kirchhoff's law of thermal radiation which states that, in thermal equilibrium, the emissivity of a gray body equals its absorptivity [42]. The expression that Hirst and Ekins-Daukes proposed for this emission loss, denoted here L_{Em}, is [9]

$$L_{\mathrm{Em}} = E_{\mathrm{g}} \int_{E_{\mathrm{g}}}^{\infty} n(E, T_{\mathrm{c}}, qV, F_{\mathrm{emi}})\ \mathrm{d}E, \tag{3.25}$$

which reads as the energy loss due to radiative recombination (Fig. 3.3.b) assuming that the average energy of the emitted photons equals the cells energy gap.

The last two mechanisms of energy loss that Hirst and Ekins-Daukes describe in their work limits to the obtainable voltage. This is easily seen in the expression for V_{mpp}[1] that

[1] In their work, the authors refer to it as the optimal voltage, V_{opt}.

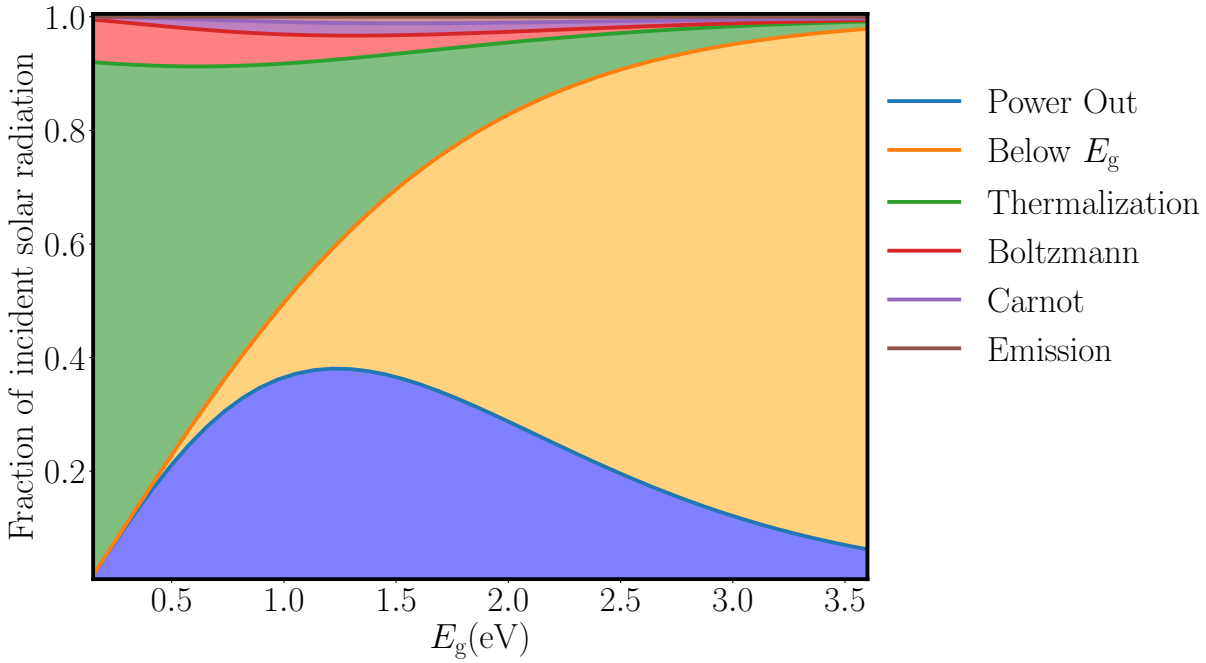

Figure 3.4: Intrinsic energy losses and power output as a function of the bandgap under 1000 suns illumination. Reproduced from [9].

the authors provided in Ref. [9],

$$qV_{\mathrm{mpp}} = E_{\mathrm{g}}\left(1 - \frac{T_{\mathrm{c}}}{T_{\mathrm{sun}}}\right) - kT_{\mathrm{c}}\log\left(\frac{F_{\mathrm{emi}}}{F_{\mathrm{abs}}}\right). \tag{3.26}$$

The first term on the right-hand side of Eq. (3.26) is referred to in Ref. [9] as the *Carnot factor* due to its similarity with the efficiency of a Carnot cycle, Eq. (3.18). The second term affecting the voltage appears due to the possible mismatch between the solid angles of emission and absorption of radiation, which results in part of the incoming energy being lost in entropy generation [43]. The physical explanation for this energy loss is provided by Markvart in Refs. [44], [45] and [46] and reads as follows: when a solar cell absorbs light, entropy needs to be created, in form of an energy loss, to ensure conservation of optical etendue[2][3] [48, 49]. As étendue cannot decrease, the solid angle of emission, Ω_{emi}, must be greater (or equal) than the solid angle of absorption, Ω_{abs}. The last term in Eq. (3.26) will always be positive, or zero for $\Omega_{\mathrm{abs}} = \Omega_{\mathrm{emi}}$. In the context of Fig. 3.2, this loss accounts for the irreversibility of solar energy conversion. As for the Carnot loss, because of its mathematical expression resembles *Boltzmann's entropy equation*, it is referred to in Ref. [9] as the *Boltzmann factor*.

In Fig. 3.4 the fraction of the incident solar radiation is plotted as a function of the

[2]Recall that the geometrical factors, F_{s}, are related to the solid angles Ω_{s} ($\mathrm{s} = \mathrm{abs}, \mathrm{emi}$) through the étendue, Eq. (2.4)

[3]We would like to refer to Ref. [47] for an entertaining, yet accurate, explanation of the law of conservation of étendue.

energy gap, E_g. Here, the contribution of each of the energy losses presented in this section is displayed. The cell is assumed to be at $T = 300$ K and to emit radiation in a whole hemisphere. This is obtained by setting the solid angle of emission to 2π. The solid angle of absorption has been set so that it is equivalent to a Sun concentration factor of 1000. The figure is reproduced from Ref. [9].

3.3 Temperature sensitivity of solar cells

The temperature of a solar cell plays a very important role in its overall power efficiency. See, e.g., the thermodynamic efficiency limits presented in section 3.2.1. The efficiencies η_{Carnot} in Eq. (3.18) and η_{DV}, in Eq. (3.22), decrease with increasing temperature. The fundamental energy losses presented in section 3.2 are also dependent on the cell temperature; the emission, Carnot and Boltzmann losses present an explicit dependence with the cell temperature, whereas the losses due to thermalization and unabsorbed photons depend on the cell temperature through the semiconductor bandgap [50, 51, 52]. Solar cell devices are usually characterized and optimized at standard test conditions (STC), defined as a global standard solar spectrum AM1.5G, an irradiance of 1000 $\text{W} \cdot \text{m}^{-2}$, and a cell temperature of $T = 300$ K. However, real operating conditions can differ significantly from STC depending on, e.g., the climate [53, 54]. This is exemplified in Fig. 3.5, where the normalized efficiency of various solar cell materials is displayed as a function of the operating cell temperatures. Being able to accurately quantify temperature variations is therefore relevant in the pursue of optimal efficiency.

3.3.1 Temperature Coefficient

The temperature sensitivity of a solar cell parameter (V_{oc}, i_{sc}...) is usually described by its *temperature coefficient* (TC). The *absolute temperature coefficient* of a parameter X, as a function of the temperature, T, denoted here $\beta_X(T)$, is defined as the rate of change of X over the considered temperature range, i.e., the derivative of X with respect to the temperature. The *relative temperature coefficient* of X, denoted here β_X^r, is defined as the absolute TC of X normalized by X, i.e., [56]

$$\beta_X^r(T) = \frac{1}{X}\beta_X(T) = \frac{1}{X}\frac{\mathrm{d}X}{\mathrm{d}T} = \frac{\mathrm{d}}{\mathrm{d}T}\log X(T). \tag{3.27}$$

The dependence with the temperature of most solar cell parameters, such as V_{oc} or the efficiency, is approximately linear for normal operating temperatures [10, 57]. The derivative in Eq. (3.27) is then nearly constant and, therefore, β_X can be referred to as the temperature *coefficient*.

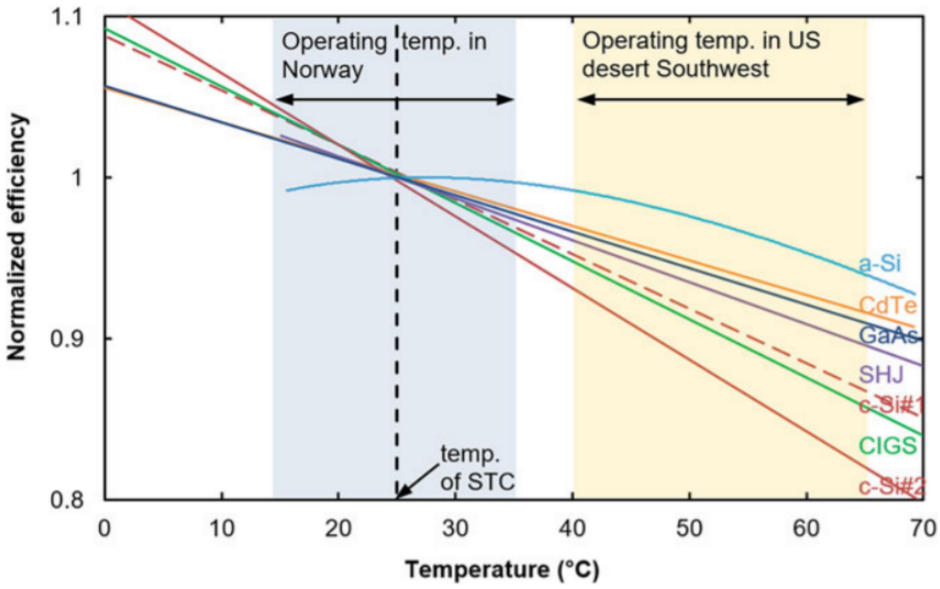

Figure 3.5: Normalized efficiency as a function of the temperature for various solar cell materials (c-Si: crystalline silicon; a-Si: Amorphous silicon; CdTe: Cadmium telluride. GaAs: Gallium arsenide; SHJ: Silicon hetero-junction; CIGC: Copper-indium-gallium selenide) [55]

3.3.2 The temperature coefficient of the open-circuit voltage

The TC of V_{oc}, $\beta_{V_{\mathrm{oc}}}$, has been studied from an analytical perspective in multiple works. This is because $\beta_{V_{\mathrm{oc}}}$ accounts for approximately 80–90% of the total temperature sensitivity of the cell [10]. For the thesis work, two articles are of particular relevance: Refs. [11] and [13]. In this section, we reproduce the derivations of the relevant expressions derived in these works.

Starting with Ref. [13], Green derived an expression for the TC of V_{oc}. From the expression for V_{oc} given in Eq. (2.20), Green wrote

$$J_{\mathrm{sc}}(T) = J_0\left(\exp\left(\frac{qV_{\mathrm{oc}}}{kT}\right) - 1\right) = AT^{\gamma}\exp\left(\frac{-E_{\mathrm{g0}}}{kT}\right)\exp\left(\frac{qV_{\mathrm{oc}}}{kT}\right), \tag{3.28}$$

where A is a constant, E_{g0} is the bandgap extrapolated to 0 K and γ is a parameter that includes the temperature dependencies of the remaining parameters determining J_0. The last equality of Eq. (3.28) was proposed by Green in Ref. [13] and this form of J_0 is derived and justified later in the present text. Taking the derivative with respect to the temperature at both sides of Eq. (3.28) yields

$$\frac{\mathrm{d}J_{\mathrm{sc}}}{\mathrm{d}T} = \left(A\gamma T^{\gamma-1} + AT^{\gamma}\frac{q}{kT_{\mathrm{c}}}\left[\frac{\mathrm{d}V_{\mathrm{oc}}}{\mathrm{d}T} - \left(\frac{V_{\mathrm{oc}} - {}^{E_{\mathrm{g0}}}\!/_{q}}{T}\right)\right]\right)\exp\left(\frac{q(V_{\mathrm{oc}} - {}^{E_{\mathrm{g0}}}\!/_{q})}{kT}\right) \tag{3.29}$$

Here, Green noted that the absolute value of ${}^{\mathrm{d}J_{\mathrm{sc}}}\!/_{\mathrm{d}T}$ can be neglected in comparison with the remaining terms of the equality. The parenthesis on the RHS of Eq. (3.29) is then

zero. Making use of the definition of TC to write ${}^{\mathrm{d}V_{\mathrm{oc}}}/_{\mathrm{d}T} = \beta_{V_{\mathrm{oc}}}$ and a bit of manipulation yields [13]

$$\beta_{V_{\mathrm{oc}}} = \frac{\mathrm{d}V_{\mathrm{oc}}}{\mathrm{d}T} = -\frac{{}^{E_{\mathrm{g0}}}/_{q} - V_{\mathrm{oc}} + {}^{\gamma kT}/_{q}}{T}, \tag{3.30}$$

from where Green concluded a approximately linear decrease in V_{oc} with increasing temperature.

3.3.2.1 The external radiative efficiency

As the diode equation presented in Eq. (2.19) is derived from the detailed balance, it describes a solar cell operating at the radiative limit. However, as noted in section 2.4, non-radiative recombination processes, such as SRH recombination, are the most important processes occurring in real semiconductors. In order to account for non-radiative recombination, Green introduced the concept of External Radiative Efficiency (ERE) in Ref. [58]. The ERE is defined as *the fraction of the total dark current recombination in the cell that results in radiative emission from the cell* [58]. In Ref. [11], Dupré made use of the ERE to explicitly quantify the mechanism affecting the temperature sensitivity of V_{oc}. For this, Dupré introduced the ERE in Eqs. (2.19) and (2.20) by making the substitution $J_0 \rightarrow {}^{J_0}/_{\mathrm{ERE}}$ [11] and wrote

$$J = J_{\mathrm{sc}} - \frac{1}{\mathrm{ERE}} J_0 \exp\left(\frac{qV}{kT}\right), \tag{3.31}$$

$$V_{\mathrm{oc}}(T) = \frac{kT}{q} \log\left(\mathrm{ERE}_{\mathrm{oc}} \frac{J_{\mathrm{sc}}}{J_0}\right), \tag{3.32}$$

where $\mathrm{ERE}_{\mathrm{oc}}$ is the ERE evaluated at open-circuit. From Eq. (3.32), an expression for $\beta_{V_{\mathrm{oc}}}$ can be obtained by taking the derivative with respect to the temperature. This gives

$$\begin{aligned} \beta_{V_{\mathrm{oc}}} = \frac{\mathrm{d}V_{\mathrm{oc}}}{\mathrm{d}T} &= \frac{k}{q} \log\left(\mathrm{ERE}_{\mathrm{oc}} \frac{J_{\mathrm{sc}}}{J_0}\right) + \frac{kT}{q} \frac{\mathrm{d}}{\mathrm{d}T} \log\left(\mathrm{ERE}_{\mathrm{oc}} \frac{J_{\mathrm{sc}}}{J_0}\right) \\ &= \frac{V_{\mathrm{oc}}}{T} + \frac{kT}{q}\left[\frac{J'_{\mathrm{sc}}}{J_{\mathrm{sc}}} + \frac{\mathrm{ERE}'_{\mathrm{oc}}}{\mathrm{ERE}_{\mathrm{oc}}} - \frac{J'_0}{J_0}\right], \end{aligned} \tag{3.33}$$

where the prime implies derivative with respect to the temperature. The thermal recombination current, J_0, is given by the integral in Eq. (2.17), which is well approximated by

$$J_0(T) = \frac{2\pi}{c^2 h^3} \int_{E_{\mathrm{g}}(T)}^{\infty} E^2 \exp\left[-\frac{E}{kT}\right] \mathrm{d}E \approx \frac{2\pi}{c^2 h^3} kT E_{\mathrm{g}}(T)^2 \exp\left[-\frac{E_{\mathrm{g}}(T)}{kT}\right]. \tag{3.34}$$

Note from Eq. (3.34) that the bandgap is dependent on the cell's temperature, $E_{\mathrm{g}}(T)$. This originates from interaction between electrons and lattice phonons [59]. The bandgap

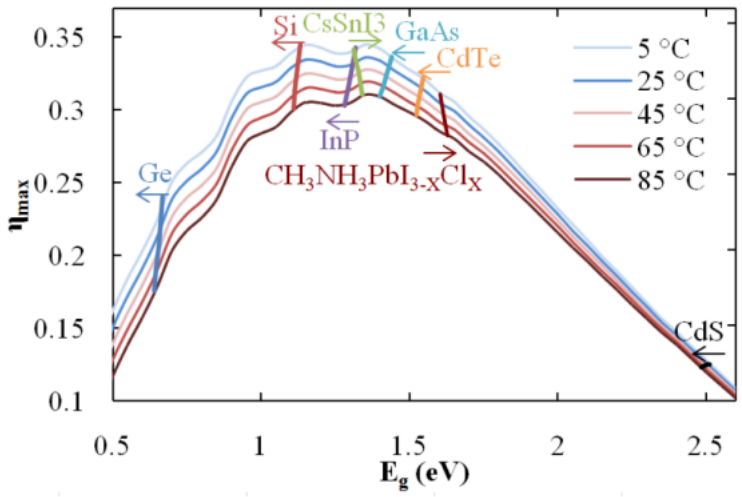

Figure 3.6: Limiting efficiency of single-junction solar cells as a function the energy gap for various temperatures. An AM1.5G spectrum is assumed. The plot also displays the temperature sensitivity of the bandgap of various semiconductors, as well as their limiting efficiencies [11, 55].

of most semiconductors decreases with increasing temperature. This excludes $CH_3NH_3PbI_3$ and related perovskite compound which shows the opposite behavior [55]. The temperature sensitivity of the bandgap is well approximated by [13, 50, 60],

$$E_{\mathrm{g}}(T) = E_{\mathrm{g0}} - T \left.\frac{\mathrm{d}E_{\mathrm{g}}}{\mathrm{d}T}\right|_{T=T_{\mathrm{c}}} + \mathcal{O}(T_{\mathrm{c}}^2)\ldots \tag{3.35}$$

where E_{g0} is the bandgap extrapolated to $T = 0$ K. In Fig. 3.6, the limiting efficiency of single-junction solar cells is displayed as a function of the bandgap for temperatures ranging from 5°C up to 85°C [11, 55]. Here, the temperature sensitivity of the bandgap of various solar cell materials is also displayed.

Inserting Eq. (3.34) into (3.33) and accounting for the linear temperature dependence of the bandgap in Eq.(3.35) yields [11]

$$\beta_{V_{\mathrm{oc}}} = \frac{V_{\mathrm{oc}} - {}^{E_{\mathrm{g0}}}/_{q} - \gamma {}^{kT_{\mathrm{c}}}/_{q}}{T_{\mathrm{c}}}, \tag{3.36}$$

with

$$\gamma = 1 + 2T_{\mathrm{c}}\frac{E_{\mathrm{g}}'}{E_{\mathrm{g}}} - T_{\mathrm{c}}\frac{\mathrm{ERE}'}{\mathrm{ERE}} - T_{\mathrm{c}}\frac{J_{\mathrm{sc}}'}{J_{\mathrm{sc}}}. \tag{3.37}$$

Comparing Eq. (3.36) to (3.30), Dupre noted that they had arrived at the same expression[4] and concluded that Eq. (3.37) explicitly quantifies the recombination parameter γ introduced in section 3.3.2. Recalling the definition of γ, given by Green in Ref. [10], Dupré concluded that Eq. (3.37) allows for an explicit identification of the temperature

[4] In Ref. [11], the author used the notation $\frac{\mathrm{d}\log X}{\mathrm{d}\log T}$, which is equivalent to $T\frac{X'}{X}$

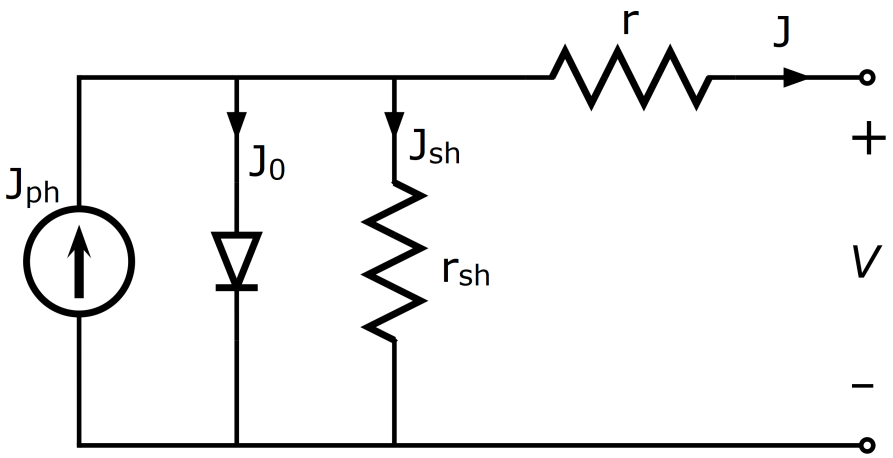

Figure 3.7: Equivalent circuit for a solar cell including series (r) and shunt (r_{sh}) resistance. J_{ph} and J_0 are the photogeneration and thermal recombination current introduced in chapter 2. J_{sh} equals the last term in Eq. (3.38).

sensitivity of the mechanisms determining V_{oc} [11, 61].

3.4 The effect of the series resistance

So far, all the expressions that we have presented in this thesis have been derived from the diode equation, Eq. (2.19). Non-radiative recombination has been accounted for through the ERE, Eq. (3.31). In real solar cells, however, power is lost not only through recombination but also through resistance of the metal contacts and current leakages. To account for these effects in the characterization of solar cell devices, the diode equation in Eq. (2.19) needs to be modified to the general form [26, 29, 62]

$$J = J_{\mathrm{ph}} - J_0 \exp\left[\frac{q(V + Jr)}{kT}\right] - \frac{V + Jr}{r_{\mathrm{sh}}}, \tag{3.38}$$

where r and r_{sh} are the series and shunt resistances, respectively. Note that, as Eq. (3.38) describes current density, the units of the resistance are $\Omega \cdot \mathrm{cm}^2$ and therefore, these are sometimes refer to as *area-normalized* resistances [63]. In Fig. 3.7, we display the equivalent circuit of a solar cell. Here, J_{sh} equals the last term in Eq. (3.38). Shunt resistance effects do not usually have a relevant impact in laboratory cells, as these typically appear due to defects in manufacturing. We will therefore assume $r_{\mathrm{sh}} \to \infty$ in Eq. (3.38), so that the last term is negligible, and limit our discussion to only series resistance.

3.4.1 Closed-form of the diode equation with series resistance

Banwell showed in Ref. [14] that Lambert's W function, introduced in section 3.1.1, allows for an exact analytical solution of Eq. (3.38). In this section, we reproduce the derivation.

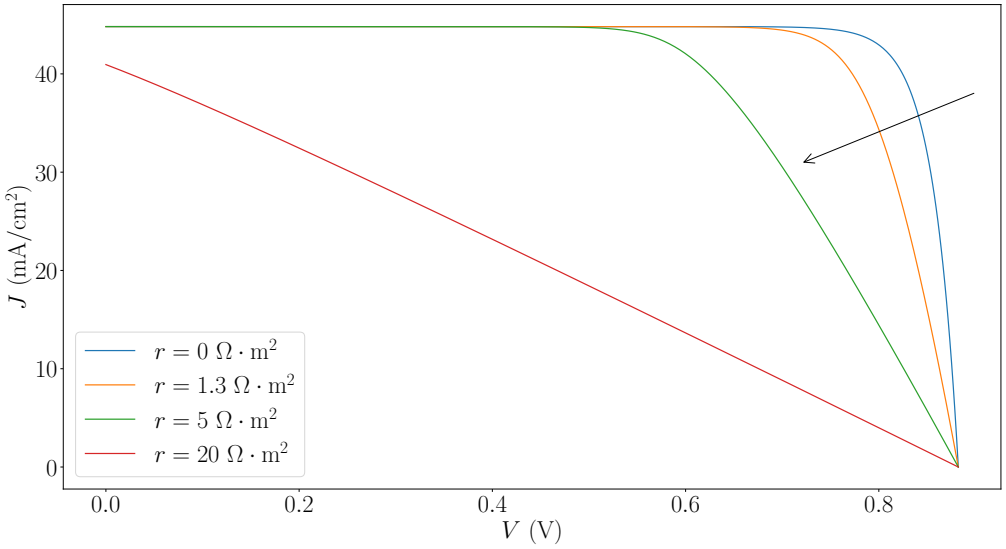

Figure 3.8: $J - V$ characteristic corresponding to a semiconductor with bandgap $E_\mathrm{g} = 1.125$ eV at $T_\mathrm{c} = 300$ K under an AM 1.5G spectrum for various values of the series resistance.

Multiplying both sides of the equality by $\frac{qr}{kT}\exp(-\frac{qr(J-J_\mathrm{ph})}{kT})$ allows to rewrite Eq. (3.38) as

$$\frac{qr}{kT}(J_\mathrm{ph} - J)\exp\left[\frac{qr(J_\mathrm{ph} - J)}{kT}\right] = \frac{qr}{kT}J_0\exp\left[\frac{q(V + J_\mathrm{ph}r)}{kT}\right]. \tag{3.39}$$

Note that the left-hand side of the equality is of the form ze^z, with $z = \frac{qr}{kT}(J_\mathrm{ph} - J)$. Applying W to both sides of Eq. (3.1) yields

$$\frac{qr}{kT}(J_\mathrm{ph} - J) = \mathrm{W}\left[\frac{qr}{kT}J_0\exp\left[\frac{q}{kT}(V + J_\mathrm{ph}r)\right]\right], \tag{3.40}$$

and therefore

$$J = J_\mathrm{ph} - \frac{kT}{qr}\mathrm{W}\left[\frac{qr}{kT}J_0\exp\left[\frac{q}{kT}(V + J_\mathrm{ph}r)\right]\right]. \tag{3.41}$$

From Eq. (3.41), it is now straight forward to obtain an expression for the short-circuit current, J_sc, by setting $V = 0$. This gives

$$J_\mathrm{sc} = J_\mathrm{ph} - \frac{kT}{qr}\mathrm{W}\left[\frac{qr}{kT}J_0\exp\left[\frac{qJ_\mathrm{ph}r}{kT}\right]\right]. \tag{3.42}$$

In Fig. 3.8, we display $J - V$ characteristics corresponding to a solar cell with $E_\mathrm{g} = 1.125$ eV at $T = 300$ K under an AM1.5G spectrum for various values of the series resistance ($[r] = \Omega\cdot\mathrm{cm}^2$). Here, the arrow indicates increasing series resistance. Note that the the series resistance reduces the fill factor. As a final note, it is worth mentioning the work of Jain and Kapoor in Ref. [64], where, the authors derived an analogue expression to Eq. (3.41) that also included the effect of the shunt resistance.

3.4.2 Singal's model for the maximum power point

Already in 1981, Singal derived approximate analytical expressions for V_{mpp}, J_{mpp} and P_{mpp} [12]. Because this work came before Banwell's close-form expression for the current with series resistance, Eq. (3.41), Singal's model did not make use of Lambert's W function. In this section, we derive Singal's expressions. First, setting $r_{\mathrm{sh}} \to \infty$, we can solve Eq. (3.38) for V and obtain

$$V = \frac{kT}{q} \log\left[\frac{J_{\mathrm{ph}} - J}{J_0}\right] - Jr. \tag{3.43}$$

The power density, P, is given by $P = VJ$ and at the maximum power point, it holds

$$0 = \left.\frac{\mathrm{d}P}{\mathrm{d}J}\right|_{J=J_{\mathrm{mpp}}} = \frac{kT}{q} \log\left[\frac{J_{\mathrm{ph}} - J_{\mathrm{mpp}}}{J_0}\right] - \frac{kT}{q}\frac{J_{\mathrm{mpp}}}{J_{\mathrm{ph}} - J_{\mathrm{mpp}}} - 2J_{\mathrm{mpp}}r. \tag{3.44}$$

For convenience, Singal defined the dimensionless variables v and y as

$$v = \frac{q}{kT}V_{\mathrm{oc}}, \tag{3.45}$$

$$y = \frac{kT}{qV_{\mathrm{oc}}} \log\left[\frac{J_{\mathrm{ph}} - J_{\mathrm{mpp}}}{J_0}\right] = \frac{1}{v} \log\left[\frac{J_{\mathrm{ph}} - J_{\mathrm{mpp}}}{J_0}\right]. \tag{3.46}$$

Note that $yV_{\mathrm{oc}} = V_{\mathrm{mpp}}$. This can be seen by evaluating Eq. (3.43) at the MPP with $r = 0$:

$$V_{\mathrm{mpp}} = \frac{kT}{q} \log\left[\frac{J_{\mathrm{ph}} - J_{\mathrm{mpp}}}{J_0}\right] = \frac{V_{\mathrm{oc}}}{v} \log\left[\frac{J_{\mathrm{ph}} - J_{\mathrm{mpp}}}{J_0}\right] = yV_{\mathrm{oc}}, \tag{3.47}$$

where we used Eqs. (3.45) and (3.46). Since $yV_{\mathrm{oc}} = V_{\mathrm{mpp}}$, y is necessarily less than one. Note that, from Eq. (2.20), it follows that ${}^{J_{\mathrm{ph}}}/_{J_0} = \exp\left({}^{qV_{\mathrm{oc}}}/_{kT}\right) = \exp(v)$. Additionally, note that $J_{\mathrm{mpp}} = J_{\mathrm{ph}} - J_0 \exp(yv)$ follows from Eq. (3.46). The variables v and y can be found in Eq. (3.44) by dividing the equality by V_{oc}. The presented identities together with the Eqs. (3.45) and (3.46) allow for Eq. (3.44) to be expressed as

$$\begin{aligned} 1 + vy &= e^{v - vy} + \frac{2qrJ_0}{kT}(e^v - e^{vy}) \\ &= e^{v-vy}\left[1 + \frac{2qrJ_0}{kT}e^{vy}(1 - e^{vy-v})\right], \end{aligned} \tag{3.48}$$

and taking the logarithm at both sides of the equality and a bit of manipulation finally gives

$$y = 1 - \frac{1}{v}\log v - \frac{1}{v}\left[\log y + \frac{1}{v}\right] + \frac{1}{v}\log\left[1 + \frac{2qrJ_0}{kT}e^{vy}(1 - e^{vy-v})\right]. \tag{3.49}$$

From here, Singal noted that for most solar cells, it holds that $qV_{\mathrm{oc}} >> kT$, implying

that $v >> 1$. Additionally, as noted above, we have $y \leq 1$. This allowed him to make a series of Taylor expansions and approximations that yielded an approximate analytical solution of the form $y = f(v)$. We refer to Ref. [12] for the further-detailed derivation. The obtained analytical solutions for V_{mpp} and J_{mpp} were

$$V_{\mathrm{mpp}} = V_{\mathrm{oc}}\Bigg[1 - \frac{1}{v}\log(1+v-\log(v)) + \frac{1}{v}\log\left(1 + \frac{2J_{\mathrm{sc}}r}{V_{\mathrm{oc}}}\frac{v(v-\log(v))}{(1+v-\log(v))^2}\right) - \frac{J_{\mathrm{sc}}r}{V_{\mathrm{oc}}}\frac{v-\log(v)}{1+v-\log(v)} + \left(\frac{J_{\mathrm{sc}}r}{V_{\mathrm{oc}}}\right)^2\frac{2v(v-\log(v))}{(1+v-\log(v))^3}\Bigg], \tag{3.50}$$

$$J_{\mathrm{mpp}} = J_{\mathrm{sc}}\left[1 - \frac{1}{1+v-\log(v)} - \frac{2J_{\mathrm{sc}}r}{V_{\mathrm{oc}}}\frac{v(v-\log(v))}{(1+v-\log(v))^3}\right]. \tag{3.51}$$

The corresponding expression for P_{mpp} is obtained by multiplying, i.e., Eqs. (3.50) and (3.51)

$$\begin{aligned} P_{\mathrm{mpp}} = V_{\mathrm{oc}}J_{\mathrm{sc}}&\left[1 - \frac{1}{1+v-\log(v)} - \frac{2J_{\mathrm{sc}}r}{V_{\mathrm{oc}}}\frac{v(v-\log(v))}{(1+v-\log(v))^3}\right] \\ &\times\Bigg[1 - \frac{1}{v}\log(1+v-\log(v)) + \frac{1}{v}\log\left(1 + \frac{2J_{\mathrm{sc}}r}{V_{\mathrm{oc}}}\frac{v(v-\log(v))}{(1+v-\log(v))^2}\right) \\ &- \frac{J_{\mathrm{sc}}r}{V_{\mathrm{oc}}}\frac{v-\log(v)}{1+v-\log(v)} + \left(\frac{J_{\mathrm{sc}}r}{V_{\mathrm{oc}}}\right)^2\frac{2v(v-\log(v))}{(1+v-\log(v))^3}\Bigg]. \end{aligned} \tag{3.52}$$

With these expressions, Singal obtained estimated numerical errors below 1%, compared to numerical models. As a final note, we want to note the work in Ref. [65], where Green made use of Banwell's expression in Eq. (3.41) to derive an implicit analytical expression of V_{mpp} that accounted for the effect of the series resistance.

Chapter 4

Summary of Papers

In this chapter, we present a summary and the motivation of the attached papers.

Author contributions: Alfredo Sanchez Garcia and Rune Strandberg are the authors of the six attached papers. In all six papers, the conceptualization, mathematical modeling and numerical computations were made by Alfredo Sanchez. The writing of all six papers was also done by Alfredo Sanchez. Rune Strandberg supervised the process, reviewed and helped in the writing and, overall, catalyze the work through fruitful discussions. In the papers that involved experimental verification of the models, it was Sissel Tind Kristensen who coordinated the experiments and therefore shares co-authorship.

Paper A: Analytical expressions for radiative losses in solar cells

In Ref. [9], Hirst and Ekin-Daukes derived a set of analytical expression to describe the fundamental losses intrinsic to single-junction solar cells. As Khanna's model for the maximum power point [8] had not yet been derived, the authors in Ref. [9] made use of various approximations to obtain their model. In this paper, we investigate how Khanna's model and Lambert's W function can be used to describe fundamental energy losses intrinsic to single-junction solar cells. We derive a new set of exact analytical expressions. The new expression for the thermalization loss is derived accounting for the fermionic nature of electrons. We show that Khanna's model allows for an expression that combines the emission, Carnot and Boltzmann losses.

Published as:
Garcia, A.S. and Strandberg, R., 2019, June. Analytical expressions for radiative losses in solar cells. In 2019 IEEE 46th Photovoltaic Specialists Conference (PVSC) (pp. 1774-1779). IEEE.

Paper B: Temperature Coefficients of Solar Cell Parameters at Maximum Power Point

Motivated by the works of Green in Ref. [13] and Dupré in Ref. [11] on the modeling of TCs, we derive analytical expressions for the TC of V_{mpp} and J_{mpp}. Our approach is inspired by Dupré in Ref. [11], as we also use the ERE to account for non-radiative recombination. We explore the effects of making use of certain approximations and the choice of bandgap model. The recombination parameter γ is found to play role in the temperature sensitivity of the maximum power point. From both theory and experiments, we show that J_{mpp} does not change linearly with the cell temperature. This work sets the ground for **paper C**.

Published as:
Garcia, A.S., Kristensen, S.T., Christiansen, S.N. and Strandberg, R., 2020, June. Temperature Coefficients of Solar Cell Parameters at Maximum Power Point. In 2020 47th IEEE Photovoltaic Specialists Conference (PVSC) (pp. 1232-1237). IEEE.

Paper C: Analytical Modeling of the Temperature Sensitivity of the Maximum Power Point

This paper extends on **paper B**. Here, we drop the ERE approach and make use of identities that follow from Khanna's model [8] to write all the expressions for the TCs in terms of known solar cell parameters. In addition to the expressions derived in **paper B**, we derive an analytical expression for the TC of P_{mpp}, which allows for the derivation of a new exact analytical expression for the TC of the FF. The expressions are tested with experimental data obtained from suns-V_{oc} measurements and show outstanding agreement with the experiments. The limitations of a single-valued TC to describe the temperature sensitivity of a solar cell parameter are also discussed.

Published as:
Garcia, A. S., Kristensen, S. T., and Strandberg, R., 2022. Analytical Modeling of the Temperature Sensitivity of the Maximum Power Point of Solar Cells. IEEE Journal of Photovoltaics.

Paper D: Analytical Modeling of the Maximum Power Point with Series Resistance.

In this work, we derive analytical expressions for V_{mpp}, J_{mpp} and P_{mpp} that account for the effect of the series resistance of the solar cell. To obtain these, we make use of the Taylor expansion of Lambert's W function. This allows for an analytical solution of what is otherwise a transcendental equation. The new model allows for the derivation of an analytical expression that explicitly shows how the series resistance depends on other solar cell parameters. We test the new analytical model against a numerical single-diode model and show that our expressions are able to predict the maximum power point with discrepancies below 0.1% for typical values of the series resistance.

Published as:
Garcia, A.S.; Strandberg, R. Analytical Modeling of the Maximum Power Point with Series Resistance. Appl. Sci. 2021, 11, 10952.

Paper E: Assessment of a New Analytical Expression for the Maximum Power Point Voltage with Series Resistance.

In this paper, we test the applicability of the model presented in **paper D**. For this, we use experimental data obtained from 18 multi-crystalline silicon solar cells. We also compare the model to Singal's [12] and a numerical model obtained from the diode equation with series resistance. We conclude that the model presented in paper D can be successfully applied in multi-crystalline silicon solar cells, achieving, and sometimes surpassing, the level of accuracy that Singal's model has.

Published as:
Garcia, A.S., Kristensen, S.T. and Strandberg, R., 2021, June. Assessment of a New Analytical Expression for the Maximum-Power Point Voltage with Series Resistance. In 2021 IEEE 48th Photovoltaic Specialists Conference (PVSC) (pp. 0961-0965). IEEE.

Paper F: The Recombination Parameter γ: Modeling and Comments

The recombination parameter γ was introduced by Green [13], when deriving an expression for the TC of V_{oc}. Later in Ref. [11], Dupré was able to explicitly quantify γ by making

use of the ERE. Motivated by these works, we explore, from a theoretical perspective, the connection between γ and material properties, such as carrier mobility and lifetime. This is possible by assuming that all non-radiative recombination occurs in the neutral region of the cell, where carrier diffusion is dominant. We find problems in the definition of γ that hinder a further analytical investigation. Particularly, we note that γ is dependent on V_{oc}. Because of this voltage dependency, the applicability of γ is limited. We suggest solutions to the presented problems. Particularly, for low-level injection, γ is not dependent on V_{oc}. We derive analytical expressions for γ in this regime and conduct numerical experiments. We conclude that although γ may not be a fingerprint of defects in silicon, it may still be useful in conjunction with other characterization techniques for impurity identification. Particularly, we suggest its possible usability in showing how impurities distribute within silicon wafers.

Published as:
Garcia, A.S., Kristensen, S.T. and Strandberg, R., 2022. The Recombination Parameter γ: Modeling and Comments. *To be submitted*

Chapter 5

Summary and further work

In this thesis, we have developed analytical models that described some of the physical processes limiting the efficiency of single-junction solar cells. We have focused on three distinct topics: fundamental energy losses, the temperature sensitivity of single-junction solar cells and the effect of the series resistance on the maximum power point.

Our model for the fundamental energy losses improved upon the expressions presented in Ref. [9], as it made use of Lambert's W function and Khanna's model for the maximum power point. In the newly derived expression for the thermalization loss, the fermionic nature of electrons and holes was accounted for. This resulted in the need of a second thermalization to the CB edge, from where we concluded that the overall thermalization loss needed to occur step-wise. The introduction of Lambert's W allowed for an expression that combined the emission, Carnot and Boltzmann energy losses.

Regarding the temperature sensitivity of single-junction solar cells, we made use of Khanna's model to derive analytical expressions for the temperature coefficients of the maximum power point. These expressions allowed for an expression of the temperature coefficient of the fill factor, which improved upon Green's semi-empirical expression [13], as in ours being completely analytical. The derived model used solar cell parameters that can be extracted from $I - V$ characteristics as inputs. We therefore suggested the possibility of implementing our model in sun simulator softwares to allow for accurate determination of the temperature sensitivity of the maximum power point. The model was tested against experimental data obtained from 18 multi-crystalline silicon cells, with different architectures and from different ingot positions. We discussed the limitations of making use of a single-valued TC to describe the temperature sensitivity of solar cells by showing that not all solar cell parameters can vary linearly with the temperature. In contrast, our model did not make any assumptions regarding the temperature dependence of any of the solar cell parameters. We showed that the derived model predicted the temperature sensitivity of all investigated parameters with low discrepancy.

As for the recombination parameter γ, assuming that all non-radiative recombination

occurs in the neutral zone of the solar cell allowed for analytical expressions that relate γ to the carriers mobilities and lifetimes. In our attempt to further explore the utility of γ for impurity identification in semiconductor crystals, we found various problems regarding the definition of γ and its dependency with the open-circuit voltage. We suggested possible solutions to amend these problems. From these solutions, it is worth mentioning the expressions for γ derived assuming a thick cell in low-injection level regime. From numerical experiments, we concluded that γ by itself may not be enough for defect identification but may be useful in conjunction with other characterization techniques.

Finally, regarding the effect of series resistance, we made use of Banwell's closed-form expression for the current as a starting point to derive a set of analytical expressions for the maximum power point. The transcendental equations became analytically solvable by realizing that for most solar cells and typical values of the series resistance, Lambert's W function can effectively be linearized. We compared the new expressions to a numerical single-diode model and obtained discrepancies below 0.1% for typical values of the series resistance. The next step consisted in testing the experimental applicability of the model and compare it to the already existing derived by Singal in Ref. [12]. For this, we made use of 18 multi-crystalline silicon cells, from which we extracted $I-V$ characteristics at multiple temperature. We showed that our model had the same level of accuracy as Singal's, predicting experimental values of V_{mpp} and P_{mpp} with discrepancies up to 0.7% and 0.2%, respectively. Our model then improves upon Singal's as in it is much simpler and easy to use.

5.1 Outlook

The work presented in this thesis has resulted in analytical models that describe fundamental energy losses, the temperature sensitivity of the maximum power point and the effect of series resistance in single-junction solar cells.

The natural next step to our research is attempting to combine some of these results. One possibility could be to make use of the expressions that we derived to describe the effect of the series resistance on the maximum power point in **paper D** as a starting point to derive expressions for the temperature coefficients that include the series resistance and its temperature sensitivity.

Still within the block of temperature sensitivity, although we restricted the work on γ in **paper F** to just theory, experimental γ maps for wafers and cells have been investigated in the scientific literature [66, 67, 68]. The results presented in **paper F** may, e.g., help to extract more information from these maps. Further theoretical and experimental work should be performed to asses the capabilities of γ for defect characterization.

Deriving analytical expressions for the maximum power point that account for shunt

resistance effects may also be of interest. Although shunt resistance is often not relevant in laboratory cells, it may be nevertheless interesting to obtain such analytical models for outdoor characterization. These new expressions could also be used as a starting point to obtain analytical expressions for the corresponding temperature coefficients. Based on Ref. [64], it is quite likely that Lambert's W function will play a role in these new models.

The applications of Lambert's W in the field photovoltaics should be further explored. Lambert's W function has already been proven useful in describing the maximum power point, with and without series resistance, and its temperature sensitivity. We strongly believe that this function will play an important role in the derivation of future analytical models not only in single-junction but also third generation solar cells [69].

As a final note, generalizing the models that we have derived during this PhD to third generation photovoltaics may also be an interesting direction for research. Example of this could be, e.g., exploring the temperature sensitivity of multi-junction or intermediate band solar cells. For the multi-junction cells, Lambert's W function was employed in a recent work to analytically determine the maximum power point of various multi-junction solar cell configurations [69]. This sets the possibility to make use of an analogue approach as the one we used in **paper D** to obtain analytical expressions for the TCs.

Bibliography

[1] Intergovernmental Panel on Climate Change (IPCC). *An IPCC Special Report on the Impacts of Global Warming of 1.5° C above Pre-Industrial Levels and Related Global Greenhouse Gas Emission Pathways*. 2019.

[2] U.S. Energy Information Administration. "EIA projects nearly 50% increase in world energy use by 2050, led by growth in renewables". In: (2021). URL: https://www.eia.gov/todayinenergy/detail.php?id=42342.

[3] International Renewable Energy Agency (IRENA). *Renewable Power Generation Costs in 2020*. 2020. URL: https://www.irena.org/publications/2021/Jun/Renewable-Power-Costs-in-2020.

[4] REN21. *Global Status Report*. 2021. URL: https://www.ren21.net/reports/global-status-report/.

[5] M. A. Green et al. "Third generation photovoltaics". In: (2006).

[6] M. Green et al. "Solar cell efficiency tables (version 57)". In: *Progress in photovoltaics: research and applications* 29.1 (2021), pp. 3–15.

[7] L. C. Andreani et al. "Silicon solar cells: toward the efficiency limits". In: *Advances in Physics: X* 4.1 (2019), p. 1548305.

[8] A. Khanna et al. "A fill factor loss analysis method for silicon wafer solar cells". In: *IEEE Journal of Photovoltaics* 3.4 (2013), pp. 1170–1177.

[9] L. C. Hirst and N. J. Ekins-Daukes. "Fundamental losses in solar cells". In: *Progress in Photovoltaics: Research and Applications* 19.3 (2011), pp. 286–293.

[10] M. A. Green. "Solar cells: operating principles, technology, and system applications". In: *Englewood Cliffs, NJ, Prentice-Hall, Inc., 1982. 288 p.* (1982).

[11] O. Dupré, R. Vaillon, and M. A. Green. "Physics of the temperature coefficients of solar cells". In: *Solar Energy Materials and Solar Cells* 140 (2015), pp. 92–100.

[12] C. M. Singal. "Analytical expression for the series-resistance-dependent maximum power point and curve factor for solar cells". In: *Solar Cells* 3.2 (1981), pp. 163–177.

[13] M. A. Green, K. Emery, and A. W. Blakers. "Silicon solar cells with reduced temperature sensitivity". In: *Electronics Letters* 18.2 (1982), pp. 97–98.

[14] T. C. Banwell and A. Jayakumar. “Exact analytical solution for current flow through diode with series resistance”. In: *Electronics letters* 36.4 (2000), pp. 291–292.

[15] T. Markvart. *Solar electricity*. Vol. 6. John Wiley & Sons, 2000.

[16] A. E. Becquerel. “Recherches sur les effets de la radiation chimique de la lumiere solaire au moyen des courants electriques”. In: *CR Acad. Sci* 9.145 (1839), p. 1.

[17] P. Wurfel. “The chemical potential of radiation”. In: *Journal of Physics C: Solid State Physics* 15.18 (1982), p. 3967.

[18] M. Planck. “The theory of heat radiation”. In: *Entropie* 144.190 (1900), p. 164.

[19] J. Stefan. “Uber die beziehung zwischen der warmestrahlung und der temperatur, sitzungsberichte der mathematisch-naturwissenschaftlichen classe der kaiserlichen”. In: *Akademie der Wissenschaften* 79 (1879), S–391.

[20] Photovoltaic devices Part. “Part 1–10”. In: *IEC-60904* (2009).

[21] W. T. Welford and R. Winston. “Optics of nonimaging concentrators. Light and solar energy”. In: (1978).

[22] E. Fermi. “Sulla quantizzazione del gas perfetto monoatomico”. In: *Rendiconti Lincei* 145 (1926).

[23] P. A. M. Dirac. “On the theory of quantum mechanics”. In: *Proceedings of the Royal Society of London. Series A, Containing Papers of a Mathematical and Physical Character* 112.762 (1926), pp. 661–677.

[24] W. Shockley and W. T. J. Read. “Statistics of the recombinations of holes and electrons”. In: *Physical Review* 87.5 (1952), p. 835.

[25] R. N. Hall. “Electron-hole recombination in germanium”. In: *Physical review* 87.2 (1952), p. 387.

[26] R. F. Pierret and G. W. Neudeck. *Advanced semiconductor fundamentals*. Vol. 6. Addison-Wesley Reading, MA, 1987.

[27] S. M. Sze and J. C. Irvin. “Resistivity, mobility and impurity levels in GaAs, Ge, and Si at 300 K”. In: *Solid-State Electronics* 11.6 (1968), pp. 599–602.

[28] P. Auger. “Sur les rayons β secondaires produits dans un gaz par des rayons X.” In: *CR Acad. Sci.(F)* 177 (1923), p. 169.

[29] J. Nelson. *The Physics of Solar Cells*. World Scientific Publishing Company, 2003.

[30] W. Shockley and H. J. Queisser. “Detailed balance limit of efficiency of p-n junction solar cells”. In: *Journal of Applied Physics* 32.3 (1961), pp. 510–519.

[31] L. Boltzmann. “Studien uber das Gleichgewicht der lebenden Kraft”. In: *Wissenschafiliche Abhandlungen* 1 (1868), pp. 49–96.

[32] A. Cuevas. “The recombination parameter J0”. In: *Energy Procedia* 55 (2014), pp. 53–62.

[33] W. Shockley. “The Theory of p-n Junctions in Semiconductors and p-n Junction Transistors”. In: *Bell System Technical Journal* 28.3 (1949), pp. 435–489.

[34] C.-T. Sah, R. N. Noyce, and W. Shockley. “Carrier generation and recombination in pn junctions and pn junction characteristics”. In: *Proceedings of the IRE* 45.9 (1957), pp. 1228–1243.

[35] R. M. Corless et al. “On the Lambert W function”. In: *Advances in Computational Mathematics* 5.1 (1996), pp. 329–359.

[36] A. Sergeev and K. Sablon. “Exact solution, endoreversible thermodynamics, and kinetics of the generalized Shockley-Queisser model”. In: *Physical Review Applied* 10.6 (2018), p. 064001.

[37] S. Carnot. “Réflexions sur la puissance motrice du feu et sur les machines propres à développer cette puissance”. In: *Annales scientifiques de l’École Normale Supérieure*. Vol. 1. 1872, pp. 393–457.

[38] P. T. Landsberg and G. Tonge. “Thermodynamic energy conversion efficiencies”. In: *Journal of Applied Physics* 51.7 (1980), R1–R20.

[39] A. De Vos. “Thermodynamics of photochemical solar energy conversion”. In: *Solar energy materials and solar cells* 38.1-4 (1995), pp. 11–22.

[40] R. T. Ross and A. J. Nozik. “Efficiency of hot-carrier solar energy converters”. In: *Journal of Applied Physics* 53.5 (1982), pp. 3813–3818.

[41] G. Conibeer et al. “Progress on hot carrier cells”. In: *Solar Energy Materials and Solar Cells* 93.6-7 (2009), pp. 713–719.

[42] G. Kirchhoff. “Über das Verhältnis zwischen dem Emissionsvermögen und dem Absorptionsvermögen der Körper für Wärme und Licht”. In: *Von Kirchhoff bis Planck*. Springer, 1978, pp. 131–151.

[43] G. L. Araújo and A. Martıé. “Absolute limiting efficiencies for photovoltaic energy conversion”. In: *Solar Energy Materials and Solar Cells* 33.2 (1994), pp. 213–240.

[44] T. Markvart. “The thermodynamics of optical étendue”. In: *Journal of Optics A: pure and applied optics* 10.1 (2007), p. 015008.

[45] T. Markvart. “Thermodynamics of losses in photovoltaic conversion”. In: *Applied Physics Letters* 91.6 (2007), p. 064102.

[46] T. Markvart. “Solar cell as a heat engine: energy–entropy analysis of photovoltaic conversion”. In: *physica status solidi (a)* 205.12 (2008), pp. 2752–2756.

[47] R. Munroe. *What If?: Serious Scientific Answers to Absurd Hypothetical Questions*. Houghton Mifflin Harcourt, 2014. URL: https://what-if.xkcd.com/145/.

[48] R. Winston, L. Jiang, and M. Ricketts. "Nonimaging optics: a tutorial". In: *Advances in Optics and Photonics* 10.2 (2018), pp. 484–511.

[49] J. Chaves. *Introduction to nonimaging optics*. CRC press, 2008.

[50] M. A. Green. "Intrinsic concentration, effective densities of states, and effective mass in silicon". In: *Journal of Applied Physics* 67.6 (1990), pp. 2944–2954.

[51] M. A. Green. "General temperature dependence of solar cell performance and implications for device modeling". In: *Progress in Photovoltaics: Research and Applications* 11.5 (2003), pp. 333–340.

[52] J. C. C. Fan. "Theoretical temperature dependence of solar cell parameters". In: *Solar cells* 17.2-3 (1986), pp. 309–315.

[53] D. Moser, M. Pichler, and M. Nikolaeva-Dimitrova. "Filtering procedures for reliable outdoor temperature coefficients in different photovoltaic technologies". In: *Journal of solar energy engineering* 136.2 (2014).

[54] S. Kurtz et al. "Evaluation of high-temperature exposure of photovoltaic modules". In: *Progress in photovoltaics: Research and applications* 19.8 (2011), pp. 954–965.

[55] O. Dupré, R. Vaillon, and M. A. Green. *Thermal Behavior of Photovoltaic Devices: Physics and Engineering*. Springer, 2016.

[56] K. Emery et al. "Temperature dependence of photovoltaic cells, modules and systems". In: *Conference Record of the Twenty Fifth IEEE Photovoltaic Specialists Conference-1996*. IEEE. 1996, pp. 1275–1278.

[57] G. A. Landis. "Review of solar cell temperature coefficients for space". In: *XIII Space Photovoltaic Research and Technology Conference (SPRAT XIII)*. Vol. 3278. 1994, p. 385.

[58] M. A. Green. "Radiative efficiency of state-of-the-art photovoltaic cells". In: *Progress in Photovoltaics: Research and Applications* 20.4 (2012), pp. 472–476.

[59] P. Dey et al. "Origin of the temperature dependence of the band gap of PbS and PbSe quantum dots". In: *Solid state communications* 165 (2013), pp. 49–54.

[60] S. M. Sze. "Physics of Semiconductor Devices 2nd edition Awiley Inter-science John wiley and Sons". In: *New York* (1981).

[61] M. A. Green, A. W. Blakers, and C. R. Osterwald. "Characterization of high-efficiency silicon solar cells". In: *Journal of applied physics* 58.11 (1985), pp. 4402–4408.

[62] M. Wolf and H. Rauschenbach. “Series resistance effects on solar cell measurements”. In: *Advanced energy conversion* 3.2 (1963), pp. 455–479.

[63] C. B. Honsberg and S. G. Bowden. *Series Resistance*. Photovoltaics Education Website, www.pveducation.org. 2019.

[64] A. Jain and A. Kapoor. “Exact analytical solutions of the parameters of real solar cells using Lambert W-function”. In: *Solar Energy Materials and Solar Cells* 81.2 (2004), pp. 269–277.

[65] M. A. Green. “Accurate expressions for solar cell fill factors including series and shunt resistances”. In: *Applied physics letters* 108.8 (2016), p. 081111.

[66] S. T. Kristensen et al. “Temperature Coefficients of Crystal Defects in Multicrystalline Silicon Wafers”. In: *IEEE Journal of Photovoltaics* 10.2 (2020), pp. 449–457.

[67] S. Nie et al. “Photoluminescence-based spatially resolved temperature coefficient maps of silicon wafers and solar cells”. In: *IEEE Journal of Photovoltaics* 10.2 (2019), pp. 585–594.

[68] R. Eberle et al. “Temperature coefficient imaging for silicon solar cells”. In: *IEEE Journal of Photovoltaics* 8.4 (2018), pp. 930–936.

[69] R. Strandberg. “An Analytic Approach to the Modeling of Multijunction Solar Cells”. In: *IEEE Journal of Photovoltaics* 10.6 (2020), pp. 1701–1711.

Appendix A

Analytical Expressions for Radiative Losses in Solar Cells

Analytical Expressions for Radiative Losses in Solar Cells

Alfredo Sanchez Garcia and Rune Strandberg
Department of Engineering Sciences, University of Agder,
Grimstad, 4879, Norway

November 1, 2021

Abstract

Analytical expressions for the fundamental losses in single junction solar cells are revised and improved. The losses are, as far as possible, described using parameters with clear physical interpretations. One important improvement compared to earlier work is the use of Lambert's W function, which allows for analytical expressions for the voltage and current at the maximum power point. Other improvements include the use of Stefan Boltzmann's law to describe the incoming energy flux as well as taking into account the fermionic nature of the electrons when calculating the thermalization loss. A new expression, which combines emission, Boltzmann and Carnot losses, is presented. Finally, an expression which combines all energy losses derived in this work is presented.

1 Introduction

In 1961, *Shockley* and *Queisser* published an article where the theoretical efficiency limits of single-junction solar cells (SC) were studied. They presented a model based on a detailed particle balance and found a theoretical upper limit of 40.8% [1]. This *Shockley-Queisser* (SQ) limit shows that a single-junction solar cell is unable to convert almost 60% of the incoming solar radiation into useful energy. In order to understand what happens to this 60% of the total incoming radiation, five different mechanisms of energy loss were identified and studied in Ref. [2]. There, the authors mathematically modeled the energy losses that are theoretically unavoidable. These fundamental energy losses are due to: (i) unabsorbed photons, (ii) carriers

thermalizing to the bandgap, (iii) radiative emission from the cell and, voltage losses caused by (iv) the cell having a temperature higher than 0 K and, (v) a mismatch of the solid angles of absorption and emission of radiation. These five mechanisms of energy loss are further studied and discussed in section 4.

The expressions derived in Ref. [2] are based on approximations which may lead to some inaccuracies. In this work, we intend to improve those expressions.

In Ref. [3], exact expressions for both the optimal voltage and current, and consequently the efficiency, were derived by making use of *Lambert's W function*. We will follow this approach and combine it with Refs. [1] and [2] to find compact expressions for the fundamental losses in solar cells.

Before starting our discussion, let us summarize our strategies to improve the model presented in Ref. [2]. These will later on be explained in detail:

- Stefan Boltzmann's law is used to describe the incoming solar radiation.
- Lambert's W function is used to obtain exact expressions for the maximum power point voltage and current. Consequently, some of the fundamental losses are expressed in terms of Lambert's W function.
- The fermionic nature of electrons and holes is considered in the expression for the thermalization loss.
- A new expression that combines Carnot, Boltzmann and emission losses is derived. The derivation consists in computing the difference in output power when the cell is at 0 K and at a nonzero temperature T_c.
- The new expressions together with the output power account for 100% of the total incident solar radiation.

2 Conventions and notation

We will follow *Shockley* and *Queisser*'s detailed balance approach [1] and study a single junction solar cell operating at temperature $T_c = 300K$. The Sun is assumed to be a blackbody radiating at temperature $T_s = 6000K$. The flux of photons with energy in the interval $[E, E + dE]$ is given by Planck's law

$$n(E, T, \mu) = \frac{2F_s}{c^2h^3} \frac{E^2\ dE}{\exp\left(\frac{E-\mu}{kT}\right) - 1}, \tag{1}$$

where μ is the chemical potential, or the splitting of *quasi-Fermi levels*, of the material and F_s is a geometrical factor associated with the solid angle in which the cell absorbs

or emits radiation. Thermal energy emission, such as solar radiation, has a 0 chemical potential, while in the case of luminescent emission from a solar cell, the chemical potential is $\mu = qV$, where q is the electron charge and V is the voltage across the device.

The total electrical current produced by the cell is calculated as the difference between the absorbed and emitted photons times the electric charge

$$J = q \int_{E_g}^{\infty} [n(E, T_s, 0, F_{abs}) - n(E, T_c, qV, F_{emi})] \, dE, \tag{2}$$

where F_{abs} and F_{emi} are the geometrical factors associated with absorption and emission of radiation, respectively. The first term on the right hand-side of Eq. (2) is known as *generation current*, J_G, while the second is known as *recombination current*, J_R.

Let us now compute the geometrical factors. Although this is found in textbooks, we include their derivation here since they are important for the Boltzmann loss. The geometrical factors arise from integrating over the solid angles of emission, Ω_{emi}, and absorption, Ω_{abs} with respect to the normal of the cell. We will assume that the cell emits through and angle θ_{emi} and absorbs energy through an angle θ_X. Defining θ' as the polar angle with respect to the surface normal, we have

$$F_{emi} = \int_{\Omega_{emi}} \cos\theta' d\Omega = \int_0^{2\pi} \int_0^{\frac{\pi}{2}} \cos\theta' \sin\theta' d\theta' d\phi = \pi \sin^2 \theta_{emi}, \tag{3}$$

$$F_{abs} = \int_{\Omega_{abs}} \cos\theta' d\Omega = \int_0^{2\pi} \int_0^{\theta_X} \cos\theta' \sin\theta' d\theta' d\phi = \pi \sin^2 \theta_X. \tag{4}$$

θ_X can be expressed in terms of the Sun concentration factor, X, by making use of the $\sin\theta_X = \sqrt{X} \sin\theta_{sun}$, with $\theta_{sun} = 0.267°$ being the angle which the Sun subtends without any concentrators. Defining $X_{max} = 1/\sin^2\theta_{sun}$, as the maximum concentration factor, we can express F_{abs} as $F_{abs} = \pi(X/X_{max})$. With this in mind, J_G can be expressed as

$$J_G(E_g) = \frac{2\pi q}{c^2 h^3} \frac{X}{X_{max}} \int_{E_g}^{\infty} \frac{E^2}{\exp\left(\frac{E}{kT_s}\right) - 1} \, dE. \tag{5}$$

It is possible to simplify Eq. (1). When $E - \mu >> kT$, the exponential term in the denominator becomes dominant. Hence, we can neglect the -1. This is called *Boltzmann's approximation* and is valid in the regime of useful bandgaps ($E_g \geq 0.5 \, eV$ for

the normal conditions experienced by solar cells). We will use this approximation to express J_R as

$$J_R(E_g) \approx \frac{2q}{c^2h^3} F_{emi} \int_{E_g}^{\infty} E^2 \exp\left(-\frac{E}{kT_c}\right) \exp\left(\frac{\mu}{kT_c}\right) \mathrm{d}E = J_0(E_g) \exp\left(\frac{qV}{kT_c}\right), \quad (6)$$

where J_0 is known as the *dark saturation current*. Unless otherwise stated, we will assume in the following that the cell emits radiation in a hemisphere, i.e., $F_{emi} = \pi$. Finally in this section, we want to point out that Boltzmann's approximation should not be used when calculating J_G since kT_s is large compared to the photon energies in question.

3 Optimal power out efficiency

The efficiency of the solar cell is given by:

$$\eta = \frac{VJ}{P_{\text{in}}}, \quad (7)$$

where $P_{\text{in}} = \sigma T_S^4$, with σ being the Stefan-Boltzmann constant. The optimal efficiency is found by differentiating $\eta(V)$ with respect to the voltage, equating to zero and solving for V. The achieved limiting efficiency receives the name of Shockley-Queisser (SQ) limit and is 40.8%. In Fig. 1, the optimal efficiency as a function of the bandgap, E_g, is presented for Sun concentration factors, $X = X_{max}$ and $X = 1$. The limiting efficiencies are 40.8% and 30.9%, respectively.

In Ref. [3], it was shown that an analytical expression for the optimal voltage, V_{opt}, can be obtained by making use of Lambert's W function, defined as $z = \mathrm{W}(ze^z)$, to solve $\frac{\partial(JV)}{\partial V} = 0$. The obtained optimal voltage then is

$$V_{opt} = \frac{kT_c}{q} \left(\mathrm{W}\left(e\frac{J_G}{J_0}\right) - 1 \right). \quad (8)$$

An expression for the optimal current, J_{opt}, was found by plugging Eq. (8) into Eq. (2). The obtained expression is

$$J_{opt} = J_G(E_g) \left(1 - \frac{1}{\mathrm{W}\left(e\frac{J_G}{J_0}\right)} \right), \quad (9)$$

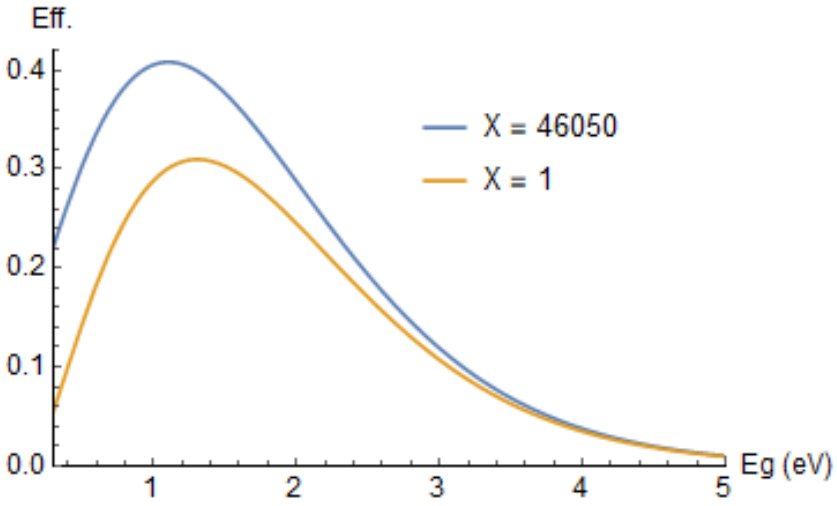

Figure 1: Power out efficiency as a function of the bandgap for different Sun concentration factors.

where they made use of $\mathrm{W}(z)\exp[\mathrm{W}(z)] = z$ to simplify the expression. The optimal power out efficiency then is found by plugging Eqs. (8) and (9) into Eq. (7). We then have

$$\eta(E_g) = \frac{kT_c}{q}\left(\mathrm{W}\left(e\frac{J_G}{J_0}\right) - 2 + \frac{1}{\mathrm{W}\left(e\frac{J_G}{J_0}\right)}\right) J_G. \tag{10}$$

A comparison between the efficiencies obtained in Ref. [3] and in Ref. [2] is presented in Fig 2. We notice a difference between the maxima of both efficiencies. The efficiency calculated with the approximations used in Ref. [2] has its maximum at 39.2%, while Ref. [3] yields a maximum of 40.8%, as expected from the *Shockley-Queisser limit* [1]. As we mentioned in section 2, Boltzmann approximation should not be used to calculate J_G. In Ref. [2], it was done in order to find a compact expression for the optimal voltage. A large drawback of using Boltzmann's approximation to calculate J_G was that the achieved power out efficiency and, later on, the intrinsic losses were slightly lower than they should be.

4 Intrinsic losses

From Fig 2, we clearly see that more than half of the incoming solar radiation is not converted into useful energy for the cell. Intrinsic losses for idealized single junction

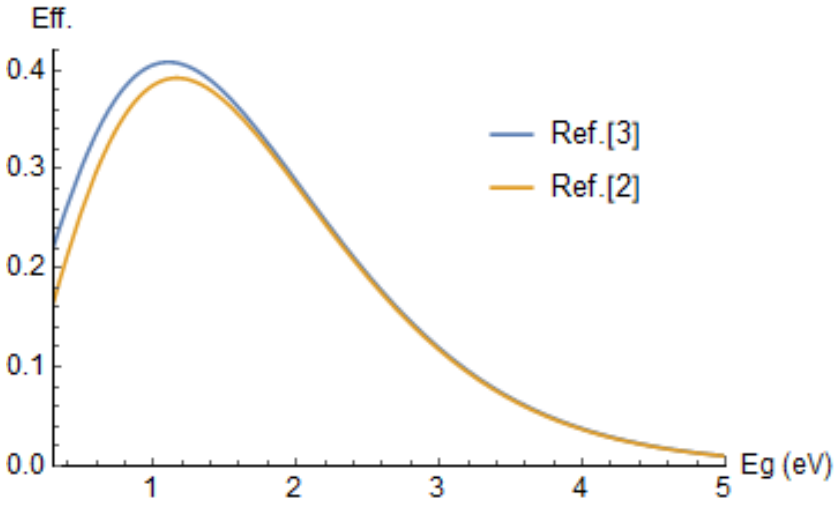

Figure 2: Power out efficiency as a function of the energy gap at maximum Sun concentration factor. Ref. [3] makes use of an expression for the efficiency that relies in fewer approximations than the one derived in Ref. [2]. This results into a higher efficiency.

solar cells are unavoidable and presented in this section. Five mechanisms of energy loss have previously been discussed in Ref. [2]. In this section, we will revise them and propose new analytical expressions with the purpose of describing them more accurately.

4.1 Thermalization

Let us start by considering the energy loss due to thermalization. If an electron absorbs a high-energetic photon, it will acquire an energy way higher than the bandgap. Through strong interactions with lattice phonons, the overexcited electrons will thermalize to the edge of the conduction band, i.e., they will emit their energy excess as heat and relax to an energy of $E = E_g$. This process of energy loss is described in Ref. [2] by

$$L_{Therm} = \int_{E_g}^{\infty} (E - E_g) \cdot n(E, T_s, 0, F_{abs})\ dE. \tag{11}$$

After relaxing to the bandgap, electrons should distribute according to Fermi-Dirac statistics, which means that their mean energy will be a little above E_g. According to the literature (e.g. in Ref. [4]), the internal energy of the electrons is given

by

$$\frac{\int_0^\infty EF(E)D(E)\ dE}{\int_0^\infty F(E)D(E)\ dE} = \frac{3}{2}kT_c, \tag{12}$$

where $F(E)$ is the Fermi-Dirac distribution and $D(E)$ is the density of states for the electrons. It should be noted that the internal energy of the electrons is equal to $\frac{3}{2}kT_c$ only when their dispersion relation is parabolic [4]. The same argument should apply to holes in the VB and, therefore, the mean energy of an electron-hole pair is $E_g + 3kT_c$.

The average energy of the exciting photons is given by

$$\overline{E}_G = \frac{q}{J_G}\int_{E_g}^\infty E \cdot n(E, T_s, 0, F_{abs})\ dE, \tag{13}$$

This quantity can be introduced together with the extra $3kT_c$ into Eq. (11) to obtained a more accurate expression for the energy loss due to thermalization of carriers. We finally have

$$L_{therm} = \frac{1}{q}(\overline{E}_G - E_g - 3kT_c)J_G. \tag{14}$$

4.2 Further Thermalization

We saw in the previous section that after thermalizing to the bandgap, carriers will carry extra energy due to their fermionic nature. As a consequence, an extra thermalization must occur in the extraction of carriers to the metal contact. This second thermalization has to be equal to the internal energy of the carriers, that is, $3kT_cJ_G$. Therefore, this second thermalization will cancel the energy gain that we discussed in section 4.1.

4.3 Emission and Voltage Losses

In this section, we will consider three mechanisms of energy loss that constitute a smaller fraction of the lost solar radiation in comparison to the loss due to thermalization (around 7%). We will first introduce each mechanism as well as the expressions used in Ref. [2] to describe them and, after that, we will present an approach to obtain an expression which will combine all three losses.

Let us first consider the energy loss due to emitted photons. According to Kirchoff's law, since the cell absorbs radiation, it should also emit. The energy loss associated with the emission of photons produced by the cell is given in Ref. [2] by

$$L_{Em} = E_g\int_{E_g}^\infty n(E, T_c, qV, F_{emi})\ dE. \tag{15}$$

Second, we have two fundamental mechanisms of energy loss that directly affect the maximum achievable voltage. This is easily seen in Ref [2], where the optimal voltage is given by

$$qV_{opt} = E_g \left(1 - \frac{T_c}{T_s}\right) - kT_c \ln\left(\frac{\Omega_{emi}}{\Omega_{abs}}\right). \tag{16}$$

The first term multiplying the energy gap on the right-hand side of Eq. (16) is called *Carnot Factor* because its mathematical form resembles of the expression for Carnot's efficiency [2, 5]. Since a solar cell may be considered a heat engine, the maximum achievable efficiency needs to be limited by Carnot's efficiency, which manifests as a voltage drop.

The second term affecting the voltage appears due to the possible mismatch between the solid angles of emission and absorption of radiation. As we saw in section 2, while we assume that the cell emits in a hemisphere, it typically absorbs solar radiation through a smaller solid angle. The mismatch between the solid angles of absorption and emission results in part of the incoming energy being lost in entropy generation [6]. As for the Carnot loss, because its mathematical expression resembles *Boltzmann's entropy equation*, it is referred to in Ref. [2] as the *Boltzmann factor*. The corresponding losses are calculated in Ref. [2] by multiplying each factor by the optimal current J_{opt}.

In the following section, we will present an expression that combines the three losses that have been explained in this section.

4.4 The CBE Loss. Derivation

From Eqs. (15) and (16), we notice that both Carnot and Boltzmann factors as well as the emission loss cancel when the temperature of the cell is 0 K. We hence should be able to find an expression that combines all three losses by calculating the difference in output power at $T_c = 0$ K and at a non-zero cell temperature, T_c. We can then define the combined loss, L_{CBE}, (Carnot, Boltzmann and Emission) as

$$L_{CBE} = V_{opt}(0)J_{opt}(0) - V_{opt}(T_c)J_{opt}(T_c). \tag{17}$$

Starting with the voltage, we first take the limit $T_c \to 0$ in Eq. (8). By doing it so, we obtain an undefined result since $\mathrm{W}(T_c^{-1} \to 0) = \mathrm{W}(\infty) \to \infty$. In order to walk this problem around, we make use of the asymptotic expansion of Lambert's W function [7], given by

$$\mathrm{W}(x) \approx \ln x - \ln\ln x + \frac{\ln\ln x}{\ln x}. \tag{18}$$

In Eq. (8), all the terms in this expansion are multiplied by the temperature of the cell, T_c. Since $T_c \to 0$ and the last two terms in the expansion grow very slowly in comparison, it is reasonable to cancel them out. This leads to

$$\begin{aligned} V_{opt}(T_c \to 0) &= \lim_{T_c \to 0} \frac{kT_c}{q} \left[\ln \left(e \frac{J_g}{J_0(T_c)} \right) - 1 \right] \\ &= \lim_{T_c \to 0} \frac{kT_c}{q} \ln \left(\frac{J_g}{J_0(T_c)} \right) \\ &= \lim_{T_c \to 0} -\frac{kT_c}{q} \ln J_0(T_c). \end{aligned} \tag{19}$$

In order to proceed now, we need to compute the integral for J_0 in Eq. (6). This is easily doable thanks to having taken Boltzmann's approximation. The integral gives

$$J_0(E_g) = \exp\left(-\frac{E_g}{kT_c} \right) kT_c \left(E_g^2 + 2E_g kT_c + 2k^2 T_c^2 \right). \tag{20}$$

Now, besides the exponential term, we have terms like $T_c \ln T_c$, $T_c \ln T_c^2$ and $T_c \ln T_c^3$, which will cancel in the limit $T_c \to 0$. We finally have

$$V_{opt}(T_c \to 0) = -\frac{kT_c}{q} \ln \left[\exp\left(-\frac{E_g}{kT_c} \right) \right] = \frac{E_g}{q}. \tag{21}$$

We now continue with the current and take the limit $T_c \to 0$ in Eq. (9). Again, we have a divergent $\mathrm{W}(T_c^{-1})$ but this time, in a denominator. This implies that the last term in Eq. (9) will cancel and, in the limit of 0 K temperature, the maximum power point current is just $J_G(E_g)$. Putting all together, we find L_{CBE} to be

$$L_{CBE} = \left(\frac{E_g}{q} - V_{opt}(T_c) \left[1 - \frac{1}{\mathrm{W}\left(e \frac{J_G}{J_0} \right)} \right] \right) J_G. \tag{22}$$

It should be noted that the asymptotic expansion for Lambert's W in Eq. (18) only holds for $x > e$. In our case, this implies that Eq. (22) only is true for $J_G > J_0$, but this is true in all interesting cases where Boltzmann's approximation can be used.

4.5 The CBE Loss. Separation

Eq. (22) has the advantage with respect to Ref. [2] that the model now is more compact, reducing the amount of equations from five to three. A disadvantage to point out is that it now becomes a bit problematic to see each contribution (emission, Carnot and Boltzmann) individually.

In the following, we show alternative ways to find each contribution separately.

Emission loss Eq. (15) assumes that the emitted photons have an average energy of E_g. Let us instead compute the total energy flux $\int E \cdot n(E, T_c, qV, F_{emi})\ dE$ as

$$\begin{aligned} L_{Em} &= \int_{E_g}^{\infty} E \cdot n(E, T_c, qV, F_{emi})\ dE \\ &= \exp\left(\frac{qV}{kT_c}\right) \int_{E_g}^{\infty} E \cdot n(E, T_c, 0, F_{emi})\ dE. \end{aligned} \tag{23}$$

The last integral in Eq. (23) equals the energy flux emitted by the cell in thermal equilibrium. We denote it E_0 and use the expression for V_{opt} in Eq. (8) to get

$$L_{Em} = \frac{E_0}{\mathrm{W}\left(e^{\frac{J_G}{J_0}}\right)} \frac{J_G}{J_0}. \tag{24}$$

Voltage Losses Both Carnot and Boltzmann losses reduce the maximum achievable voltage of a solar cell. Since this is the case, an alternative way of computing these losses may be the product of the correspondent voltage drop times the optimal current, J_{opt}, given in Eq. (9). This approach was already introduced in Ref. [2].

In the context of voltage losses, it is useful to define the ratio between the geometrical factors of emission and absorption. Let $\gamma = F_{abs}/F_{emi}$. The advantage of using γ with respect to X/X_{max} is that now, we can increase the efficiency by restricting the emission angle instead of having a high number of Suns. In terms of efficiency, it is equivalent to have a maximum Sun concentration factor and restricting the cell to emit in the same angle as it absorbs [6].

In order to incorporate γ to the notation presented in section 2, we need to make use of the general form of F_{emi} in Eq.(3). By doing this, γ appears in all the expressions where Lambert's W is involved. We have

$$\mathrm{W}\left(e\frac{J_G}{J_0}\right) = \mathrm{W}\left(\frac{\sin^2\theta_X}{\sin^2\theta_{emi}} \frac{eJ_{G,max}}{J_{0,max}}\right) = \mathrm{W}\left(\gamma \frac{eJ_{G,max}}{J_{0,max}}\right), \tag{25}$$

where $J_{G,max}$ and $J_{0,max}$ are given by Eqs. (5) and (6) evaluated at $F_{abs} = F_{emi} = \pi$. The dependence with the absorption and emission angles is now incorporated in γ. When $\gamma = 1$, the emission and the absorption angle are equal and therefore we will have maximum efficiency without having maximum Sun concentration.

In order to have a compact notation, let us introduce γ as an index in the expressions for the optimal voltage and current, defined in Eqs. (8) and (9). We make $V_{opt} \to V_{opt}^{\gamma}$ and $J_{opt} \to J_{opt}^{\gamma}$. We can now proceed to calculate the Carnot and Boltzmann losses.

Starting with Boltzmann loss, we have previously discussed that it is consequence of the possible mismatch between solid angles of emission and absorption. In terms of γ, Boltzmann loss will be zero at $\gamma = 1$ and nonzero otherwise. Hence, the Boltzmann energy loss can be computed as the difference in voltage $V_{opt}^{1} - V_{opt}^{\gamma}$ times the optimal current, that is

$$L_B = \frac{kT_c}{q}\left[\mathrm{W}\left(\frac{eJ_{G,max}}{J_{0,max}}\right) - \mathrm{W}\left(\gamma\frac{eJ_{G,max}}{J_{0,max}}\right)\right] J_{opt}^{\gamma}. \tag{26}$$

It should be noted that expanding the W functions to first order, i.e., $\mathrm{W}(x) \approx \ln x$ in Eq. (26) will result in the expression proposed in Ref. [2] for the Boltzmann loss.

Continuing with Carnot loss, the corresponding voltage drop is due to the cell having a nonzero temperature. We can hence calculate this loss as $(V_{opt}^{1}(T_c = 0) - V_{opt}^{1}(T_c))J_{opt}^{\gamma}$, where we have to set $\gamma = 1$ in the voltage drop to ensure that there is no Boltzmann loss. From Eq. (21), we have that $V_{opt}^{1}(T_c = 0) = E_g/q$. Hence, the Carnot energy loss is

$$L_C = \left(\frac{E_g}{q} - V_{opt}^{1}\right) J_{opt}^{\gamma}. \tag{27}$$

We want to point out that by introducing Eqs. (8) and (9) and further expanding the W functions to first order, the proposed expression for the Carnot loss in Ref. [2] is obtained if we also make use of Boltzmann's approximation in calculating J_G.

4.6 Unabsorbed photons

Finally, the last mechanism of energy loss is produced by the photons with energy lower than the bandgap of the material. These photons will not be absorbed. The energy lost due to unabsorbed photons is given by

$$L_{Below} = \int_0^{E_g} E \cdot n(E, T_s, 0, F_{abs})\, dE. \tag{28}$$

As for the optimal efficiency, the expression derived in Ref. [2] makes use of Boltzmann's approximation when calculating J_G. As we discussed in section 2, this approach is inaccurate. Even though the expression may not be as compact as desirable, not making use of Boltzmann's approximation in Eq. (28) gives a more accurate energy loss.

Eq. (28) can be expressed in terms of the incident solar radiation by making use of $\overline{E}_G$. Adding the energy flux of the exciting photons, $\int E \cdot n(E, T_s, 0, F_{abs})$, to

Eq. (28) gives

$$\left(\int_0^{E_g} + \int_{E_g}^{\infty}\right) E \cdot n(E, T_s, 0, F_{abs})\ dE = \int_0^{\infty} E \cdot n(E, T_s, 0, F_{abs})\ dE, \tag{29}$$

which is just $P_{\text{in}} = \sigma T_s^4$. We can hence write the energy loss due to unabsorbed photons as

$$L_{Below} = \left(\frac{\sigma T_s^4}{J_G} - \frac{\overline{E}_G}{q}\right) J_G. \tag{30}$$

4.7 The Total Loss

Finally, Eqs. (14) and (22) together with the second thermalization can be summed into a compact expression which accounts for all mechanisms of energy loss occurring in the cell. We denote it as L_T. The total sum gives

$$L_T = \left(\frac{\overline{E}_G}{q} - V_{opt}(T_c)\left[1 - \frac{1}{\mathrm{W}\left(e\frac{J_G}{J_0}\right)}\right]\right) J_G. \tag{31}$$

Note that by also adding the energy loss due to unabsorbed photons given by Eq. (30), we obtain a very obvious result which reads as: the total energy loss equals the difference between the input and the output power.

5 Numerical Results

The intrinsic losses and power out efficiency, all as a function of the energy gap, are plotted in Fig. 3 for a Sun concentration factor of $X = 1000$. The incident solar radiation is described by Stefan-Boltzmann law. A comparison between the results obtained in this work, (left), and the ones derived in Ref. [2], (right), is shown.

Tab 1 shows a comparison between the fraction of solar energy attributed to the different expressions derived both in this work and in Ref. [2]. All expressions in Tab. 1 are evaluated at the optimal bandgap of $E_g = 1.17\ eV$ for a Sun concentration factor of $X = 1000$. Due to having taken fewer approximations in Eqs. (10) and (30), the energy loss due to unabsorbed photons and the power out efficiency obtained in this work are slightly higher than the ones achieved in Ref. [2]. The sum of the two occurring thermalizations gives a fraction of the incident solar radiation that agrees with the results obtained in Ref. [2]. This is also the case with the new expression

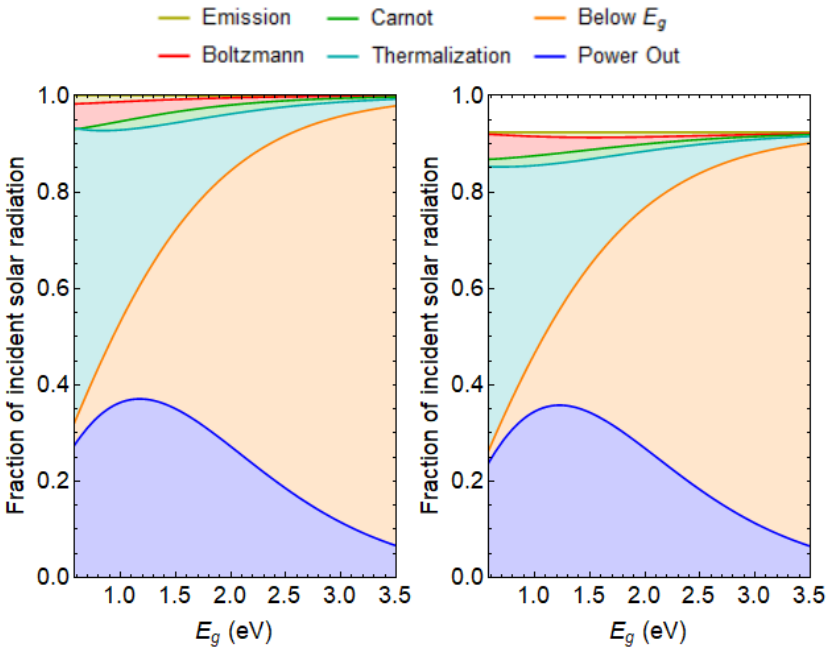

Figure 3: Comparison between this work (left) and Ref. [2] (right) of the intrinsic losses and power out efficiency as a function of E_g at Sun concentration factor of $X = 1000$.

Table 1: Fraction of solar radiation for all losses and power out efficiency at $E_g = 1.17\ eV$ and X = 1000.

X = 1000 Mechanism	Fraction of solar radiation This Work	Fraction of solar radiation Ref. [2]
Power out	0.371	0.357
Below E_g	0.235	0.180
Thermalization	0.327	0.322
Carnot	0.021	0.021
Boltzmann	0.035	0.035
Emission	0.011	0.009
Total	1.000	0.924

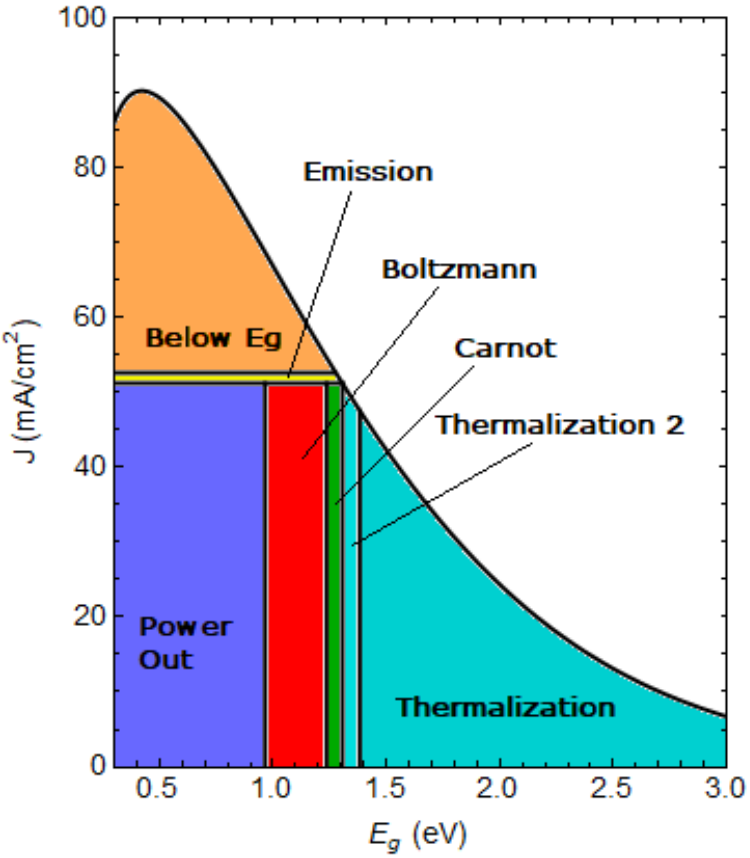

Figure 4: Intrinsic losses for a solar cell with optimal bandgap of $E_g = 1.31\ eV$ and a Sun concentration factor of $X = 1$. This type of plot was inspired by Ref. [2]

that combines emission, Carnot and Boltzmann losses, L_{CBE}. Overall, the sum of the output power and all the losses gives significant improvement with respect to the previous model, adding to 100% of the incident solar radiation.

All the expressions for the intrinsic losses presented in this work as well as the output power are also presented in Fig. 4, where a plot of the optimal current in Eq. (9), J_{opt}, as a function of the bandgap energy is showed. The intrinsic losses and output power are evaluated at a Sun concentration factor of $X = 1$, so that the Boltzmann loss is easier to notice.

6 Conclusions

With the purpose of improving the expressions for the intrinsic losses of single-junction solar cells given in Ref. [2], we have presented new analytical expressions. Our approach has its starting point in Ref. [3] where Lambert's W function was used in order to find analytical expressions for both the optimal voltage and current. We have made use of Lambert's W to find expressions for some of the fundamental energy losses. In the thermalization loss, the fermionic nature of electrons and holes was also accounted. A second thermalization, occurring in the process of carrier extraction, has been discussed. An expression that combines emission, Carnot and Boltzmann losses has been presented. Each contribution to the combined loss has also been identified. As shown in Tab. 1, our results show a significant improvement with respect to the previous model, adding up to 100% of the incident solar radiation.

References

[1] W. Shockley and H. J. Queisser. "Detailed balance limit of efficiency of p-n junction solar cells". In: *Journal of applied physics* 32.3 (1961), pp. 510–519.

[2] L. C. Hirst and N. J. Ekins-Daukes. "Fundamental losses in solar cells". In: *Progress in Photovoltaics: Research and Applications* 19.3 (2011), pp. 286–293.

[3] A. S. and K. Sablon. "Exact Solution, Endoreversible Thermodynamics, and Kinetics of the Generalized Shockley-Queisser Model". In: *Physical Review Applied* 10.6 (2018), p. 064001.

[4] J. Nelson. *The physics of solar cells*. World Scientific Publishing Company, 2003.

[5] P. T. Landsberg and V. Badescu. "Carnot factor in solar cell efficiencies". In: *Journal of Physics D: Applied Physics* 33.22 (2000), p. 3004.

[6] G. L. Araújo and A. Martí. "Absolute limiting efficiencies for photovoltaic energy conversion". In: *Solar Energy Materials and Solar Cells* 33.2 (1994), pp. 213–240.

[7] R. M. Corless et al. "On the LambertW function". In: *Advances in Computational mathematics* 5.1 (1996), pp. 329–359.

Appendix B

Temperature Coefficients of Solar Cell Parameters at Maximum Power Point

Temperature Coefficients of Solar Cell Parameters at Maximum Power Point

Alfredo Sanchez Garcia, Sissel Tind Kristensen,
Sjur Narten Christiansen and Rune Strandberg
University of Agder, Grimstad, 4879, Norway

Abstract

Analytical expressions for the temperature coefficients of the maximum power point voltage and current are presented. The temperature coefficients are calculated assuming the bandgap to be a linear function of the temperature and accounting for energy losses of non-radiative nature. The latter are introduced in the model through the External Radiative Efficiency. The so-called γ parameter, which has been shown to account for the thermal sensitivity of all mechanisms determining the open-circuit voltage, appears to also play a role in the temperature coefficient of the maximum power point voltage and current. Numerical results and a comparison with experimental measurements are also presented.

1 Introduction

Solar cells are generally characterized and optimized under standard test conditions (STC), defined as a global standard solar spectrum AM 1.5G, an irradiance of 1000 W/m^2, and a cell temperature of 298 K [1, 2, 3]. An increase in cell temperature results in a linear decrease in efficiency for most semiconductor materials [1, 4]. In order to optimize solar cells, it is therefore of high relevance to understand and being able to quantify the effect of changes in temperature.

The temperature sensitivity of any solar cell parameter is described by its temperature coefficient (TC) [1]. Some work has been done aiming to explicitly quantify the TCs of the open-circuit voltage, V_{oc}, and the short-circuit current, J_{sc} [2, 3], but, so far, there has not been much focus on the TCs for the maximum power point

voltage, V_{mpp} and current, J_{mpp}. In this work, we aim to find analytical expressions for the TCs of these two quantities.

This work is structured as follows: we make use of the expressions for V_{mpp} and J_{mpp}, previously derived by Sergeev and Sablon in Ref. [5], to derive analytical expressions for the respective TCs. Our approach is inspired by the work of Dupré et al. in Ref. [3] and, therefore, energy losses related to non-radiative recombination are also considered through the *External Radiative Efficiency* (ERE). The derived expressions also account for temperature variations of the bandgap, which we model as a linear function of the temperature. We discuss the limit case where only radiative recombination occurs and where the bandgap is a constant with respect to temperature variations. Additionally, we discuss how a more realistic temperature dependence of the bandgap affects the derived expressions for the TCs. Finally, we present numerical results and compare them with experimental measurements.

2 Theoretical Background

In the radiative limit and assuming non-degenerate conditions, so that we can approximate Fermi-Dirac by Maxwell-Boltzmann distributions, the total current produced by a solar cell is given by Shockley's diode equation [6],

$$J = J_{\mathrm{G}} - J_0 \exp\left(\frac{qV}{kT}\right), \tag{1}$$

where J_{G} is the *generation current* and J_0 is the *dark saturation current*. Assuming the Sun to be a black body radiating at $T_s = 6000$ K, J_{G} is given by

$$J_{\mathrm{G}} = \frac{2\pi q}{c^2 h^3} \frac{X}{X_{max}} \int_{E_g}^{\infty} \frac{E^2}{\exp\left(\frac{E}{kT_s}\right) - 1}\, dE, \tag{2}$$

with h, q, c and X being Planck's constant, the elementary charge, the speed of light and the Sun concentration factor, respectively. In the radiative limit, J_0 is given by [6]

$$J_0 = \frac{2\pi q}{c^2 h^3} \int_{E_g}^{\infty} E^2 \exp\left(-\frac{E}{kT}\right)\, dE. \tag{3}$$

2.1 Maximum Power Point

In Ref. [5], it was shown that an analytical expression for V_{mpp} can be obtained by making use of Lambert's W function, defined by $z = \mathrm{W}(ze^z)$ [7]. Consequently, an

analytical expression for J_{mpp} could be obtained by evaluating Eq. (1) at $V = V_{\mathrm{mpp}}$. The obtained expressions were

$$V_{\mathrm{mpp}} = \frac{kT}{q}\left[\mathrm{W}\left(e\frac{J_{\mathrm{G}}}{J_0}\right) - 1\right], \tag{4}$$

$$J_{\mathrm{mpp}} = J_{\mathrm{G}}\left[1 - \frac{1}{\mathrm{W}\left(e^{\frac{J_{\mathrm{G}}}{J_0}}\right)}\right]. \tag{5}$$

2.2 Temperature Coefficient

The efficiency of a solar cell varies linearly with temperature for the majority of semiconductor materials under normal operating temperatures [1]. This variation may be characterized by making use of the TC. The *relative temperature coefficient* of a photovoltaic cell parameter, X, as a function of the temperature, T, denoted here $\beta_X^r(T)$, is defined as the rate of change of X over the considered temperature range and normalized by X, i.e.,

$$\beta_{\mathrm{X}}^r(T) = \frac{1}{X(T)}\frac{\partial X}{\partial T}. \tag{6}$$

3 The Model

To account for non-radiative recombination, Green introduced the concept of External Radiative Efficiency (ERE) in Ref. [8]. The ERE is defined as *the fraction of the total dark current recombination in the cell that results in radiative emission from the cell* [8]. Admitting that the ERE may depend on the temperature, let us denote ERE $:= \mathcal{E}(T)$. Following Ref. [3], we modify Eq. (1) so that it also accounts for $\mathcal{E}(T)$ and obtain

$$J = J_{\mathrm{G}} - \frac{1}{\mathcal{E}(T)}J_0 \exp\left(\frac{qV}{kT}\right). \tag{7}$$

From Eq. (7), we can derive an expression for V_{mpp} in the same way as in Ref. [5]. In order to do so, let us first assume that the ERE is not dependent on the voltage. This is the case if, e.g., we restrict ourselves to a low-injection regime, or if we just assume carrier lifetimes which are constant with the injection level [9]. V_{mpp} then becomes

$$V_{\mathrm{mpp}} = \frac{kT}{q}\left[\mathrm{W}\left(\mathcal{E}(T)\frac{eJ_{\mathrm{G}}}{J_0}\right) - 1\right]. \tag{8}$$

3.1 Temperature Dependence of the Bandgap

Since both J_{G} and J_0 are functions of the bandgap, E_g, its temperature dependence will be important for computing the TCs. The bandgap decreases when the temperature increases for most semiconductors[1] [1]. This effect was considered in Ref. [3] by assuming a linear variation of the bandgap with the temperature, i.e.,

$$E_g(T) \approx E_{g0} + T \left. \frac{\partial E_g}{\partial T} \right|_{T=T_c}, \tag{9}$$

with E_{g0} being the bandgap at $T = 0$ K and the slope of the straight line resulting from linear fits around $T = 300$ K [4]. We will also assume that the bandgap is a linear function of the temperature and proceed to derive an expression for the TC of V_{mpp} by making use of Eq. (6).

3.2 Dark Saturation Current

Before computing the TC for V_{mpp}, let us take a look back at the dark saturation current, J_0, given in Eq. (3). Performing the integral yields:

$$J_0 = \frac{2\pi q}{c^2 h^3} kT \exp\left(-\frac{E_g}{kT}\right)(E_g^2 + 2kTE_g + 2k^2T^2). \tag{10}$$

In Ref. [3], the polynomial in E_g in Eq. (10) is approximated by E_g^2. We will refer to this as the *approximated form* of J_0, while Eq. (10) will be referred to as the *full form*. This approximated form simplified the derivation of the analytical expression for the temperature coefficient of the V_{oc}. This is also the case for V_{mpp} and J_{mpp}. In order to check the validity of this approximation, we display in Fig.1 a logarithmic plot of J_0 as a function of the temperature for the bandgap of silicon, which has been considered linear, as in Eq. (9). We see that the full and the approximated form of J_0 overlap. We will therefore make use of the approximated form of J_0 to compute the temperature coefficients of V_{mpp} and J_{mpp}. The numerical consequences of making use of this approximation will be discussed in section 5.

3.3 Temperature Coefficients

Let $Z := e\,\mathcal{E}\frac{J_{\mathrm{G}}}{J_0}$ and $\mathrm{W}(Z) := \mathrm{W}$. From Eq. (8), we have

$$\frac{\partial V_{\mathrm{mpp}}}{\partial T} = \frac{V_{\mathrm{mpp}}}{T} + \frac{kT}{q}\frac{\partial \mathrm{W}}{\partial T}. \tag{11}$$

[1]Exceptions of this behavior are $CH_3NH_3PbI_3$ and related perovskite compounds [4]

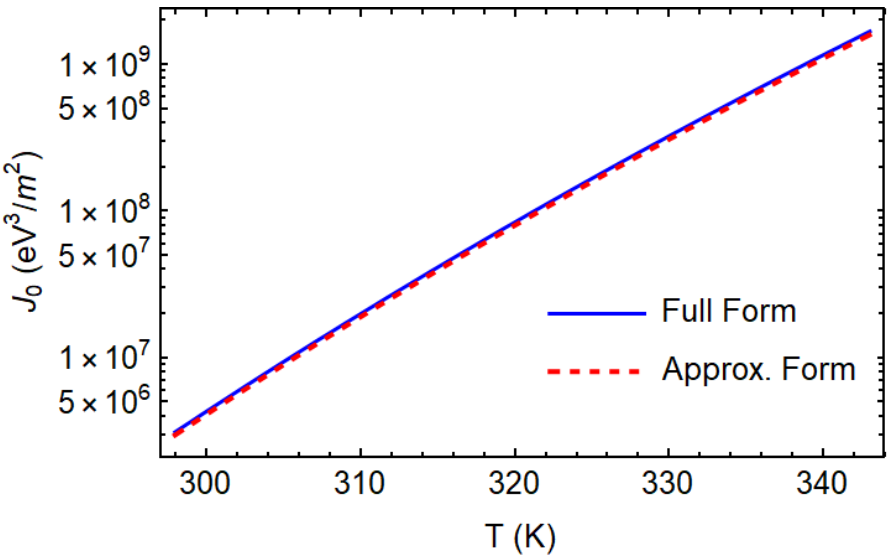

Figure 1: Dark saturation, both in full (Eq. (10)) and approximated form, as a function of the temperature.

Let us now explicitly compute the derivative of Lambert's W function with respect to the temperature. From Eqs. (3) and (9), we have

$$\begin{aligned}\frac{\partial \mathrm{W}}{\partial T} &= \frac{\partial}{\partial T}\log\left(\mathcal{E}\frac{eJ_{\mathrm{G}}}{J_0}\right)\frac{\mathrm{W}}{1+\mathrm{W}} \\ &= \left(\frac{\mathcal{E}'}{\mathcal{E}}+\frac{J'_{\mathrm{G}}}{J_{\mathrm{G}}}-\frac{J'_0}{J_0}\right)\frac{\mathrm{W}}{1+\mathrm{W}} \\ &= \left(\frac{\mathcal{E}'}{\mathcal{E}}+\frac{J'_{\mathrm{G}}}{J_{\mathrm{G}}}-\frac{1}{T}-\frac{E_{g0}}{kT^2}-2\frac{E'_g}{E_g}\right)\frac{\mathrm{W}}{1+\mathrm{W}} \\ &= -\frac{1}{T}\left(\gamma+\frac{E_{g0}}{kT}\right)\frac{\mathrm{W}}{1+\mathrm{W}},\end{aligned} \tag{12}$$

where the prime implies the derivative with respect to the temperature and

$$\gamma = 1+2T\frac{E'_g}{E_g}-T\frac{\mathcal{E}'}{\mathcal{E}}-T\frac{J'_{\mathrm{G}}}{J_{\mathrm{G}}}. \tag{13}$$

In Eq. (12), we have made use of the derivative of Lambert's W function, which can be found in, e.g., Ref. [7]. We obtain the absolute TC for V_{mpp} ($\beta_{V_{\mathrm{mpp}}}$) by

inserting Eq. (12) into Eq. (11). Let $\omega := \mathrm{W}/(1+\mathrm{W})$. We then can write $\beta_{V_{\mathrm{mpp}}}$ as

$$\beta_{V_{\mathrm{mpp}}} = \frac{V_{\mathrm{mpp}} - \omega\frac{E_{g0}}{q} - \omega\frac{kT}{q}\gamma}{T}, \tag{14}$$

which resembles the expression for $\beta_{V_{\mathrm{oc}}}$ in Ref. [3], which was

$$\beta_{V_{\mathrm{oc}}} = \frac{V_{\mathrm{oc}} - \frac{E_{g0}}{q} - \frac{kT}{q}\gamma}{T}. \tag{15}$$

The γ parameter in Eq. (13) is identical[2] to the γ used in the expression for $\beta_{V_{\mathrm{oc}}}$ in Ref. [3]. This parameter was first introduced by Green in Ref. [1] as a way to account for the temperature sensitivity of all mechanisms determining V_{oc} and was later explicitly quantified in Ref. [3]. From the work presented here, we may conclude that γ also plays a role in the temperature sensitivity of V_{mpp}.

Rearranging terms in Eq. (14), we can express $\beta_{V_{\mathrm{mpp}}}$ as

$$\beta_{V_{\mathrm{mpp}}} = \frac{V_{\mathrm{mpp}}}{T}\left[1 + \frac{\mathrm{W}}{1-\mathrm{W}^2}\left(\gamma + \frac{E_{g0}}{kT}\right)\right], \tag{16}$$

from which it is trivial to find the relative TC for $\beta_{V_{\mathrm{mpp}}}$. Likewise for J_{mpp}, we can derive expressions for its TC from Eq. (5) by making use of Eq. (6). We obtain

$$\beta_{J_{\mathrm{mpp}}} = \frac{J_{\mathrm{mpp}}}{T}\left[T\frac{J'_{\mathrm{G}}}{J_{\mathrm{G}}} + \frac{1}{1-\mathrm{W}^2}\left(\gamma + \frac{E_{g0}}{kT}\right)\right]. \tag{17}$$

3.4 The Radiative Limit with Constant Bandgap

In the radiative limit, the total current produced by the cell is given by Eq. (1). The maximum power point voltage, current and power are therefore given by Eqs. (4) and (5). All energy losses are of radiative nature and, therefore, $\mathrm{ERE} = 1$. Additionally, if the bandgap is a constant with respect to temperature variations, the γ parameter given in Eq. (13) simplifies to $\gamma = 1$. Accounting for this, Eqs. (16) and (17) become

$$\beta_{V_{\mathrm{mpp}}} = \frac{V_{\mathrm{mpp}}}{T}\left[1 + \frac{\mathrm{W}}{1-\mathrm{W}^2}\left(1 + \frac{E_{g0}}{kT}\right)\right], \tag{18}$$

$$\beta_{J_{\mathrm{mpp}}} = \frac{J_{\mathrm{mpp}}}{T}\left[\frac{1}{1-\mathrm{W}^2}\left(1 + \frac{E_{g0}}{kT}\right)\right] \tag{19}$$

[2]The notation $T\frac{X'}{X}$ is equivalent to $\frac{\partial \log X}{\partial \log T}$.

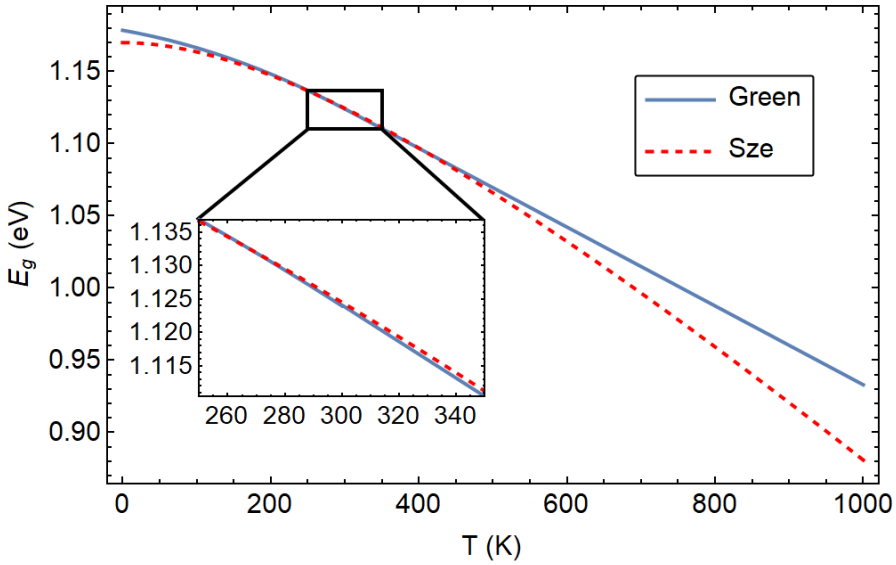

Figure 2: Temperature dependence of the energy gap, $E_g(T)$, for Green's (Eq. (9)) and Sze's (Eq. (20)) models.

3.5 A More Realistic Bandgap

In this work as well as in Ref. [3], the bandgap of silicon has been assumed to be a linear function of the temperature, as seen in Eq. (9). Sze determined in Ref. [10] the temperature dependence of E_g from the absorption edge of silicon and showed that it could be empirically described by

$$E_g(T) = E_{g0} - \frac{\alpha T^2}{T + \beta}, \tag{20}$$

where α and β are fitting parameters; and E_{g0} is the bandgap extrapolated to $T = 0$ K. Sze's model shows that at low temperatures, the bandgap has a rather quadratic dependence with the temperature, in contrasts to the linear bandgap presented in section 3.1.

Eq. (9) follows from the model for the temperature dependence of the energy gap presented by Green in Ref. [11]. There, Green modeled $E_g(T)$ as a piecewise function of the temperature, with a quadratic dependency for $T < 300$ K and a linear one for $T > 300$ K [11]. Eq. (9) represents the linear part of Green's model. Fig. 2 displays a comparison between both models. Here, we have plotted Sze's and Green's bandgap as a function of the temperature, for silicon. We see that, in the normal operating temperature range of $[300, 343]$ K, both functions overlap well.

In order to introduce Sze's bandgap in our model, we need to make use of Eq. (20) when computing J_0'. This results in one new term that should be added to the γ parameter in Eq. (13), which yields

$$\gamma = 1 + 2T\frac{E_g'}{E_g} + \frac{\alpha\beta T}{k(T+\beta)^2} - T\frac{\mathcal{E}'}{\mathcal{E}} - T\frac{J_{\mathrm{G}}'}{J_{\mathrm{G}}}. \tag{21}$$

Since we always can collect this new term into the γ parameter, the expressions for the TCs presented in this work are still valid.

Finally, as noted in Ref. [9], the deviation between Sze's and Green's models is a measure for the uncertainty of the model used. In the relevant temperature range up to 650 K, this uncertainty is below 1% and can be neglected.

4 Experimental Method

In order to validate the analytical expression for $\beta_{V_{\mathrm{mpp}}}$ and $\beta_{J_{\mathrm{mpp}}}$, 18 cells with different bulk resistivities (ρ) and cell architectures were studied. The cells were fabricated from three different compensated p-type multi-crystalline silicon (mc-Si) ingots and can be divided into three groups: (a) $\rho = 0.5\ \Omega$ cm, *Passivated Emitter Rear Cell* (PERC), (b) $\rho = 1.3\ \Omega$ cm, PERC, and (c) $\rho = 1.3\ \Omega$ cm, *Aluminum Back Surface Field* (Al-BSF) cell. Each group contains six cells from various brick positions. The $\beta_{V_{\mathrm{mpp}}}$ and $\beta_{J_{\mathrm{mpp}}}$ values were obtained from temperature dependent suns $-V_{\mathrm{oc}}$ measurements using a NeonSee$^{\mathrm{TM}}$ AAA Sun-simulator. Making use of suns $-V_{\mathrm{oc}}$ measurements allowed for TCs without the effects of series resistance.

5 Numerical Results and Discussion

In this section we present numerical results for the model presented in section 3 and compare them to experimental measurements. For all numerical evaluations, the bandgap is assumed to be a linear function of the temperature as stated in Eq. (9).

5.1 Temperature Coefficient of V_{mpp}

In Fig. 3, $\beta^r_{V_{\mathrm{mpp}}}$ is plotted as a function of V_{mpp} for $E_g' = -0.27 \times 10^{-3}$ eV K^{-1}, i.e., the temperature sensitivity of the silicon bandgap [4]. Here, Eq. (14) is represented by a dashed line and our experimental values by crosses. Note that V_{mpp} and $\beta^r_{V_{\mathrm{mpp}}}$ are increasing functions of the ERE (see Eq. (8)). The points of the dashed line in Fig. 3 are obtained by evaluating Eqs. (8) and (14) for several values of the ERE

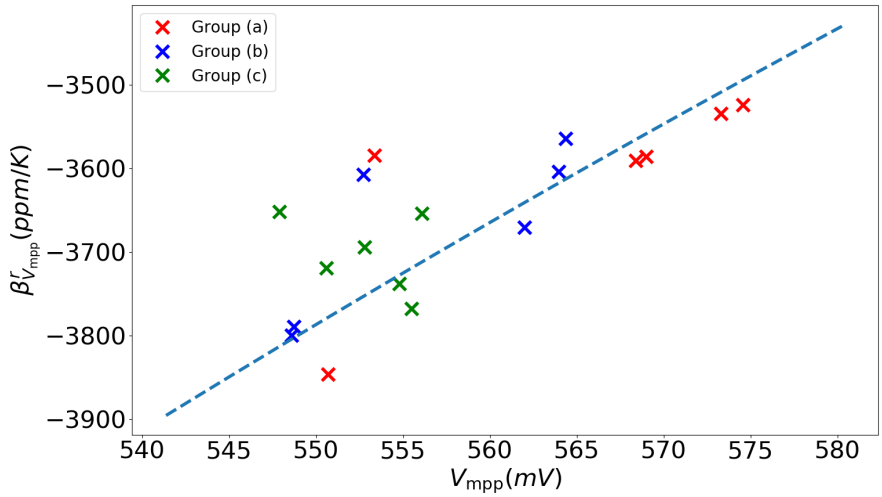

Figure 3: Relative temperature coefficient of the maximum power point voltage as a function of V_{mpp}. Eq. (14) is represented by the dashed line. The crosses represent experimental measurements of V_{mpp} of the three sets of mc-Si samples described in section IV: (a) PERC: $\rho = 0.5\ \Omega$ cm, (b) PERC: $\rho = 1.3\ \Omega$ cm and (c) Al-BSF: $\rho = 1.3\ \Omega$ cm

within the interval $\mathcal{E} \in [3,\ 15] \times 10^{-5}$. The ERE of each measurement can be calculated by subtracting the ideal and the measured V_{oc} as

$$\mathcal{E}(T) = \exp\left[\frac{q}{kT}(V_{\mathrm{oc}} - V_{\mathrm{oc}}^{\mathrm{id}})\right], \tag{22}$$

where $V_{\mathrm{oc}}^{\mathrm{id}}$ is the open-circuit voltage in the radiative limit, given in, e.g., Ref. [12]. For the samples presented in this work, we find an average value of the ERE of $\mathcal{E} = 6.99 \times 10^{-5}$. A rather low value of the ERE is expected since silicon is dominated by non-radiative recombination [1, 12]. In the light of Fig. 3, we may conclude that Eq. (14) gives food predictions of the temperature behavior of V_{mpp}.

5.2 Dark Saturation Current

As mentioned in section 3, we have been making use of the approximated form of J_0 to simplify the derivation of $\beta_{V_{\mathrm{mpp}}}$ and $\beta_{J_{\mathrm{mpp}}}$. We have numerically computed these TCs by making use of both the full and approximated form J_0 to check whether there is a significant difference. The results show a difference of 12 ppm K^{-1} at $T = 300$ K and $\mathcal{E} = 1$ up to 66 ppm K^{-1} at $T = 343$ K and $\mathcal{E} = 10^{-7}$ for $\beta^r_{V_{\mathrm{mpp}}}$ and, 0.5 ppm K^{-1} at $T = 300$ K and $\mathcal{E} = 1$ up to 10 ppm K^{-1} at $T = 343$ K and $\mathcal{E} = 10^{-7}$ for $\beta^r_{J_{\mathrm{mpp}}}$. From the measured values, as well as from Fig. 3, we see that typical values of $\beta^r_{V_{\mathrm{mpp}}}$

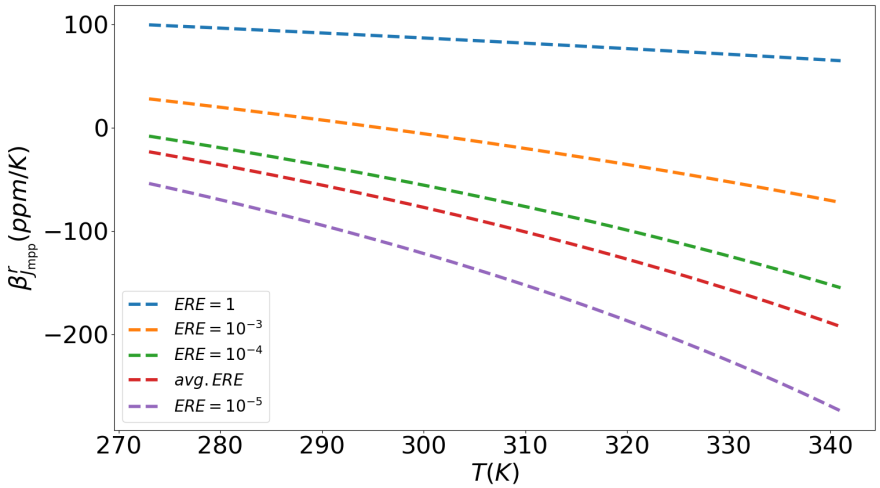

Figure 4: Relative temperature coefficient of the maximum power point current as a function of the temperature calculated from Eq. (17) for several values of the ERE.

range from -3500 to -4000 ppm K^{-1}. We can therefore conclude that having made use of the approximated form of J_0 for computing the TCs does not have significant effects in $\beta_{V_{mpp}}$ and $\beta_{J_{mpp}}$, in our cases.

5.3 Temperature Coefficient of J_{mpp}

In Fig. 4, we have plotted Eq. (17) as a function of the temperature for different values of the ERE. Here, we can see that the temperature behavior of J_{mpp} changes with a decreasing ERE. For $\mathcal{E} = 1$, $\beta^r_{J_{mpp}}(T)$ has positive values, implying that J_{mpp} increases with temperature. But when the ERE starts decreasing, we encounter negative values of $\beta^r_{J_{mpp}}(T)$, implying that J_{mpp} is decreasing with increasing temperature. Fig. 4 shows that $\beta_{J_{mpp}}$ is not a constant but rather temperature dependent, which implies J_{mpp} does not vary linearly with the temperature. Note that for $\mathcal{E} = 6.99 \times 10^{-5}$, i.e., the average ERE of our samples (sec. 5.1), we have $\beta^r_{J_{mpp}} < 0$ (red line in Fig. 4) and, particularly, $\beta^r_{J_{mpp}}(\text{avg. ERE}) = -122$ ppm K^{-1} for $T = 300$ K. Let us also note that, for $\mathcal{E} = 10^{-3}$, $\beta^r_{J_{mpp}}$ crosses zero at a temperature, denoted here T_{crit}, which equals 284 K in this specific case. $J(T_{crit})$ therefore is a maximum J_{mpp}. Note also that for $\mathcal{E} = 1$, $\beta^r_{J_{mpp}}$ is decreasing with the temperature and will eventually cross zero. Fig. 4 therefore suggests that T_{crit} is decreasing with the ERE.

Our experiments show a variety of temperature behaviors for the measured J_{mpp}. In Fig. 5, we display our measurements of J_{mpp} for three of the six investigated Al-

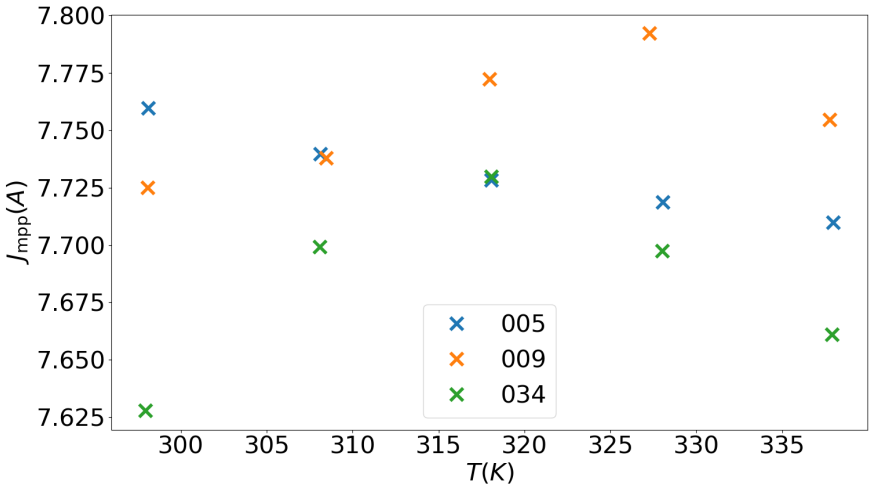

Figure 5: Measurements of J_{mpp} of the Al-BSF cell for different temperatures. Each color represents a position within the brick.

BSF cells (group (c) in sec. 4). The cells are numbered according to their position within the brick starting from the bottom, i.e., position 005 will be lower in the brick than 009. In Fig. 5, we can see that in brick position 005, J_{mpp} is clearly decreasing with the temperature. This is also the case for three other cells in positions 012, 022 and 027. These are not displayed in Fig. 5. In positions 009 and 034, J_{mpp} appears to increase with temperature, reach a maximum and then decrease. In our measurements of the PERC cells (groups (a) and (b) in sec. 4), J_{mpp} is increasing with the temperature in most brick positions. There are however a few positions where the measured values J_{mpp} vary in a non-systematic manner, and it is hard to see any increasing or decreasing trend. A similar behavior as the one found in positions 009 and 034 of group (c) is found in positions 012 and 041 of group (a).

The TC of J_{mpp} in each position is calculated by least-square fitting the measured values of J_{mpp} to a straight line. $\beta_{J_{\text{mpp}}}$ will therefore be the value of the slope. This method gives reasonable fitting errors in those brick positions where J_{mpp} shows a clear increasing, or decreasing, trend. In the case of position 005 in Fig. 5, we find $\beta^r_{J_{\text{mpp}}} = -156 \pm 16$ ppm K^{-1}. In the case of positions 009 and 034, where J_{mpp} shows both an increasing and a decreasing behavior, the fit gives $\beta^r_{J_{\text{mpp}}} = 147 \pm 96$ ppm K^{-1} and $\beta^r_{J_{\text{mpp}}} = 85 \pm 180$ ppm K^{-1}, respectively. The non-linearity of J_{mpp} originates these large uncertainties. It is therefore reasonable to conclude that making use of a single TC to describe the temperature behavior of J_{mpp} may be misleading.

Our model has limitations that may be able to explain the discrepancy with our

experiments. First, the spectral response of the solar cell. Eq. (7), assumes unit absorptivity [6]. In real solar cells, the absorption coefficients are not step-functions but rather smooth functions of the incoming wavelength which also depend on the cell temperature [13] and, therefore, they will play a role in the temperature coefficients. Particularly, the spectral response of the cell will affect the value of J'_{G}. Second, whereas our model assumes an ideality factor of 1, the IV-curve of real cells are often better described by a larger ideality factor [14]. A temperature dependent ideality factor, $n(T)$, will possibly also affect the TCs.

These two factors may not be sufficient to explain the discrepancies, so let us focus now on the experiments. The biggest source of uncertainty in our measurements comes from the difficulty in stabilizing the temperature during the relatively long data-acquisition times. This results in not only uncertainty in the temperature, but possibly also in the measured values of V_{mpp} and J_{mpp}. The uncertainty of the temperature propagates in the calculation of the TCs further increasing the fitting errors. Within the investigated temperature range, $\beta_{J_{\mathrm{mpp}}}$ varies with temperature (see Fig. 4) while $\beta_{V_{\mathrm{mpp}}}$ is nearly constant. Small temperature fluctuations will therefore cause a bigger, and significant, effect on $\beta_{J_{\mathrm{mpp}}}$ than on $\beta_{V_{\mathrm{mpp}}}$.

Finally, T_{crit} may be the last piece of the puzzle to explain the discrepancies between Eq. (17) and our experiments. A T_{crit} dependent on the brick position and the cell architecture may explain the variety of temperature behaviors that our experiments show. J_{mpp} has not reached T_{crit} in the cells that show an only increasing J_{mpp}. At the same time, those cells only showing a decreasing J_{mpp} have a T_{crit} lower than the temperature range in which the measurements were performed, as seen, for example, in Fig. 5 in the measurements of the cell from position 005. Finally, the positions where J_{mpp} first increases and then decreases with the cell temperature reach their correspondent T_{crit} within the investigated temperature range. This is the case for brick positions 009 and 034 in Fig. 5, where we can see that their correspondent T_{crit} is around 328 K and 318 K, respectively.

6 Conclusion

In this paper, we have presented analytical expressions for the TCs of V_{mpp} and J_{mpp}. It was discussed in Ref. [3] that the γ parameter, first introduced in Ref. [1], accounts for the temperature sensitivity of all mechanisms determining the V_{oc}. From the results presented in section 3, we conclude that γ may also determine the thermal sensitivity of V_{mpp} and J_{mpp}.

Numerical results as well as a comparison with experimental measurements of $\beta_{V_{\mathrm{mpp}}}$ and $\beta_{J_{\mathrm{mpp}}}$ have also been presented and discussed. We have found that our

model gives good predictions of the temperature behavior of the measured values of $\beta_{V_{\mathrm{mpp}}}$. The mismatch between the experimental measurements of $\beta_{J_{\mathrm{mpp}}}$ and Eq. (17) suggests that there are one or more factors, which are not accounted for in our model, that affect the temperature sensitivity of J_{mpp}. The solar cell spectral response and a temperature dependent ideality factor have been proposed as possible explanations to the discrepancy. The uncertainty of the measurements due to small temperature fluctuations may also contribute to the discrepancy between the experiments and Eq. (17). Finally, Fig. 4 shows that $\beta_{J_{\mathrm{mpp}}}$ is not a constant within the investigated temperature range. Additionally, it can be seen in Fig. 4 that $\beta_{J_{\mathrm{mpp}}}(T)$ crosses zero at an ERE-dependent critical temperature, implying that J_{mpp} reaches a maximum at this temperature.

References

[1] M. A. Green. "Solar cells: operating principles, technology, and system applications". In: *Englewood Cliffs, NJ, Prentice-Hall, Inc., 1982. 288 p.* (1982).

[2] M. A. Green. "General temperature dependence of solar cell performance and implications for device modeling". In: *Progress in Photovoltaics: Research and Applications* 11.5 (2003), pp. 333–340.

[3] O. Dupré, R. Vaillon, and M. A. Green. "Physics of the temperature coefficients of solar cells". In: *Solar Energy Materials and Solar Cells* 140 (2015), pp. 92–100.

[4] O. Dupré, R. Vaillon, and M. A. Green. *Thermal Behavior of Photovoltaic Devices: Physics and Engineering*. Springer, 2016.

[5] A. Sergeev and K. Sablon. "Exact solution, endoreversible thermodynamics, and kinetics of the generalized Shockley-Queisser model". In: *Physical Review Applied* 10.6 (2018), p. 064001.

[6] W. Shockley and H. J. Queisser. "Detailed balance limit of efficiency of p-n junction solar cells". In: *Journal of Applied Physics* 32.3 (1961), pp. 510–519.

[7] R. M. Corless et al. "On the Lambert W function". In: *Advances in Computational Mathematics* 5.1 (1996), pp. 329–359.

[8] M. A. Green. "Radiative efficiency of state-of-the-art photovoltaic cells". In: *Progress in Photovoltaics: Research and Applications* 20.4 (2012), pp. 472–476.

[9] S. Rein. *Lifetime Spectroscopy: A Method of Defect Characterization in Silicon for Photovoltaic Applications*. Vol. 85. Springer Science & Business Media, 2006.

[10] S. M. Sze. "Physics of Semiconductor Devices 2nd edition Awiley Inter-science John wiley and Sons". In: *New York* (1981).

[11] M. A. Green. "Intrinsic concentration, effective densities of states, and effective mass in silicon". In: *Journal of Applied Physics* 67.6 (1990), pp. 2944–2954.

[12] J. Nelson. *The Physics of Solar Cells*. World Scientific Publishing Company, 2003.

[13] K. Rajkanan, R. Singh, and J. Shewchun. "Absorption coefficient of silicon for solar cell calculations". In: *Solid-State Electronics* 22.9 (1979), pp. 793–795.

[14] A. McEvoy and T. Markvart. *Solar cells: materials, manufacture and operation*. Academic Press, 2012.

Appendix C

Analytical Modeling of the Temperature Sensitivity of the Maximum Power Point of Solar Cells

Analytical Modeling of the Temperature Sensitivity of the Maximum Power Point of Solar Cells

Alfredo Sanchez Garcia, Sissel Tind Kristensen, and Rune Strandberg
University of Agder, Grimstad, 4879, Norway

Abstract

This work presents new analytical expressions for the temperature coefficients of the voltage, current and power of a solar cell at its maximum power point. A new analytical expression of the temperature coefficient of the fill factor is also derived. The new expressions are written as functions of solar cell parameters that can be extracted from the current-voltage characteristic of the cell. Non-ideal diode behavior is partially accounted for through a temperature dependent ideality factor. The recombination parameter γ, which has been shown to account for the thermal sensitivity of all mechanisms determining the open-circuit voltage, appears to play a role also for the temperature coefficient of the maximum power point. The expressions are tested against experimental data, which covers measurements from 18 multicrystalline silicon solar cells with different bulk resistivities and cell architectures. It is found that the new model captures the essence of the temperature variation shown by the investigated parameters.

1 Introduction

The temperature sensitivity of a solar cell parameter, such as the open-circuit voltage, V_{oc}, is usually described by its temperature coefficient (TC) [1]. Some work has been done aiming to explicitly quantify the TCs of V_{oc} and the short-circuit current, i_{sc} [2, 3], but so far, there has not been much focus on the temperature sensitivity of the maximum power point (MPP). Quantification of TCs, particularly at the MPP, is of special importance as it is desirable to accurately predict the temperature dependent performance of solar cells under real operating conditions. The lack of

analytical models describing the temperature sensitivity of the MPP represents a gap in the scientific literature which this work seeks to fill. To this end, Khanna's model for the maximum power point [4] is used as a starting point to derive analytical expressions for the TCs of the voltage, current and power at the MPP. Inspired by the work of Dupré et al. in Ref. [3], the influence of the recombination parameter γ in the temperature sensitivity of the MPP is also explored. For this, energy losses related to non-radiative recombination are considered through the *External Radiative Efficiency* (ERE), as defined in Ref. [5]. The derived expressions also account for temperature variations of the bandgap, which are modeled with a linear function of the temperature. Some preliminary results have already been presented in Ref. [6]. This extended version includes the derivation of the expressions for the TCs of photovoltaic parameters that were not included in the preliminary version. In the present work, non-ideal diode behavior is also accounted for through a temperature dependent ideality factor. The derived quantities are expressed as functions of each other and of well-known parameters, such as V_{oc} and i_{sc}. This allows for the derivation of an analytical expression for the TC of the fill factor. Finally, the new expressions are tested with experimental data obtained from suns-V_{oc} measurements of 18 multicrystalline silicon solar cells with different bulk resistivities and cell architectures.

2 Theoretical Background

Assuming non-degenerate conditions, the total current density, i, produced by a solar cell as a function of its voltage V, is given by Shockley's diode equation [7],

$$i = i_{\mathrm{G}} - i_0 \exp\left(\frac{V}{mV_{\mathrm{t}}}\right) \approx i_{\mathrm{sc}} - i_0 \exp\left(\frac{V}{mV_{\mathrm{t}}}\right), \tag{1}$$

where i_0 is the thermal recombination current [8] and the photogeneration current, i_{G}, has been approximated by the short-circuit current, i_{sc}. This assumption is valid for practically all solar cells [9]. The *thermal voltage* V_{t} is defined by $qV_{\mathrm{t}} = kT$, where k is Boltzmann's constant and T is the cell temperature. Non-ideal diode behavior is accounted for through the ideality factor m which is assumed to be constant with respect to the voltage but allowed to vary with the temperature. As commonly found in literature on solar cells, the open-circuit voltage V_{oc} is easily obtained from Eq. (1) by setting $i = 0$, which gives

$$V_{\mathrm{oc}} = mV_{\mathrm{t}} \log\left(\frac{i_{\mathrm{sc}}}{i_0}\right). \tag{2}$$

The power P delivered by the cell is given by the product $P = Vi$ [9]. At the maximum power point, it holds that ${}^{dP}/_{dV} = 0$. In Ref [4], Khanna et al. found that Lambert's W function, defined by $z = \mathrm{W}(ze^z)$ [10], allows for an analytical expression of the maximum power point voltage, V_{mpp}, of the form

$$\begin{aligned} V_{\mathrm{mpp}} = &\ mV_{\mathrm{t}} \left[\mathrm{W}\left(e\frac{i_{\mathrm{sc}}}{i_0} \right) - 1 \right] \\ = &\ mV_{\mathrm{t}} \left[\mathrm{W}\left(e^{1+V_{\mathrm{oc}}/mV_{\mathrm{t}}} \right) - 1 \right], \end{aligned} \tag{3}$$

where Eq. (2) was made use of in order to write ${}^{i_{\mathrm{sc}}}/_{i_0} = \exp\left[{}^{V_{\mathrm{oc}}}/_{mV_{\mathrm{t}}}\right]$. The maximum power point current, i_{mpp}, is obtained by inserting Eq. (3) into Eq. (1). This yields

$$i_{\mathrm{mpp}} = i_{\mathrm{sc}} \left[1 - \frac{1}{\mathrm{W}\left(e^{1+V_{\mathrm{oc}}/mV_{\mathrm{t}}} \right)} \right]. \tag{4}$$

The maximum power that a solar cell can produce is given by [9]

$$P_{\mathrm{mpp}} = V_{\mathrm{mpp}} i_{\mathrm{mpp}} = V_{\mathrm{oc}} i_{\mathrm{sc}} \mathrm{FF}, \tag{5}$$

where FF is the *Fill Factor*. Inserting Eqs. (3) and (4) yields [4, 11]

$$P_{\mathrm{mpp}} = mV_{\mathrm{t}} i_{\mathrm{sc}} \left[\mathrm{W}\left(e^{1+V_{\mathrm{oc}}/mV_{\mathrm{t}}} \right) - 2 + \frac{1}{\mathrm{W}\left(e^{1+V_{\mathrm{oc}}/mV_{\mathrm{t}}} \right)} \right]. \tag{6}$$

2.1 Temperature Coefficient

The TC of a solar cell parameter (V_{oc}, i_{sc}...) describes how this parameter changes with the temperature. The *relative temperature coefficient* of a parameter, X, as a function of the temperature, T, denoted here $\beta_X^r(T)$, is defined as the rate of change of X over the considered temperature range and normalized by X, i.e., [12]

$$\beta_X^r(T) = \frac{1}{X}\frac{\mathrm{d}X}{\mathrm{d}T} = \frac{\mathrm{d}}{\mathrm{d}T} \log\left[X(T)\right]. \tag{7}$$

The temperature dependence of many solar cell parameters, such as V_{oc} or the efficiency, is approximately linear for normal operating temperatures [1]. The derivative in Eq. (7) is then nearly constant and the temperature coefficient becomes a single valued parameter, hence its designation. Inserting Eq. (5) in Eq. (7), it is seen that the relative TC of P_{mpp} can be expressed as the sum of the relative TCs of V_{oc}, i_{sc} and FF, i.e., [3]

$$\beta_{P_{\mathrm{mpp}}}^r = \ \beta_{V_{\mathrm{oc}}}^r + \beta_{i_{\mathrm{sc}}}^r + \beta_{\mathrm{FF}}^r = \beta_{V_{\mathrm{mpp}}}^r + \beta_{i_{\mathrm{mpp}}}^r. \tag{8}$$

2.2 The recombination parameter γ

For a solar cell operating at the radiative limit, the thermal recombination current, i_0 in Eq. (1), is well approximated by

$$i_0 \approx qV_\mathrm{t} \exp\left(-\frac{E_\mathrm{g}}{qV_\mathrm{t}}\right) E_\mathrm{g}^2. \tag{9}$$

To account for non-radiative recombination, Green introduced the concept of External Radiative Efficiency (ERE) in Ref. [5]. The ERE is defined as *the fraction of the total dark current recombination in the cell that results in radiative emission from the cell* [5]. Following Ref. [3], the ERE is introduced in Eq. (1) by making the substitution $i_0 \to {}^{i_0}/_{\mathrm{ERE}}$. Assuming that the ERE is independent on the voltage, the expression for V_oc in Eq. (2) becomes

$$V_\mathrm{oc} = V_\mathrm{t} \log\left(\mathrm{ERE}\frac{i_\mathrm{sc}}{i_0}\right), \tag{10}$$

where m is set to 1 to match the expression presented in Ref. [3]. Using Eqs. (10) and (7) as a starting point, it can be shown that the *absolute TC* of V_oc, β_{V_oc}, is given by [3]

$$\beta_{V_\mathrm{oc}} = \frac{V_\mathrm{oc} - \frac{E_\mathrm{gc}}{q} - \frac{kT}{q}\gamma}{T}, \tag{11}$$

with

$$\gamma = 1 + 2T\frac{E_\mathrm{g}'}{E_\mathrm{g}} - T\frac{\mathrm{ERE}'}{\mathrm{ERE}} - T\frac{i_\mathrm{sc}'}{i_\mathrm{sc}}, \tag{12}$$

where the prime denotes derivative with respect to the temperature. This explicit expression for the γ parameter is obtained by making use of the explicit form of i_0 found in Eq. (9). To obtain Eqs. (11) and (12), one also needs to assume a bandgap that changes linearly with the temperature [1], i.e.,

$$\begin{aligned} E_\mathrm{g}(T) \approx\ & E_\mathrm{g}(T_c) + (T - T_c)\frac{\mathrm{d}E_\mathrm{g}}{\mathrm{d}T}\bigg|_{T=T_c} + \mathcal{O}(T^2) \\ =\ & E_\mathrm{gc} + TE_\mathrm{g}' + \mathcal{O}(T^2), \end{aligned} \tag{13}$$

with $E_\mathrm{gc} = E_\mathrm{g}(T_c) - T_cE_\mathrm{g}'$. For, e.g., crystalline silicon, $E_\mathrm{gc} = 1.206$ eV and $E_\mathrm{g}' = -2.73 \times 10^{-4}$ eVK^{-1} [1]. The recombination parameter γ in Eq. (12) was first introduced by Green in Ref. [1] as a way to account for the temperature sensitivity of all mechanisms determining V_oc and was later explicitly quantified by Dupré et al. in Ref. [3][1].

[1]The notation $T\frac{X'}{X}$ is equivalent to $\frac{\mathrm{d}\log X}{\mathrm{d}\log T}$.

3 The model

To shorten the notation, the argument of Lambert's W function in Eqs. (3), (4) and (6) is denoted by z_{oc}. Foreseeing its usability in the coming derivations, note from Eq. (4) that

$$\frac{1}{\mathrm{W}(z_{\mathrm{oc}})} = 1 - \frac{i_{\mathrm{mpp}}}{i_{\mathrm{sc}}}. \tag{14}$$

This identity will be used in the derivation of the expressions for the TCs to eliminate the W functions when this is advantageous. From Eqs. (3) and (7), the relative TC of V_{mpp}, $\beta^r_{V_{\mathrm{mpp}}}$, is given by

$$\begin{aligned}
\beta^r_{V_{\mathrm{mpp}}} &= \frac{\mathrm{d}}{\mathrm{d}T}\log V_{\mathrm{mpp}} \\
&= \frac{\mathrm{d}}{\mathrm{d}T}\log\left[mV_{\mathrm{t}}\left[\mathrm{W}\left(e^{1+V_{\mathrm{oc}}/V_{\mathrm{t}}}\right)-1\right]\right] \\
&= \frac{1}{T}+\frac{m'}{m}+\frac{1}{\mathrm{W}(z_{\mathrm{oc}})-1}\frac{\mathrm{d}}{\mathrm{d}T}\mathrm{W}(z_{\mathrm{oc}}) \\
&= \frac{1}{T}+\frac{m'}{m}+\frac{1}{\mathrm{W}(z_{\mathrm{oc}})-1}\frac{\mathrm{W}(z_{\mathrm{oc}})}{1+\mathrm{W}(z_{\mathrm{oc}})}\frac{\mathrm{d}}{\mathrm{d}T}\left[1+\frac{V_{\mathrm{oc}}}{V_{\mathrm{t}}}\right] \\
&= \frac{1}{T}+\frac{m'}{m}+\frac{mV_{\mathrm{t}}}{V_{\mathrm{mpp}}}\frac{\mathrm{W}(z_{\mathrm{oc}})}{1+\mathrm{W}(z_{\mathrm{oc}})}\frac{\mathrm{d}}{\mathrm{d}T}\left[1+\frac{V_{\mathrm{oc}}}{mV_{\mathrm{t}}}\right],
\end{aligned} \tag{15}$$

where the derivative of Lambert's W function, which can be found in, e.g., Ref. [10] was used. Additionally, Eq. (3) was used to make $(\mathrm{W}(z_{\mathrm{oc}})-1)^{-1} = {}^{mV_{\mathrm{t}}}\!/_{V_{\mathrm{mpp}}}$. The last derivative in Eq. (15) can be written as

$$\begin{aligned}
\frac{\mathrm{d}}{\mathrm{d}T}\left[1+\frac{V_{\mathrm{oc}}}{mV_{\mathrm{t}}}\right] &= \frac{\mathrm{d}V_{\mathrm{oc}}}{\mathrm{d}T}\frac{q}{mkT}-\frac{qV_{\mathrm{oc}}}{mkT^2}-\frac{m'}{m} \\
&= \frac{V_{\mathrm{oc}}}{mV_{\mathrm{t}}}\left[\beta^r_{V_{\mathrm{oc}}}-\frac{1}{T}-\frac{m'}{m}\right],
\end{aligned} \tag{16}$$

where the definitions of relative TC in Eq. (7) was used. Inserting now Eq. (16) into the last line of Eq. (15) yields

$$\beta^r_{V_{\mathrm{mpp}}} = \frac{1}{T}+\frac{m'}{m}+\frac{\mathrm{W}(z_{\mathrm{oc}})}{1+\mathrm{W}(z_{\mathrm{oc}})}\left[\beta^r_{V_{\mathrm{oc}}}-\frac{1}{T}-\frac{m'}{m}\right]\frac{V_{\mathrm{oc}}}{V_{\mathrm{mpp}}}. \tag{17}$$

Employing Eq. (14) to eliminate the W functions, the factor in front of the parenthesis of Eq. (17) becomes

$$\frac{\mathrm{W}(z_{\mathrm{oc}})}{1+\mathrm{W}(z_{\mathrm{oc}})} = \frac{i_{\mathrm{sc}}}{2i_{\mathrm{sc}}-i_{\mathrm{mpp}}} = \mathcal{I}. \tag{18}$$

To shorten the notation, note that ${}^{1}\!/\!_{T} + {}^{m'}\!/\!_{m}$ equals the derivative with respect to the temperature of the logarithm of mV_t, i.e., $\beta^r_{mV_\mathrm{t}}$. Eq. (17) then becomes

$$\beta^r_{V_\mathrm{mpp}} = \beta^r_{mV_\mathrm{t}} + \mathcal{I}\left[\beta^r_{V_\mathrm{oc}} - \beta^r_{mV_\mathrm{t}}\right]\frac{V_\mathrm{oc}}{V_\mathrm{mpp}}. \tag{19}$$

Performing the same type of derivation with Eqs. (4) and (6) as starting points, the relative TCs of i_mpp and P_mpp can be expressed as

$$\beta^r_{i_\mathrm{mpp}} = \beta^r_{i_\mathrm{sc}} + (1-\mathcal{I})\left[\beta^r_{V_\mathrm{oc}} - \beta^r_{mV_\mathrm{t}}\right]\frac{V_\mathrm{oc}}{V_\mathrm{mpp}}, \tag{20}$$

$$\beta^r_{P_\mathrm{mpp}} = \beta^r_{mV_\mathrm{t}} + \beta^r_{i_\mathrm{sc}} + \left[\beta^r_{V_\mathrm{oc}} - \beta^r_{mV_\mathrm{t}}\right]\frac{V_\mathrm{oc}}{V_\mathrm{mpp}}, \tag{21}$$

where it is straightforward to show that Eqs. (19), (20) and (21) satisfy Eq. (8). Finally, using Eqs. (8) and (21), the relative TC of the fill factor, FF, can be written as

$$\begin{aligned}\beta^r_\mathrm{FF} &= \beta^r_{P_\mathrm{mpp}} - \beta^r_{V_\mathrm{oc}} - \beta^r_{i_\mathrm{sc}} \\ &= \beta^r_{mV_\mathrm{t}} - \left(\beta^r_{mV_\mathrm{t}} - \beta^r_{V_\mathrm{oc}}\right)\frac{V_\mathrm{oc}}{V_\mathrm{mpp}} - \beta^r_{V_\mathrm{oc}} \\ &= \left(\beta^r_{mV_\mathrm{t}} - \beta^r_{V_\mathrm{oc}}\right)\left(1 - \frac{V_\mathrm{oc}}{V_\mathrm{mpp}}\right).\end{aligned} \tag{22}$$

4 The recombination parameter γ

As mentioned in section 2, Green introduced the recombination parameter γ as a way to account for the temperature sensitivity of all mechanisms determining V_oc [9]. Eqs. (3), (4) and (6) show a direct link between the open-circuit voltage and the maximum power point. The parameter γ should therefore be expected to play a role in the temperature sensitivity of the maximum power point. In this section, the expressions for the TCs are derived in an alternative way to include the γ parameter. To match Dupré's expression in Ref. [3], $m = 1$ will be assumed in this section. By combining Eqs. (11) and (16), it becomes clear that

$$\frac{V_\mathrm{oc}}{V_\mathrm{t}}\left(\beta^r_{V_\mathrm{oc}} - \frac{1}{T}\right) = \frac{1}{V_\mathrm{t}}\left(\beta_{V_\mathrm{oc}} - \frac{V_\mathrm{oc}}{T}\right) = -\frac{1}{T}\left(\gamma + \frac{E_\mathrm{gc}}{kT}\right), \tag{23}$$

with γ being given by Eq. (12). Substituting this identity into Eq. (17) yields

$$\begin{aligned}\beta^r_{V_{\mathrm{mpp}}} &= \frac{1}{T} - \frac{\mathrm{W}(z_{\mathrm{oc}})}{1+\mathrm{W}(z_{\mathrm{oc}})}\frac{1}{\mathrm{W}(z_{\mathrm{oc}})-1}\frac{V_{\mathrm{oc}}}{V_{\mathrm{t}}}\left[\frac{1}{T} - \beta^r_{V_{\mathrm{oc}}}\right] \\ &= \frac{1}{T} - \frac{\mathrm{W}(z_{\mathrm{oc}})}{1+\mathrm{W}(z_{\mathrm{oc}})}\frac{1}{\mathrm{W}(z_{\mathrm{oc}})-1}\frac{-1}{T}\left(\gamma + \frac{E_{\mathrm{gc}}}{kT}\right) \\ &= \frac{1}{T}\left[1 + \frac{i_{\mathrm{sc}}(i_{\mathrm{sc}} - i_{\mathrm{mpp}})}{i_{\mathrm{mpp}}(i_{\mathrm{mpp}} - 2i_{\mathrm{sc}})}\left(\gamma + \frac{E_{\mathrm{gc}}}{kT}\right)\right], \end{aligned} \tag{24}$$

where Eq. (14) has been used to eliminate the W functions. Likewise with $\beta^r_{i_{\mathrm{mpp}}}$ and $\beta^r_{P_{\mathrm{mpp}}}$, inserting Eq. (23) into (20) and (21) yields

$$\beta^r_{i_{\mathrm{mpp}}} = \frac{1}{T}\left[T\frac{i'_{\mathrm{sc}}}{i_{\mathrm{sc}}} + \frac{(i_{\mathrm{sc}} - i_{\mathrm{mpp}})^2}{2i_{\mathrm{sc}}i_{\mathrm{mpp}} - i^2_{\mathrm{mpp}}}\left(\gamma + \frac{E_{\mathrm{gc}}}{kT}\right)\right], \tag{25}$$

$$\beta^r_{P_{\mathrm{mpp}}} = \frac{1}{T}\left[1 + T\frac{i'_{\mathrm{sc}}}{i_{\mathrm{sc}}} + \left(1 - \frac{i_{\mathrm{sc}}}{i_{\mathrm{mpp}}}\right)\left(\gamma + \frac{E_{\mathrm{gc}}}{kT}\right)\right]. \tag{26}$$

As for Eqs. (19), (20) and (21), it is straight forward to show that Eqs. (24), (25) and (26) also satisfy Eq. (8). Finally, it should be mentioned that alternative preliminary forms of Eqs. (24) and (25) were presented in Ref. [6].

5 Experimental Method

The theoretical expressions are compared to measurements of 18 solar cells with different bulk resistivities, ρ, and cell architectures. The cells are industrially fabricated from three different compensated p-type multi-crystalline silicon (mc-Si) ingots and can be divided into three groups: (a) $\rho = 1.3\ \Omega \cdot \mathrm{cm}$, *Aluminum Back Surface Field* (Al-BSF) cells, (b) $\rho = 0.5\ \Omega \cdot \mathrm{cm}$, *Passivated Emitter and Rear Cells* (PERC), (c) $\rho = 1.3\ \Omega \cdot \mathrm{cm}$, PERC. Each group contains six cells from various brick positions, numbered from 001-060, with position 001 denoting a cell from the bottom of the brick and position 060 denoting a cell from the top. The performance of the cells was measured with temperature dependent suns-V_{oc} using a NeonSee$^{\mathrm{TM}}$ AAA sun simulator with a built-in water heater. This allowed for the acquisition of $i-V$ data without series resistance effects at a temperature range between 293 K and 343 K, and subsequently, calculation of the TCs. The suns-V_{oc} method was chosen to enable better comparison with the theoretical expressions, which do not account for series resistance effects.

6 Numerical Method

From the temperature dependent suns-V_{oc} measurements, the experimental values of V_{oc}, i_{sc}, V_{mpp}, i_{mpp}, P_{mpp} and FF were extracted at multiple temperatures. The corresponding TCs were determined by fitting the measured values to second degree polynomials of the temperature before calculating the derivative at each of the measured temperatures. This method is chosen over a simpler linear regression because some of the measured solar cell parameters (particularly i_{sc} and i_{mpp}) show dependencies with the temperature that are far from linear. Regarding the temperature dependence of the ideality factor, Eq. (1) was evaluated at the MPP to obtain

$$m = \frac{1}{V_{\mathrm{t}}} \frac{V_{\mathrm{mpp}} - V_{\mathrm{oc}}}{\log\left(1 - \frac{i_{\mathrm{mpp}}}{i_{\mathrm{sc}}}\right)}, \tag{27}$$

where Eq. (2) was used to eliminate i_{G} and i_0. Note that m is voltage dependent for most common solar cells. This was also the case for the studied cells. If one assumes that $m(V)$ is not going to vary significantly from V_{mpp} to V_{oc}, Eq. (27) can be used to estimate m at the measured temperatures and then fit to a polynomial to obtain $m(T)$.

7 Experimental and numerical results

In this section, the polynomials of the temperature corresponding to the measured values of V_{oc}, i_{sc}, V_{mpp}, i_{mpp}, $\beta^r_{V_{\mathrm{oc}}}$ and $\beta^r_{i_{\mathrm{sc}}}$ are used to evaluate Eqs. (19), (20), (21) and (22). The obtained values are then compared to the experimental relative TCs, which are calculated according to the method explained in section 6.

Figs. 1, 2, and 3 present the numerical results as follows: In the upper graph of each subfigure, the parameter of interest is plotted as a function of the cell temperature. Here, the crosses represent measured values. For example, in the top graph of Fig. 1(a), the crosses correspond to the experimental values of V_{mpp}. The continuous lines display the polynomials that fit the measurements. Each color represents a cell from the ingot position stated in the legend. In the lower graph of each subfigure, the relative TC is plotted as a function of the cell temperature. Here, the experimental TCs are displayed with crosses. The dashed lines show the TCs calculated with the proposed model. In the bottom graph of, e.g., Fig. 1(a), the dashed lines display TCs calculated with Eq. (19).

Starting with V_{mpp}, Figs. 1- 3(a) show a nearly linear dependence with the temperature for the measured cells. Eq. (19) describes reasonably well the measured

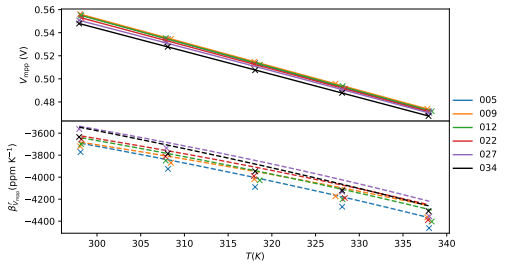

(a) V_{mpp} (top) and $\beta^r_{V_{\mathrm{mpp}}}$ (bottom) as a function of the cell temperature.

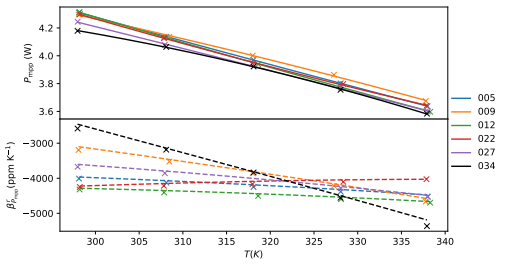

(b) P_{mpp} (top) and $\beta^r_{P_{\mathrm{mpp}}}$ (bottom) as a function of the cell temperature.

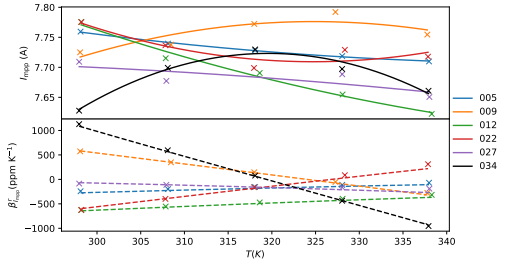

(c) i_{mpp} (top) and $\beta^r_{i_{\mathrm{mpp}}}$ (bottom) as a function of the cell temperature.

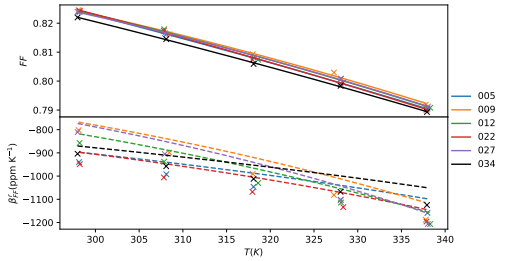

(d) FF (top) and β^r_{FF} (bottom) as a function of the cell temperature.

Figure 1: V_{mpp}, i_{mpp}, P_{mpp}, FF and their corresponding relative TCs as a function of the temperature for the cells in group (a). In all eight graphs, the experimental values and their TC are displayed with crosses. The continuous lines at the top graphs represent the polynomial fit of the measurements. The dashed lines at the bottom graphs correspond to the new expressions presented in this work.

$\beta^r_{V_{\rm mpp}}$ values, although discrepancies can be observed. In Fig. 1(a), the maximum discrepancy is of 3.2 %, found for the cell in position 022 at $T = 338$ K. A possible explanation for the discrepancies involves the possible non-ideal diode behavior of the measured cells. Some non-ideality is accounted for by the temperature dependent ideality factor, but this is still an approximation since the ideality factor in general may show some voltage dependency. Crystalline silicon cells are often better described with two-diode models rather than with Eq. (1). Noise in the measurements originating from the difficulties in stabilizing the temperature during the relatively long data acquisition times may also explain some of the discrepancy between the model and the experiments.

As for the temperature dependence of $P_{\rm mpp}$, some small nonlinearities can be observed in Figs. 1- 3(b) (see, e.g., the curves corresponding to the cells in positions 022 and 044 at the in the top graph of Fig. 1(b)) but the overall dependence with the temperature is approximately linear. Figs. 1- 3(b) show an excellent agreement between the measurements and the values predicted by Eq. (21). Here the relative discrepancies between the proposed model and the experiments are much smaller, typically below 1.5% for the cells in groups (a) and (c) and below 3% for the cells in groups (b).

In Figs. 1- 3(c), $i_{\rm mpp}$ and $\beta^r_{i_{\rm mpp}}$ are plotted as functions of the temperature. Here, a nonlinear dependence of $i_{\rm mpp}$ with the temperature of the cell can be observed. Moreover, in some of the measured cells, $i_{\rm mpp}$ appears to even have a local extremum. An example of this is the cell from position 034 in Fig. 1(c), where $i_{\rm mpp}(T)$ is clearly observed to have a maximum. This is mirrored in the bottom figure, where it can be seen that the curve for $\beta^r_{i_{\rm mpp}}(T)$ crosses zero. The nonlinear behavior of $i_{\rm mpp}$ can also be observed in Figs. 2(c) and 3(c) and it is particularly clear in cell 003 of group (b) and in cells 003 and 052 of group (c). In all three groups, the cells that show the clearest nonlinear behavior are positioned towards the top and bottom of the ingot. This may be coincidental, but it is worth noting that the concentration of impurities is higher towards the top (segregation) and bottom (diffusion) of the ingot. This suggests a connection between the nonlinear behavior of $i_{\rm mpp}$ and high impurity concentration. Despite the non-linear behavior of $i_{\rm mpp}$, the proposed model shows a reasonably good agreement with experimental values of $\beta^r_{i_{\rm mpp}}$ for all the studied cells. It can be concluded from Fig. 1(c) that restricting the temperature sensitivity of $i_{\rm mpp}$ of the studied cells to a single coefficient may be misleading. Although these nonlinearities originate, from a physical point of view, from the dependence of $\beta^r_{i_{\rm mpp}}$ with $\beta^r_{i_{\rm sc}}$ [3]; the nonlinear behavior of $i_{\rm mpp}$ can be implied from Eq. (5). If a single coefficient can describe the temperature sensitivity of $V_{\rm mpp}$ and $P_{\rm mpp}$, then, one can write $V_{\rm mpp} = a_1 T + b_1$ and $P_{\rm mpp} = a_2 T + b_2$. Here a_i are the slopes of the straight

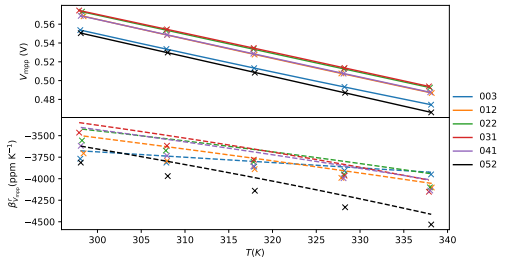

(a) V_{mpp} and $\beta^r_{V_{\text{mpp}}}$ as a function of the cell temperature.

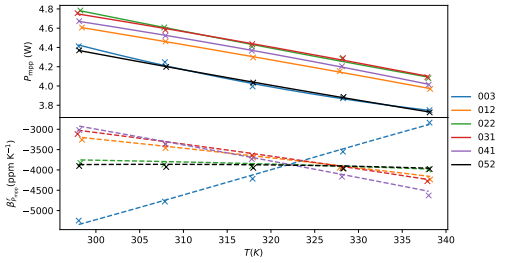

(b) P_{mpp} and $\beta^r_{P_{\text{mpp}}}$ as a function of the cell temperature.

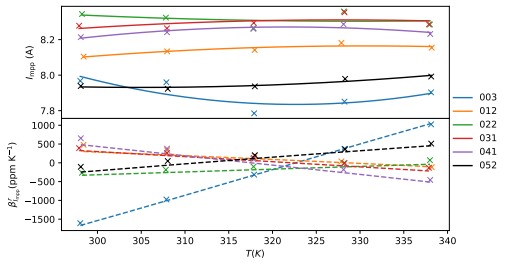

(c) i_{mpp} and $\beta^r_{i_{\text{mpp}}}$ as a function of the cell temperature.

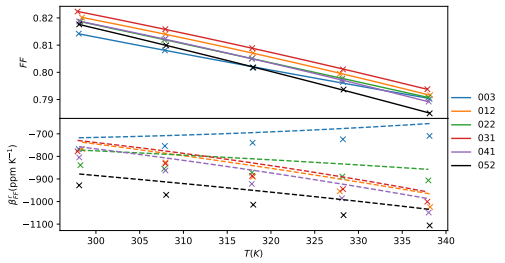

(d) FF and β^r_{FF} as a function of the cell temperature.

Figure 2: V_{mpp}, i_{mpp}, P_{mpp}, FF and their corresponding relative TCs as a function of the temperature for the cells in group (b).

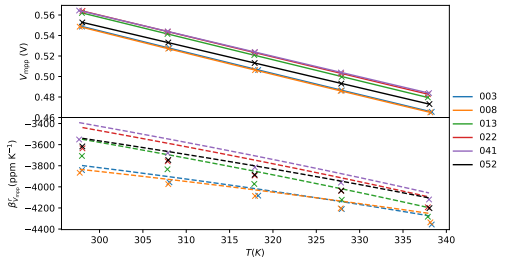

(a) V_{mpp} and $\beta^r_{V_{\mathrm{mpp}}}$ as a function of the cell temperature.

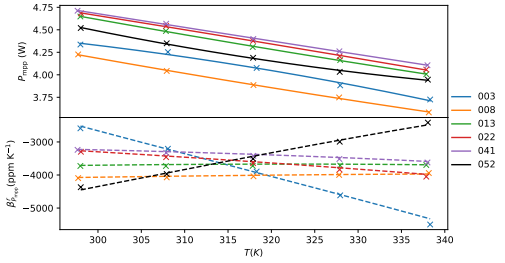

(b) P_{mpp} and $\beta^r_{P_{\mathrm{mpp}}}$ as a function of the cell temperature.

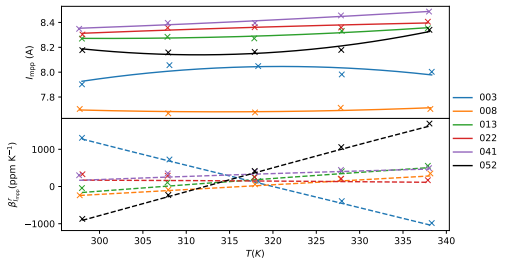

(c) i_{mpp} and $\beta^r_{i_{\mathrm{mpp}}}$ as a function of the cell temperature.

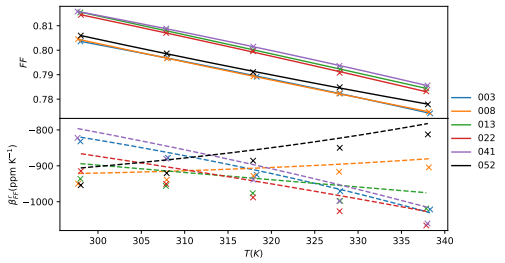

(d) FF and β^r_{FF} as a function of the cell temperature.

Figure 3: V_{mpp}, i_{mpp}, P_{mpp}, FF and their corresponding relative TCs as a function of the temperature for the cells in group (c).

lines, equal to the corresponding absolute TC, i.e., $a_1 = \beta_{V_{\mathrm{mpp}}}$ and $a_2 = \beta_{P_{\mathrm{mpp}}}$, and b_i are the parameters in question at $T = 0$ K. Since V_{mpp} and P_{mpp} must follow Eq. (5), i_{mpp} must be given by

$$i_{\mathrm{mpp}} = \frac{a_2 T + b_2}{a_1 T + b_1}, \tag{28}$$

which is not a linear function and, therefore, its derivative is not a constant. Therefore V_{mpp}, i_{mpp} and P_{mpp} cannot be linearly dependent on the temperature simultaneously.

Figs. 1- 3(d) show FF and β^r_{FF} plotted as functions of the temperature for the cells in groups (a), (b) and (c), respectively. Here, some small bends in the curves can be observed but, overall, the dependence with the temperature of the measurements is well described by straight lines. Here, the discrepancy between the predicted values and the experiments may also be attributed to temperature noise in the measurements and the diode model employed in the derivation of the expressions. Still, the proposed model predicts reasonably well the experimental values.

8 Conclusions

In this work, analytical expressions that describe the temperature sensitivity of the maximum power point have been derived. The expressions were tested with measurements from 18 multicrystalline silicon solar cells with different bulk resistivities and cell architectures. It was found that the new model describes with low discrepancy the temperature sensitivity of the investigated parameters and is in very good agreement with the experimental values.

From Eq. (28), it was concluded that not all parameters of a solar cell can vary linearly with the temperature at the same time. Using a single valued TC, though practical, may therefore be misleading. Additionally, it is worth noting that a single TC does not provide any information of the temperature sensitivity of the solar cell outside of the normal operating temperature interval, where linear dependence with temperature is usually assumed [3]. Contrary to previous literature, the model presented in this work shows how the temperature coefficient of solar cell parameters may vary with the temperature and, since no assumptions have been made regarding the temperature dependence of the parameters, the derived expressions describe the temperature sensitivity of the maximum power point at any given temperature. Finally, with respect to further developments, the techniques and methods employed in this work may be used to derive expressions for the TCs that include the effect of the series resistance [13, 14]. This would not only allow for a more accurate description of

the temperature sensitivity of the MPP, but also potentially gaining understanding of the temperature sensitivity of the series resistance.

Appendix D

Analytical Modeling of the Maximum Power Point with Series Resistance

Analytical Modeling of the Maximum Power Point with Series Resistance

Alfredo Sanchez Garcia and Rune Strandberg
University of Agder, Grimstad, 4879, Norway

Abstract

This paper presents new analytical expressions for the maximum power point voltage, current, and power that have an explicit dependence on the series resistance. An explicit expression that relates the series resistance to well-known solar cell parameters was also derived. The range of the validity of the model, as well as the mathematical assumptions taken to derive it are explained and discussed. To test the accuracy of the derived model, a numerical single-diode model with solar cell parameters whose values can be found in the latest installment of the solar cell efficiency tables was used. The accuracy of the derived model was found to increase with increasing bandgap and to decrease with increasing series resistance. An experimental validation of the analytical model is provided and its practical limitations addressed. The new expressions predicted the maximum power obtainable by the studied cells with estimated errors below 0.1% compared to the numerical model, for typical values of the series resistance.

1 Introduction

Shockley's diode equation describes how a solar cell responds to bias and illumination [1]. Analytical expressions for photovoltaic parameters, such as the open-circuit voltage, V_{oc}, or the short-circuit current, i_{sc}, can easily be derived from it. When series resistance is accounted for, however, the diode equation becomes an implicit expression of the current, which is not as straightforward to work with. Some work has been performed aiming to quantify analytically the effect of series resistance on various solar cell parameters. Banwell et al. showed that Lambert's W function allows for a closed-form expression of the current when the effect of series resistance

is considered [2]. Jain et al. derived, in [3], an analogue to Banwell's expression that also accounted for the effect of shunt resistance. The latter authors later made use of this expression to derive analytical expressions for V_{oc} and i_{sc}. The maximum power point (MPP) has been little explored from an analytical perspective, although some exceptions exist [4, 5, 6, 7, 8]. The reason for this lies in the fact that, when series resistance is considered, deriving an expression for the maximum power point voltage, V_{mpp}, involves solving a transcendental equation. Such equations often do not have closed-form solutions and need to be solved numerically. It is worth mentioning the work presented in [4], where Singal was able to obtain an approximate closed-form expression of V_{mpp}, in terms of V_{oc}. In contrast with a numerical model, an analytical model would allow identifying the physical parameters affecting the MPP. Accounting for the series resistance in the analytical model for the MPP would also allow for better characterization of real solar cells. In this sense, such a model would describe the MPP with higher accuracy than other analytical models that do not account for the effect of series resistance. The lack of an accurate analytical model for the MPP, which includes series resistance, in the scientific literature represents a research gap that this work aims to fill. To this end, a closed-form expression for the maximum power point voltage that accounts for the effect of the series resistance is derived. The starting point of the derivation is the analytical expression for the current, derived by Banwell in [2], in terms of Lambert's W function. It is then argued that, at the maximum power point, the argument of the W function is small enough to accurately approximate the function value. This makes the transcendental problem analytically solvable. The accuracy of the derived model was found to increase with increasing bandgap energy and to decrease with increasing series resistance. From the new expression for V_{mpp}, an analytical expression for the series resistance was then derived. Additionally, approximate analytical expressions for the maximum power point current, i_{mpp}, and power, P_{mpp}, were derived. Numerical results were calculated using parameters typical for seven different solar cell technologies. The accuracy of the model was tested through a comparison with reference values that were obtained from a numerical single-diode model. The results showed that the analytic model can predict the maximum power with relative errors below 0.1% when compared to the numerical model, when typical values of the series resistance are used. Still, it must be kept in mind that the analytical approach derived in the present work corresponds to a one-diode model. This implies that it should not be used with solar cells that follow, e.g., the double-diode equation. For such cells, different techniques, such as those proposed in [9], should be employed. Finally, the practical limitations of the model are discussed based on its experimental validation, provided in [10]. Whereas the present work focuses on the derivation, range of validity, and

theoretical limitations of the model from a formal perspective, in [10] the focus was on its experimental applicability.

To summarize, this work presents a novel approach based on the use of Lambert's W function to obtain closed-form analytical expressions for the MPP that account for the effect of the series resistance.

2 Background

Assuming nondegenerate conditions, the total current density, i, produced by a solar cell is given by Shockley's diode equation [11],

$$i = i_{\mathrm{G}} - i_0 \exp\left[\frac{V}{V_{\mathrm{t}}}\right], \tag{1}$$

where V is the voltage and i_{G} and i_0 are the *generation* and *thermal recombination* [12] currents, respectively. Here, the thermal voltage, V_{t}, given by $qV_{\mathrm{t}} = kT$ with T, k, and q being the cell temperature, Boltzmann's constant, and the electron charge, respectively, is introduced. The total power density, P, is given by the product $P = Vi$ [13]. At the maximum power point, it holds that:

$$\frac{\mathrm{d}}{\mathrm{d}V}P = i + V\frac{\mathrm{d}}{\mathrm{d}V}i = 0. \tag{2}$$

Khanna et al. found that Equation (2) is solved by [14, 15]:

$$V_{\mathrm{mpp}} = V_{\mathrm{t}}\left(\mathrm{W}\left[\frac{i_{\mathrm{G}}}{i_0}e\right] - 1\right), \tag{3}$$

where $\mathrm{W}(x)$, defined by $x = \mathrm{W}(xe^x)$, is Lambert's W function [16]. An expression for the maximum power point current, i_{mpp}, can be obtained by inserting Equation (3) into Equation (1), and an expression for the maximum power, P_{mpp}, is obtained from the product $P_{\mathrm{mpp}} = V_{\mathrm{mpp}}i_{\mathrm{mpp}}$. This yields [14, 15]:

$$i_{\mathrm{mpp}} = i_{\mathrm{G}}\left(1 - \frac{1}{\mathrm{W}\left[\frac{i_{\mathrm{G}}}{i_0}e\right]}\right), \tag{4}$$

$$P_{\mathrm{mpp}} = i_{\mathrm{G}}V_{\mathrm{t}}\left(\mathrm{W}\left[\frac{i_{\mathrm{G}}}{i_0}e\right] - 2 + \frac{1}{\mathrm{W}\left[\frac{i_{\mathrm{G}}}{i_0}e\right]}\right). \tag{5}$$

When series resistance is accounted for, Equation (1) becomes [13]:

$$i = i_{\mathrm{G}} - i_0 \exp\left[\frac{V + ir}{V_{\mathrm{t}}}\right], \tag{6}$$

where r is the cell series resistance ($[r] = \Omega \cdot \mathrm{cm}^2$). Banwell et al. proved in [2] that Lambert's W function allows for an explicit expression for i. Defining the voltages V_{G} and V_0 as $V_{\mathrm{G}} = i_{\mathrm{G}} r$ and $V_0 = i_0 r$, Equation (6) becomes [2]:

$$i = i_{\mathrm{G}} - \frac{V_{\mathrm{t}}}{r}\mathrm{W}\left[\frac{V_0}{V_{\mathrm{t}}}\exp\left[\frac{V_{\mathrm{G}}}{V_{\mathrm{t}}} + \frac{V}{V_{\mathrm{t}}}\right]\right], \tag{7}$$

from which it can be seen that in the limit $r \to 0$, Equation (1) is recovered.

3 The Maximum Power Point

Let $z(V)$ denote the argument of Lambert's W function in Equation (7), and let $z_{\mathrm{mpp}} := z(V_{\mathrm{mpp}})$. Inserting Equation (7) into Equation (2) yields:

$$\begin{aligned}
0 = \left[i + V\frac{\mathrm{d}}{\mathrm{d}V}i\right]_{V=V_{\mathrm{mpp}}} &= i(V_{\mathrm{mpp}}) + V_{\mathrm{mpp}}\frac{-V_{\mathrm{t}}}{r}\frac{\mathrm{W}(z_{\mathrm{mpp}})}{1+\mathrm{W}(z_{\mathrm{mpp}})}\left[\frac{\mathrm{d}}{\mathrm{d}V}\log z\right]_{V=V_{\mathrm{mpp}}} \\
&= i_{\mathrm{G}} - \frac{V_{\mathrm{t}}}{r}\mathrm{W}(z_{\mathrm{mpp}}) - \frac{V_{\mathrm{mpp}}}{r}\frac{\mathrm{W}(z_{\mathrm{mpp}})}{1+\mathrm{W}(z_{\mathrm{mpp}})} \\
&= \frac{V_{\mathrm{t}}}{r}\mathrm{W}(z_{\mathrm{mpp}})\left[\frac{1}{\mathrm{W}(z_{\mathrm{mpp}})}\frac{i_{\mathrm{G}} r}{V_{\mathrm{t}}} - 1 - \frac{V_{\mathrm{mpp}}/V_{\mathrm{t}}}{1+\mathrm{W}(z_{\mathrm{mpp}})}\right] \\
&= \frac{1}{\mathrm{W}(z_{\mathrm{mpp}})}\frac{V_{\mathrm{G}}}{V_{\mathrm{t}}} - \frac{1+\mathrm{W}(z_{\mathrm{mpp}}) + \frac{V_{\mathrm{mpp}}}{V_{\mathrm{t}}}}{1+\mathrm{W}(z_{\mathrm{mpp}})},
\end{aligned} \tag{8}$$

where the derivative of Lambert's W function, found in, e.g., [16], is used. Equation (8) is a transcendental equation in V_{mpp} and does not have a closed-form solution. Values for V_{mpp} can be calculated by solving Equation (8) numerically.

3.1 Maximum Power Point Voltage

The Taylor expansion of the principal branch of Lambert's W function, W_0, is given by:

$$\mathrm{W}_0(x) = \sum_{n=1}^{\infty}\frac{(-n)^{n-1}}{n!}x^n = x - x^2 + \frac{3}{2}x^3 - \frac{8}{3}x^4 \ldots \tag{9}$$

which converges as long as $x \leq {}^{1}/_{e}$. The series expansion in Equation (9) can be used to find an approximate analytical solution to Equation (8). To do so, notice that z_{mpp} may be small for typical solar cells. To see this, note that i_0 is given by $i_0 \approx qCV_{\mathrm{t}} \exp\left[-{}^{E_g}/_{qV_{\mathrm{t}}}\right] E_g^2$, where E_{g} is the bandgap of the semiconductor and C is a constant involving the speed of light, Planck's constant, and the external radiative efficiency (ERE) [17]. The latter is used to account for nonradiative recombination. $z(V)$ can then be written as:

$$z(V) = rCE_{\mathrm{g}}^2 \exp\left[\frac{V}{V_{\mathrm{t}}} - \frac{E_{\mathrm{g}}/q}{V_{\mathrm{t}}} + \frac{i_{\mathrm{G}} r}{V_{\mathrm{t}}}\right]. \tag{10}$$

The voltage is limited by the bandgap, and therefore, it holds that $V - {}^{E_{\mathrm{g}}}/_{q} < 0$. As long as the value of r is not excessively large, the exponent in Equation (10) will be negative, resulting in a small z. Assuming a reasonable cell quality, the series expansion in Equation (9) can be used to approximate $\mathrm{W}(z_{\mathrm{mpp}})$ by z_{mpp} in Equation (8). To show this, Figure 1 displays the values of $\mathrm{W}(z_{\mathrm{mpp}})$ (continuous lines) and z_{mpp} (crosses) as a function of the bandgap for various values of r. There, it is confirmed that, for large bandgaps, $\mathrm{W}(z_{\mathrm{mpp}})$ is well approximated by z_{mpp}, even for values of r up to 5 $\Omega \cdot \mathrm{cm}^2$. As expected from Equation (10), Figure 1 shows that the approximation is more accurate for lower values of r. In this context, it is worth noting that typical values for area-normalized series resistance usually are below 2 $\Omega \cdot \mathrm{cm}^2$ for both laboratory and commercial solar cells [18]. Therefore, $\mathrm{W}(z_{\mathrm{mpp}})$ should be well approximated by z_{mpp} for most solar cells. Figure 1 is obtained assuming an AM1.5G spectrum and ERE value of 10^{-4}. The displayed values correspond to values of V_{mpp} that were obtained by solving Equation (8) numerically for various values of r and E_{g}. Approximating $\mathrm{W}(z_{\mathrm{mpp}})$ by z_{mpp} in Equation (8) results in:

$$\frac{1}{z_{\mathrm{mpp}}} \frac{V_{\mathrm{G}}}{V_{\mathrm{t}}} = \frac{1 + z_{\mathrm{mpp}} + \frac{V_{\mathrm{mpp}}}{V_{\mathrm{t}}}}{1 + z_{\mathrm{mpp}}}. \tag{11}$$

Focusing now on the right-hand side of Equation (11), since z_{mpp} needs to be small so that the approximation $\mathrm{W}(z_{\mathrm{mpp}}) \approx z_{\mathrm{mpp}}$ is accurate, the term ${}^{V_{\mathrm{mpp}}}/_{V_{\mathrm{t}}}$ will dominate over z_{mpp} in the numerator. Equation (11) can then be simplified to:

$$\frac{1}{z_{\mathrm{mpp}}} \frac{V_{\mathrm{G}}}{V_{\mathrm{t}}} = \frac{1 + \frac{V_{\mathrm{mpp}}}{V_{\mathrm{t}}}}{1 + z_{\mathrm{mpp}}}, \tag{12}$$

which is analytically solvable. The first step in finding the solution is to insert z_{mpp}.

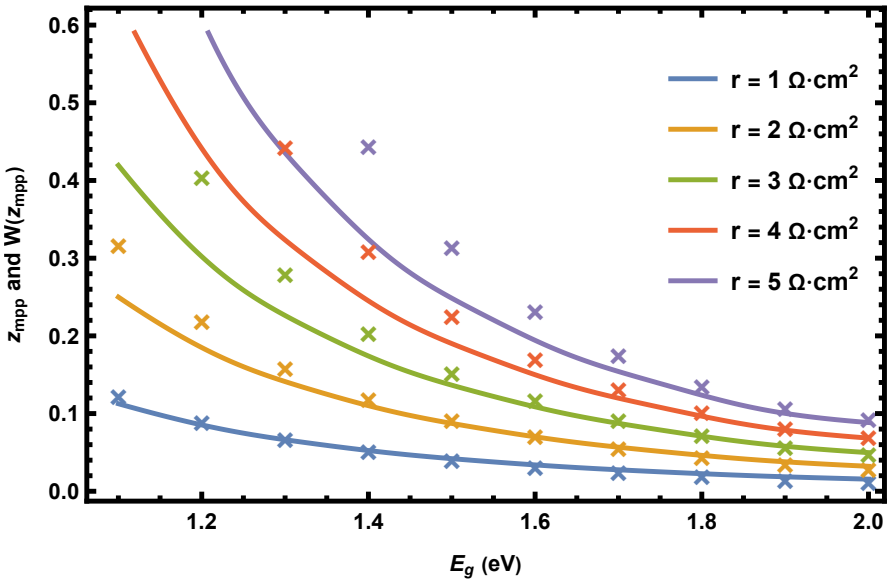

Figure 1: $\mathrm{W}(z_{\mathrm{mpp}})$ (continuous lines) and z_{mpp} (crosses) as a function of the energy gap, E_{g}, for various values of r. The graph is obtained assuming an AM 1.5G spectrum and ERE $= 10^{-4}$. The V_{mpp} values are obtained by solving Equation (8) numerically.

After a bit of manipulation, Equation (12) becomes:

$$\left(1+\frac{V_{\mathrm{mpp}}-V_{\mathrm{G}}}{V_{\mathrm{t}}}\right)\exp\left[1+\frac{V_{\mathrm{mpp}}-V_{\mathrm{G}}}{V_{\mathrm{t}}}\right]=\frac{V_{\mathrm{G}}}{V_0}\exp\left[1-2\frac{V_{\mathrm{G}}}{V_{\mathrm{t}}}\right], \tag{13}$$

which has the closed-form solution:

$$V_{\mathrm{mpp}}=V_{\mathrm{G}}+V_{\mathrm{t}}\left(\mathrm{W}\left[\frac{V_{\mathrm{G}}}{V_0}\exp\left[1-2\frac{V_{\mathrm{G}}}{V_{\mathrm{t}}}\right]\right]-1\right). \tag{14}$$

Finally, inserting the definitions for V_{G} and V_0 yields:

$$V_{\mathrm{mpp}}=i_{\mathrm{G}}r+V_{\mathrm{t}}\left(\mathrm{W}\left[\frac{i_{\mathrm{G}}}{i_0}\exp\left[1-2\frac{i_{\mathrm{G}}r}{V_{\mathrm{t}}}\right]\right]-1\right), \tag{15}$$

from which it can be seen that, in the limit $r\to 0$, Equation (15) becomes Equation (3).

3.2 Maximum Power Point Current and Power

In order to obtain expressions for i_{mpp} and P_{mpp}, Equation (15) has to be inserted into Equation (7). This results in a composite of W functions that cannot be simplified. A simpler approximate expression for i_{mpp} can be obtained by noting that at the maximum power point, the W function in Equation (7) is evaluated at $z(V) = z_{\mathrm{mpp}}$. Since z_{mpp} needs to be small for Equation (15) to be accurate, $\mathrm{W}(z_{\mathrm{mpp}})$ can be approximated by z_{mpp} here as well. From Equation (7), this yields:

$$\begin{aligned} i_{\mathrm{mpp}} = i_{\mathrm{G}} - \frac{V_{\mathrm{t}}}{r}\mathrm{W}(z_{\mathrm{mpp}}) &\approx\ i_{\mathrm{G}} - \frac{V_{\mathrm{t}}}{r} z_{\mathrm{mpp}} \\ &=\ i_{\mathrm{G}} - i_0 \exp\left[\frac{V_{\mathrm{mpp}}}{V_{\mathrm{t}}} + \frac{V_{\mathrm{G}}}{V_{\mathrm{t}}}\right]. \end{aligned} \tag{16}$$

An analytical expression for i_{mpp} can now be obtained by inserting Equation (15) into (16), and an analytical expression for P_{mpp} can be found by evaluating $V_{\mathrm{mpp}} \cdot i_{\mathrm{mpp}}$. To shorten the notation, let $\alpha(r)$ denote the argument of the W function in Equation (15). The approximate analytical expressions for i_{mpp} and P_{mpp} then become:

$$i_{\mathrm{mpp}} = i_{\mathrm{G}}\left(1 - \frac{1}{\mathrm{W}\left[\alpha(r)\right]}\right), \tag{17}$$

$$P_{\mathrm{mpp}} = i_{\mathrm{G}}^2 r\left(1 - \frac{1}{\mathrm{W}\left[\alpha(r)\right]}\right) + i_{\mathrm{G}} V_{\mathrm{t}}\left(\mathrm{W}\left[\alpha(r)\right] - 2 + \frac{1}{\mathrm{W}\left[\alpha(r)\right]}\right). \tag{18}$$

Note that in the limit $r \to 0$, Equations (4) and (5) are recovered.

3.3 Practical Note

For practical applications of Equations (15), (17), and (18), it is worth noting that i_{G} is well approximated by i_{sc}, even though the latter is dependent on the series resistance. In the case of, e.g., silicon under an AM 1.5G spectrum, i_{G} and i_{sc} practically overlap for values of r up to about 11 $\Omega \cdot \mathrm{cm}^2$. Additionally, note that the quotient ${}^{i_{\mathrm{sc}}}\!/_{i_0}$ can be expressed as $\exp\left({}^{V_{\mathrm{oc}}}\!/_{V_{\mathrm{t}}}\right)$. Equation (15) then becomes:

$$V_{\mathrm{mpp}} = i_{\mathrm{sc}} r + V_{\mathrm{t}}\left(\mathrm{W}\left[\exp\left[1 + \frac{V_{\mathrm{oc}}}{V_{\mathrm{t}}} - 2\frac{i_{\mathrm{sc}} r}{V_{\mathrm{t}}}\right]\right] - 1\right). \tag{19}$$

These practical substitutions may be also applied to Equations (17) and (18).

4 Analytical Expression for the Series Resistance

From Equation (19), it is possible to obtain r as a function of V_{mpp}. To see this, note that Equation (19) can be rewritten as:

$$1 + \frac{V_{\mathrm{mpp}} - i_{\mathrm{sc}} r}{V_{\mathrm{t}}} = \mathrm{W}\left[\exp\left[1 + \frac{V_{\mathrm{oc}}}{V_{\mathrm{t}}} - 2\frac{i_{\mathrm{sc}} r}{V_{\mathrm{t}}}\right]\right], \tag{20}$$

which is equivalent to:

$$\left(1 + \frac{V_{\mathrm{mpp}} - i_{\mathrm{sc}} r}{V_{\mathrm{t}}}\right) \exp\left[1 + \frac{V_{\mathrm{mpp}} - i_{\mathrm{sc}} r}{V_{\mathrm{t}}}\right] = \exp\left[1 + \frac{V_{\mathrm{oc}}}{V_{\mathrm{t}}} - 2\frac{i_{\mathrm{sc}} r}{V_{\mathrm{t}}}\right], \tag{21}$$

which is seen by applying Lambert's W function to both sides of Equation (21) and using the definition $x = \mathrm{W}(xe^x)$. Multiplying both sides by $\exp\left[-2^{V_{\mathrm{mpp}}}/_{V_{\mathrm{t}}} + 2^{i_{\mathrm{sc}} r}/_{V_{\mathrm{t}}}\right]$ yields:

$$\exp\left[1 + \frac{V_{\mathrm{oc}}}{V_{\mathrm{t}}} - 2\frac{V_{\mathrm{mpp}}}{V_{\mathrm{t}}}\right] = \left(1 + \frac{V_{\mathrm{mpp}} - i_{\mathrm{sc}} r}{V_{\mathrm{t}}}\right) \exp\left[1 - \frac{V_{\mathrm{mpp}} - i_{\mathrm{sc}} r}{V_{\mathrm{t}}}\right]. \tag{22}$$

Finally, multiplying both sides by $-e^{-2}$ gives:

$$-\exp\left[-1 + \frac{V_{\mathrm{oc}}}{V_{\mathrm{t}}} - 2\frac{V_{\mathrm{mpp}}}{V_{\mathrm{t}}}\right] = \left(-1 - \frac{V_{\mathrm{mpp}} - i_{\mathrm{sc}} r}{V_{\mathrm{t}}}\right) \exp\left[-1 - \frac{V_{\mathrm{mpp}} - i_{\mathrm{sc}} r}{V_{\mathrm{t}}}\right], \tag{23}$$

which can be inverted by making use of Lambert's W function. After some manipulation, r can be expressed as:

$$r = \frac{V_{\mathrm{mpp}}}{i_{\mathrm{sc}}} + \frac{V_{\mathrm{t}}}{i_{\mathrm{sc}}}\left(\mathrm{W}\left[-\exp\left[-1 + \frac{V_{\mathrm{oc}}}{V_{\mathrm{t}}} - 2\frac{V_{\mathrm{mpp}}}{V_{\mathrm{t}}}\right]\right] + 1\right). \tag{24}$$

4.1 Validity of the Approximate Expression

Equation (24) sets the limit for the range of r where Equation (19) describes the physical behavior of V_{mpp}. As the exponential function only yields positive values, the argument of Lambert's W in Equation (24) is negative. The principal branch of Lambert's W function, $\mathrm{W}_0(z)$, is only defined for $z \geq -1/e$, which implies that $\mathrm{W}(z) \notin \mathcal{R}$ for $z \leq -1/e$. Since the series resistance is a real-valued physical quantity, the argument of the W function in Equation (24) must fulfill:

$$\exp\left[-1 + \frac{V_{\mathrm{oc}}}{V_{\mathrm{t}}} - 2\frac{V_{\mathrm{mpp}}}{V_{\mathrm{t}}}\right] \leq \frac{1}{e}, \tag{25}$$

which implies:

$$V_{\mathrm{mpp}} \geq \frac{1}{2} V_{\mathrm{oc}}. \tag{26}$$

Equation (26) sets an upper limit for the series resistance, as having V_{mpp} less than $\frac{1}{2}V_{\mathrm{oc}}$ would require a complex-valued r. This translates into Equation (15) not describing a physical V_{mpp} for any value of the series resistance, which would make V_{mpp} smaller than $V_{\mathrm{oc}}/2$. This maximum value of the resistance, which is denoted in the present work by r_{max}, is found by evaluating Equation (24) at $V_{\mathrm{mpp}} = V_{\mathrm{oc}}/2$. This yields:

$$r_{\mathrm{max}} = r\left[\frac{V_{\mathrm{oc}}}{2}\right] = \frac{V_{\mathrm{oc}}/2}{i_{\mathrm{sc}}} + \frac{V_{\mathrm{t}}}{i_{\mathrm{sc}}}\left(\mathrm{W}\left[-\frac{1}{e}\right] + 1\right) = \frac{V_{\mathrm{oc}}}{2i_{\mathrm{sc}}}.$$

Note that at $r = r_{\mathrm{max}}$, the parentheses in Equation (19) cancel out. For $r \geq r_{\mathrm{max}}$, the W function tends asymptotically to zero. This results in V_{mpp} increasing linearly with r with slope i_{sc}, which is not physical.

4.2 Accuracy of the Approximation

The accuracy of Equation (15) decreases with increasing series resistance. For sufficiently large r, the term involving z_{mpp} in the numerator on the right-hand side of Equation (11) will not be small in comparison to $V_{\mathrm{mpp}}/V_{\mathrm{t}}$, implying that Equation (15) will be less accurate. Therefore, it is relevant to determine the value of the series resistance, r_{L}, until the derived model gives the acceptable results. The value $r_{\mathrm{L}} = r_{\mathrm{max}}/3$ is proposed as a rule of thumb. This corresponds roughly to $z_{\mathrm{mpp}} \approx 1/e$, which seems a natural choice since for $z_{\mathrm{mpp}} \geq 1/e$, the Taylor expansion in Equation (9) should not be applicable as z_{mpp} would be larger than the convergence radius of the expansion. Determining the actual value of r that makes $z_{\mathrm{mpp}} = 1/e$ would require solving simultaneously $z_{\mathrm{mpp}} - 1/e = 0$ and Equation (8), which is rather counterproductive, since the main point of making use of Equation (15) is to avoid solving Equation (8) numerically.

5 Numerical Results

In this section, the accuracy of Equation (19) is tested. For this, the focus is on V_{mpp} and P_{mpp}, given by $P_{\mathrm{mpp}} = V_{\mathrm{mpp}} i(V_{\mathrm{mpp}})$, with i being given by Equation (7). The label "mod" is used to denote the values of V_{mpp} and P_{mpp} obtained from Equation (19). The label "ref" is used to denote the reference values to which $V_{\mathrm{mpp}}^{\mathrm{mod}}$ and $P_{\mathrm{mpp}}^{\mathrm{mod}}$ are compared. The "ref" quantities are obtained by numerically solving Equation (8).

The accuracy of Equations (17) and (18) is also tested, and the label "app" is used to denote these.

For all numerical calculations, the AM 1.5G spectrum was assumed. The numerical single-diode model used to test the accuracy of Equation (19) was fed with cell parameters corresponding to six different technologies found in the latest installment of the solar cell efficiency tables [19]. The parameters corresponding to these cells are summarized in Table 1. As a seventh case, the derived model was also tested against a numerical single-diode model using $E_\mathrm{g} = 1.125$ eV and ERE $= 10^{-4}$. These values are typical for silicon cells. This case is therefore referred to as a numerically modeled silicon cell. All cells were assumed to be at a temperature of 300 K. Figure 2 displays (a) V_mpp, (b) i_mpp, and (c) P_mpp as a function of the series resistance. Additionally, the corresponding current–voltage characteristic (Figure 2d) is shown for several values of the series resistance. All curves correspond to the numerically modeled silicon cell described above. In Figure 2d, dotted lines show how the maximum power point changes with increasing series resistance. The red dotted line was obtained by solving Equation (8) numerically, for multiple values of the series resistance, and evaluating Equation (7) with the obtained V_mpp values. The purple dotted line was obtained from Equation (15). The values for r_L and r_max (Figure 2a–c) and their correspondent values of V_mpp (Figure 2d) are displayed with black vertical dashed lines. From Figure 2a–c, it can be seen that the values calculated with the new analytical model were in good agreement with the numerical reference model for $r \leq r_\mathrm{L}$. For $r \geq r_\mathrm{L}$, $V_\mathrm{mpp}^\mathrm{mod}$ appears to be underestimated (Figure 2a) and $i_\mathrm{mpp}^\mathrm{mod}$ overestimated (Figure 2b). As a result, $P_\mathrm{mpp}^\mathrm{mod}$ overlaps well with $P_\mathrm{mpp}^\mathrm{ref}$ (Figure 2c). Finally, for $r \geq r_\mathrm{max}$, $V_\mathrm{mpp}^\mathrm{mod}$ appears to increase with increasing series resistance.

Table 1: Parameters for selected single-junction solar cell technologies. The ERE values were estimated from Equation (27).

Device	$\boldsymbol{E_\mathrm{g}}$ **(eV)**	$\boldsymbol{V_\mathrm{oc}}$ **(V)**[1]	$\boldsymbol{i_\mathrm{sc}}$ **(mA/cm²)**[1]	**ERE (%)**
InP	1.34	0.939	31.15	0.365
GaAs	1.42	1.107	29.60	14.510
CdTe	1.51	0.876	30.25	10^{-4}
CIGS	1.08	0.734	39.58	1.750
a-Si	1.69	0.896	16.36	1.96×10^{-7}
PSC [2]	1.60	1.042	20.40	0.002

[1] The V_oc and i_sc values were measured under the AM 1.5G spectrum at T = 300 K [19].
[2] Perovskite solar cell.

The accuracy of the expression for $V_\mathrm{mpp}^\mathrm{mod}$, Equation (19), decreases with increasing

Table 2: Comparison of V_{mpp} and P_{mpp} for various values of area-normalized series resistance. The values correspond to a numerically modeled Si cell ($E_{\mathrm{g}} = 1.125$ eV) with ERE $= 10^{-4}$ at T $= 300$ K.

r ($\Omega \cdot \mathrm{cm}^2$)	V_{mpp} (V)		Error (%)	P_{mpp} (W)		Error (%)
	$V_{\mathrm{mpp}}^{\mathrm{mod}}$	$V_{\mathrm{mpp}}^{\mathrm{ref}}$		$P_{\mathrm{mpp}}^{\mathrm{mod}}$	$P_{\mathrm{mpp}}^{\mathrm{ref}}$	
0	0.559	0.559	10^{-4}	5.414	5.414	10^{-8}
0.5	0.539	0.540	0.153	5.213	5.213	0.003
1.5	0.500	0.503	0.629	4.813	4.815	0.034
2.0	0.480	0.485	1.032	4.615	4.618	0.066
5.0	0.371	0.390	4.906	3.477	3.502	0.728

resistance. This can be seen in Figure 3, where V_{mpp} is plotted as a function of the series resistance for the six technologies presented in Table 1. The dashed lines correspond to the reference values, $V_{\mathrm{mpp}}^{\mathrm{ref}}$ and the continuous lines to $V_{\mathrm{mpp}}^{\mathrm{mod}}$. The points corresponding to a series resistance equal to r_{L} are marked with crosses. Focusing on the graphs representing the CIGS cell, the mismatch between $V_{\mathrm{mpp}}^{\mathrm{ref}}$ and $V_{\mathrm{mpp}}^{\mathrm{mod}}$ becomes noticeable for $r \geq r_{\mathrm{L}}$. For additional comparison, the V_{mpp} calculated from Equation (3) (i.e., without series resistance) for the GaAs cell is displayed in Figure 3. This is represented by the blue straight line with zero slope. At $r = 0\ \Omega \cdot \mathrm{cm}^2$, $V_{\mathrm{mpp}}^{\mathrm{ref}}$, $V_{\mathrm{mpp}}^{\mathrm{mod}}$, and Equation (3) overlap, but as soon as r starts increasing, Equation (19) predicts the value of $V_{\mathrm{mpp}}^{\mathrm{ref}}$ with higher accuracy. Finally, it is worth mentioning that the overlap between $V_{\mathrm{mpp}}^{\mathrm{mod}}$ and $V_{\mathrm{mpp}}^{\mathrm{ref}}$ is particularly good with the perovskite (PSC) and the amorphous silicon (a-Si) solar cells due to their large bandgaps. Table 2 displays the values of V_{mpp} and P_{mpp} corresponding to the numerically modeled Si cell shown in Figure 2 for various values of the series resistance. From the left, the first column presents five values of area-normalized series resistance. In the second column, the values of $V_{\mathrm{mpp}}^{\mathrm{mod}}$ and $V_{\mathrm{mpp}}^{\mathrm{ref}}$ are presented, followed by their relative discrepancy in %. The three remaining columns follow the same structure, but with the values of $P_{\mathrm{mpp}}^{\mathrm{mod}}$ and $P_{\mathrm{mpp}}^{\mathrm{ref}}$. Table 2 shows that the higher the series resistance, the higher the discrepancy is. Nevertheless, the model derived in the present work has a reasonable accuracy and is able to predict the value of P_{mpp} with an error below 0.75% for series resistance up to $5\ \Omega \cdot \mathrm{cm}^2$ for this numerically modeled cell.

Figure 4 displays the base-10 logarithm of the relative discrepancy (in %) between $P_{\mathrm{mpp}}^{\mathrm{mod}}$ and $P_{\mathrm{mpp}}^{\mathrm{ref}}$ as a function of the bandgap energy and the ERE for $r = 2\ \Omega \cdot \mathrm{cm}^2$. The relative discrepancy between $P_{\mathrm{mpp}}^{\mathrm{mod}}$ and $P_{\mathrm{mpp}}^{\mathrm{ref}}$ for the six solar cell technologies presented in Table 1 is also shown. The white dotted lines represent levels of fixed relative discrepancy. To compute this figure, the ERE values of the solar cells presented

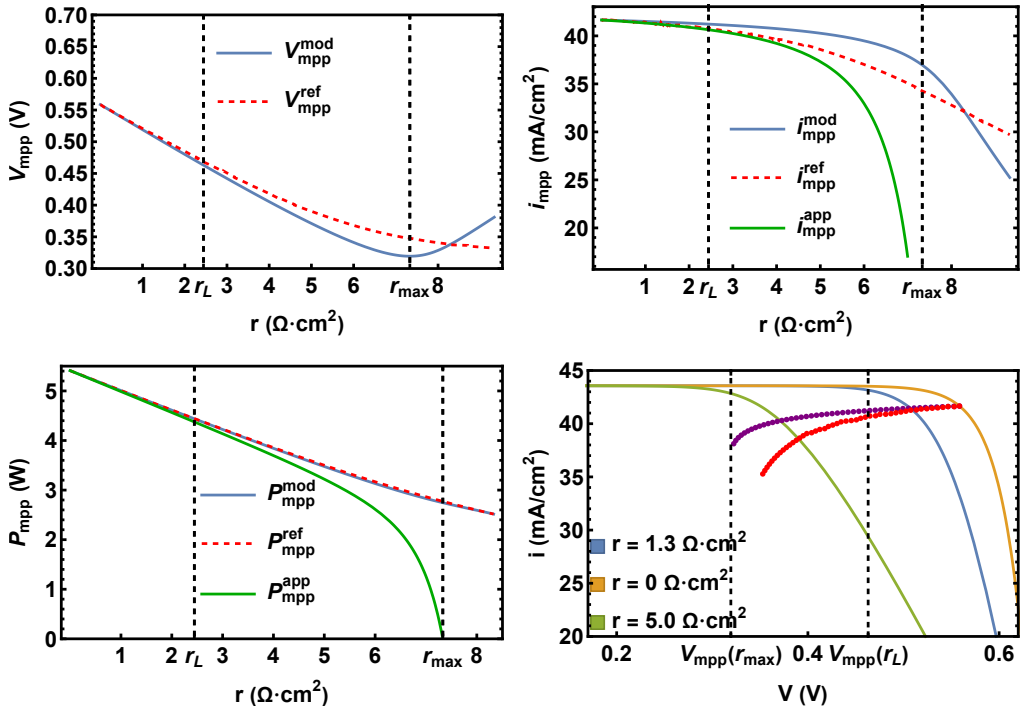

Figure 2: V_{mpp} (**a**), i_{mpp} (**b**), and P_{mpp} (**c**) as a function of the series resistance. For (**c**), a typical Si solar cell size of 6×6 inch^2 (0.0232 m^2) was assumed. (**d**) Current–voltage characteristics for three different values of series resistance. The dotted lines (Equation (15) in purple and Equation (8) in red) represent the maximum power point changing with increasing series resistance.

in Table 1 were estimated by making use of:

$$\mathrm{ERE} = \exp\left[\frac{V_{\mathrm{oc}} - V_{\mathrm{oc}}^{\mathrm{rad}}}{V_{\mathrm{t}}}\right], \tag{27}$$

where $V_{\mathrm{oc}}^{\mathrm{rad}}$ can be calculated from Equation (1) by assuming that i_0 results only from radiative recombination. Figure 4 shows that, for a given series resistance, the accuracy of Equation (15) increases with increasing bandgap and decreases with decreasing ERE. Note that the P_{mpp} of all the investigated cases was predicted with a discrepancy below 0.07%. Finally, Figure 5 displays the base-10 logarithm of the relative discrepancy (in %) between $P_{\mathrm{mpp}}^{\mathrm{ref}}$ and $P_{\mathrm{mpp}}^{\mathrm{mod}}$ (Figure 5a) and between $P_{\mathrm{mpp}}^{\mathrm{ref}}$ and $P_{\mathrm{mpp}}^{\mathrm{app}}$ (Figure 5b) as a function of the series resistance for the six devices presented in Table 1. Here, it can be seen that the discrepancy between $P_{\mathrm{mpp}}^{\mathrm{ref}}$ and $P_{\mathrm{mpp}}^{\mathrm{app}}$ is

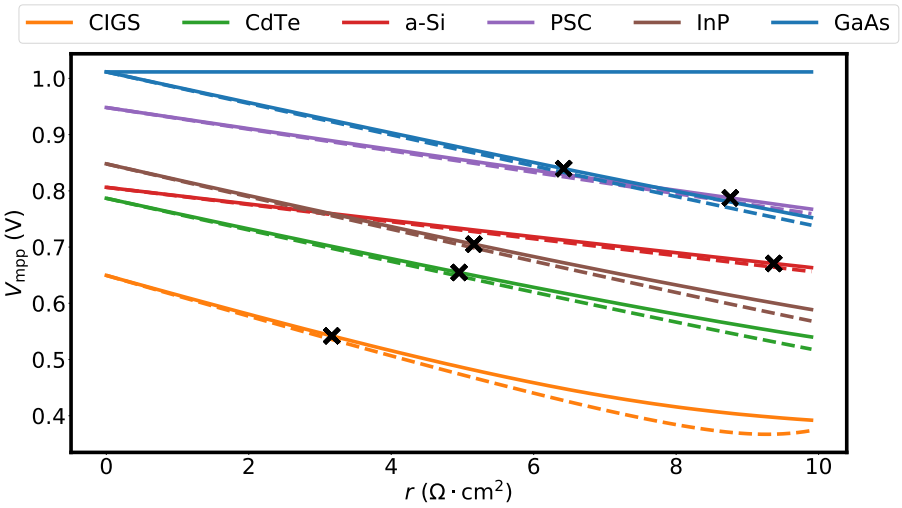

Figure 3: V_{mpp} as a function of the series resistance at T = 300 K. $V_{\mathrm{mpp}}^{\mathrm{mod}}$ (Equation (15)) is represented by continuous lines and $V_{\mathrm{mpp}}^{\mathrm{ref}}$ (Equation (8)) by dashed lines.

around one order of magnitude larger than between $P_{\mathrm{mpp}}^{\mathrm{mod}}$ and $P_{\mathrm{mpp}}^{\mathrm{ref}}$. $P_{\mathrm{mpp}}^{\mathrm{app}}$ could still predict P_{mpp} in most of the studied cases with errors below 1% for values of the series resistance up to 5 $\Omega \cdot \mathrm{cm}^2$.

6 Experimental Validation and Remarks

Now that the analytical model has been numerically validated, its applicability in real cells should be tested. This was performed in [10], where 18 multicrystalline silicon solar cells with different bulk resistivities and cell architectures were measured at multiple temperatures. For the studied cells, Equations (18) and (19) predicted the experimental P_{mpp} and V_{mpp} with relative discrepancies below 0.2% and 0.7%, respectively. It is worth mentioning that low relative discrepancies were obtained at all the measured temperatures.

Besides the numerical limitations that the model derived in the present work may have (e.g., Equation (26)), practical limitations of the model should be addressed. These may include factors that real cells will eventually experience, for instance, degradation due to aging or shunt resistance effects. Although the derived model cannot account for, e.g., cell degradation, it is worth noting that neither can the diode equation in Equation (1), nor the modified diode equation in Equation (6).

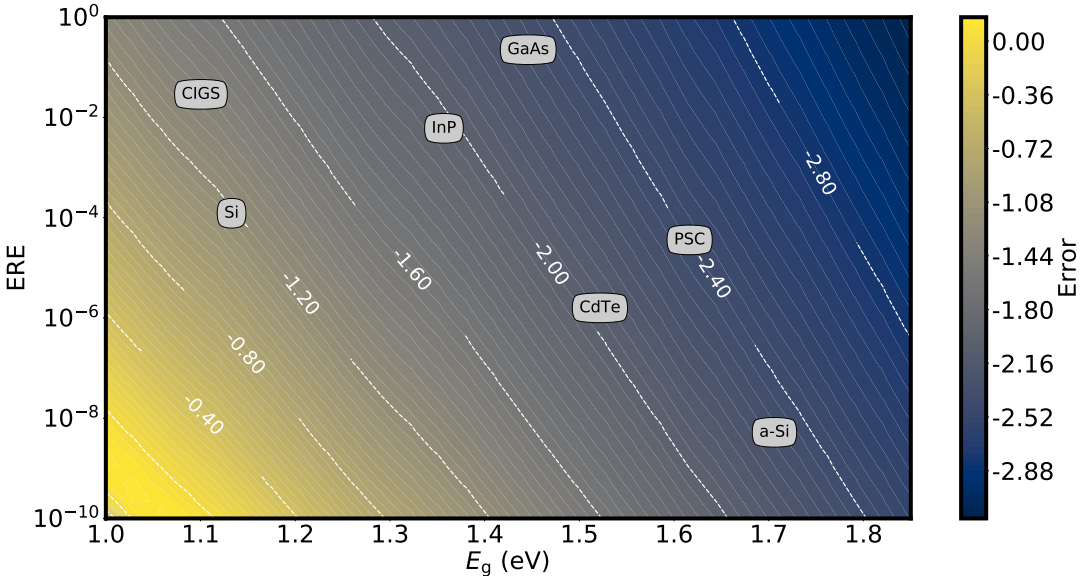

Figure 4: Logarithm of the relative discrepancy (in %) between $P_{\mathrm{mpp}}^{\mathrm{mod}}$ (Equation (15)) and $P_{\mathrm{mpp}}^{\mathrm{ref}}$ (Equation (8)) as a function of the bandgap energy and the ERE at T = 300 K and $r = 2\ \Omega \cdot \mathrm{cm}^2$. The small bends in the dashed lines originated from the irregular shape of the AM 1.5G spectrum.

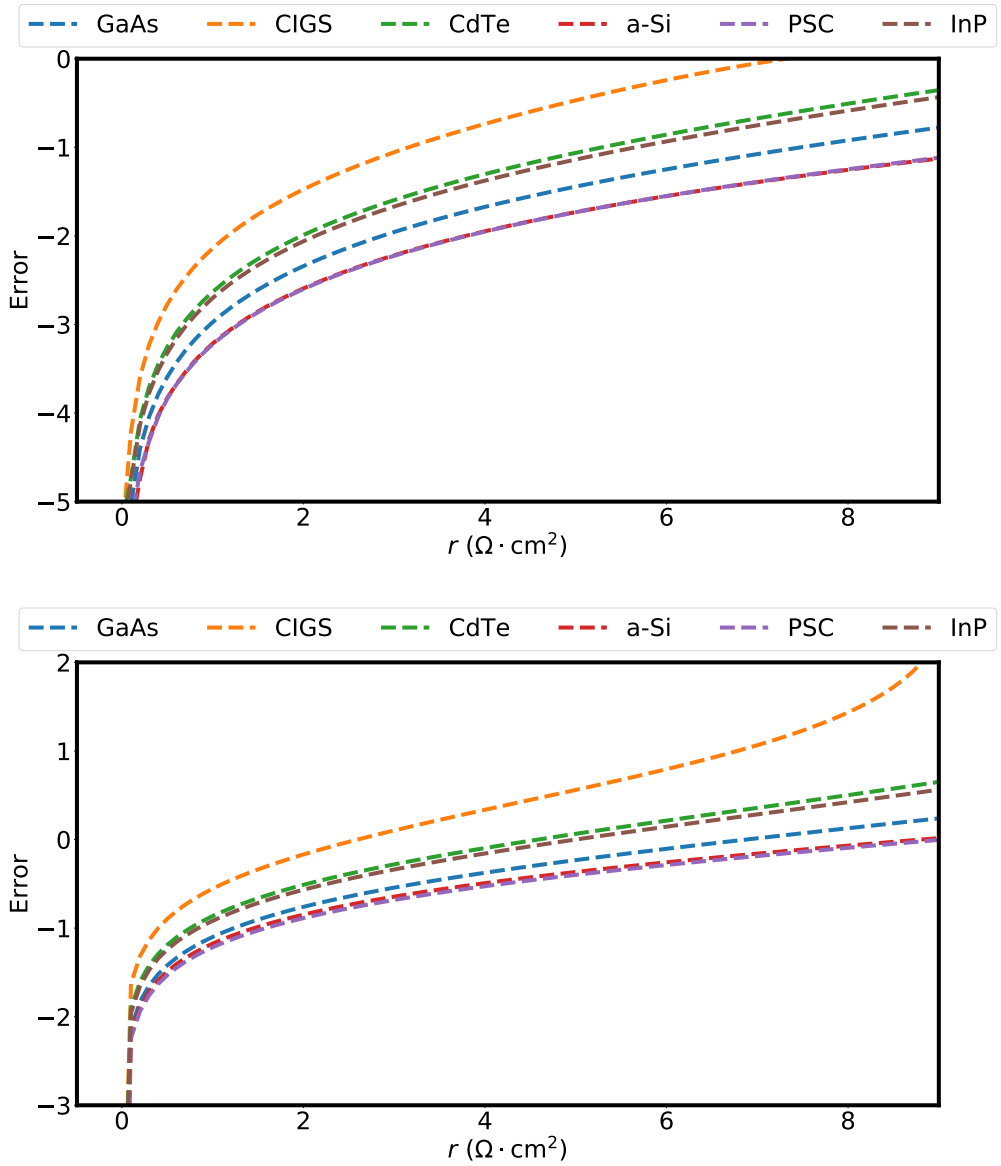

Figure 5: Logarithm of the relative discrepancy (in %) between (**a**) $P_{\text{mpp}}^{\text{ref}}$ (Equation (8)) and $P_{\text{mpp}}^{\text{mod}}$ (Equation (15)) and (**b**) $P_{\text{mpp}}^{\text{ref}}$ and $P_{\text{mpp}}^{\text{app}}$ (Equation (18)) as a function of the series resistance at T = 300 K.

The analytical expressions derived in the present work were subjected to the same practical limitations that the modified diode equation was. The advantage that the derived model presents with respect to Equation (6) is that it allows seeing how the series resistance affects the MPP analytically. On the other hand, shunt resistance effects do not usually have a relevant impact in laboratory cells, as these typically appear due to defects in manufacturing. In fact, in [10], the shunt resistance in the measured cells had only a negligible effect on the comparison between the model and the experiments. Although it might be possible to obtain an expression analogous to Equation (19) that also accounts for the effect of shunt resistance, this goes beyond the scope of the present work.

7 Conclusions

In this work, a new analytical expression for the maximum power point voltage that explicitly accounts for the effect of the series resistance was derived. Approximate analytical expressions for the current and power at the maximum power point were also presented. To derive these expressions, it was shown that Lambert's W function may be approximated by its argument, as long as the value of the series resistances is not excessively large. This makes what otherwise would be a transcendental problem analytically solvable. The accuracy of the new expressions was tested with a numerical single-diode model. It was shown that the new model accurately predicts the maximum power of all the investigated cases with small discrepancies between the analytical model and the numerically simulated values. This was the case even when considering values of the series resistance above 2 $\Omega \cdot \mathrm{cm}^2$, which is larger than typical values for laboratory and commercial cells [18]. The accuracy of the approximation was shown to decrease with increasing series resistance, but also to increase with increasing bandgap energy. This makes the derived model of particular interest for semiconductors with large bandgaps such as perovskite or organic solar cells. Based on the results presented in this work, together with the results published in [10], it may be concluded that the derived analytical model can successfully be utilized to predict the maximum power point for solar cells that follow the diode equation when series resistance is accounted for. Moreover, the employment of Lambert's W function allowed for accurate and simpler expressions than what is currently found in the scientific literature. With respect to new developments, the derived model opens the possibility of analytically studying the effect of the series resistance on the temperature coefficients of the maximum power point. Further enhancements may also include attempts to generalize the model derived in the present work to also include the effect of the shunt resistance.

References

[1] W. Shockley and H. J. Queisser. "Detailed balance limit of efficiency of p-n junction solar cells". In: *Journal of Applied Physics* 32.3 (1961), pp. 510–519.

[2] T. C. Banwell and A. Jayakumar. "Exact analytical solution for current flow through diode with series resistance". In: *Electronics letters* 36.4 (2000), pp. 291–292.

[3] A. Jain and A. Kapoor. "Exact analytical solutions of the parameters of real solar cells using Lambert W-function". In: *Solar Energy Materials and Solar Cells* 81.2 (2004), pp. 269–277.

[4] C. M. Singal. "Analytical expression for the series-resistance-dependent maximum power point and curve factor for solar cells". In: *Solar Cells* 3.2 (1981), pp. 163–177.

[5] M. A. Green. "Accurate expressions for solar cell fill factors including series and shunt resistances". In: *Applied physics letters* 108.8 (2016), p. 081111.

[6] M. Arjun et al. "An iterative analytical solution for calculating maximum power point in photovoltaic systems under partial shading conditions". In: *IEEE Transactions on Circuits and Systems II: Express Briefs* 66.6 (2018), pp. 973–977.

[7] A. Laudani et al. "An analytical approach for maximum power point calculation for photovoltaic system". In: *2017 European Conference on Circuit Theory and Design (ECCTD)*. IEEE. 2017, pp. 1–4.

[8] A. Xenophontos and A. M. Bazzi. "Model-based maximum power curves of solar photovoltaic panels under partial shading conditions". In: *IEEE Journal of Photovoltaics* 8.1 (2017), pp. 233–238.

[9] A. Ramadan et al. "Parameter Estimation of Modified Double-Diode and Triple-Diode Photovoltaic Models Based on Wild Horse Optimizer". In: *Electronics* 10.18 (2021), p. 2308.

[10] A. S. Garcia, S. T. Kristensen, and R. Strandberg. "Assessment of a New Analytical Expression for the Maximum-Power Point Voltage with Series Resistance". In: *2021 IEEE 48th Photovoltaic Specialists Conference (PVSC)*. IEEE. 2021, pp. 0961–0965.

[11] W. Shockley. "The Theory of p-n Junctions in Semiconductors and p-n Junction Transistors". In: *Bell System Technical Journal* 28.3 (1949), pp. 435–489.

[12] A. Cuevas. "The recombination parameter J0". In: *Energy Procedia* 55 (2014), pp. 53–62.

[13] J. Nelson. *The Physics of Solar Cells*. World Scientific Publishing Company, 2003.

[14] A. Khanna et al. "A fill factor loss analysis method for silicon wafer solar cells". In: *IEEE Journal of Photovoltaics* 3.4 (2013), pp. 1170–1177.

[15] A. Sergeev and K. Sablon. "Exact solution, endoreversible thermodynamics, and kinetics of the generalized Shockley-Queisser model". In: *Physical Review Applied* 10.6 (2018), p. 064001.

[16] R. M. Corless et al. "On the Lambert W function". In: *Advances in Computational Mathematics* 5.1 (1996), pp. 329–359.

[17] M. A. Green. "Radiative efficiency of state-of-the-art photovoltaic cells". In: *Progress in Photovoltaics: Research and Applications* 20.4 (2012), pp. 472–476.

[18] C. B. Honsberg and S. G. Bowden. *Series Resistance*. `https://www.pveducation.org/pvcdrom/solar-cell-operation/series-resistance`. Accessed on March 19, 2021. 2019.

[19] M. A. Green et al. "Solar cell efficiency tables (version 57)". In: *Progress in photovoltaics: research and applications* 25.1 (2017), pp. 3–13.

Appendix E

Assessment of a New Analytical Expression for the Maximum-Power Point Voltage with Series Resistance

Assessment of a New Analytical Expression for the Maximum-Power Point Voltage with Series Resistance

Alfredo Sanchez Garcia, Sissel Tind Kristensen, and Rune Strandberg
University of Agder, Grimstad, 4879, Norway

Abstract

This work compares a recently developed analytical expression for the maximum-power point voltage with experimental data, to test its usability for crystalline silicon solar cells. The experimental data covers measurements from 18 multicrystalline silicon solar cells with different bulk resistivities and cell architectures. We show that the expression is able to predict the maximum power obtainable by the measured cells with relative discrepancies below 1%. Additionally, we compare the accuracy of this new expression with two already existing models.

1 Introduction

The maximum-power point of solar cells that follow Shockley's diode equation has been studied from an analytical perspective in a number of works, such as Refs. [1] and [2]. There, the authors showed that Lambert's W function [3] allowed for a simple analytical expression of the maximum-power point voltage, V_{mpp}, and, consequently the maximum-power point current and power, i_{mpp} and P_{mpp}, respectively.

Some work has been done aiming to quantify analytically the effect of series resistance on various solar cell parameters [4, 5, 6, 7]. Particularly in Ref. [6], Singal obtained an approximate closed-form expression of V_{mpp} in terms of the open-circuit voltage, V_{oc}.

Recently, a new expression for V_{mpp} that accounts for the effect of series resistance, and is comparable in simplicity to the expression derived by Khanna in Ref. [1], has been derived and tested against a numeric one-diode model for a number of different bandgaps [8].

In this paper, we aim to test the applicability of this new expression for V_{mpp} in crystalline silicon (c-Si) solar cells. The current-voltage (I-V) characteristics of 18 compensated multicrystalline silicon (mc-Si) solar cells, as well as the series resistance and sample characteristics, were measured at various temperatures. We compare the measured values of V_{mpp}, i_{mpp} and P_{mpp} of the measured cells to their corresponding counter parts predicted by the expression derived in Ref. [8]. Additionally, we test the accuracy of the expressions derived in Ref. [8] against Singal's expressions (Ref. [6]) and a numerical model.

2 Theoretical Framework

When series resistance is accounted for in Shockley's diode equation [9], the total current, i, produced by a solar cell is given by [10]

$$i = i_{\mathrm{G}} - i_0 \exp\left(\frac{V + iR}{V_{\mathrm{t}}}\right) \tag{1}$$

where i_{G} and i_0 are the generation and the thermal recombination [11] currents, respectively; V is the voltage and $qV_{\mathrm{t}} = kT$ with q and k being the elementary charge and Boltzmann's constant; and R is the series resistance. Banwell et al. showed in Ref. [4], that Lambert's W function, defined by $x = \mathrm{W}(xe^x)$ allows for Eq. (1) to be expressed in closed-form as

$$i = i_{\mathrm{sc}} - \frac{V_t}{R}\mathrm{W}\left(\frac{i_{\mathrm{sc}}R}{V_{\mathrm{t}}}\exp\left[\frac{V}{V_{\mathrm{t}}} - \frac{V_{\mathrm{oc}}}{V_{\mathrm{t}}} + \frac{i_{\mathrm{sc}}R}{V_{\mathrm{t}}}\right]\right), \tag{2}$$

where we have approximated i_{G} by i_{sc} and made use of the identity $i_0 = i_{\mathrm{sc}}/\exp\left({}^{V_{\mathrm{oc}}}/_{V_{\mathrm{t}}}\right)$. The latter follows from Eq. (1) by noting that $i(V_{\mathrm{oc}}) = 0$ [10].

At the maximum-power point, it holds that ${}^{\mathrm{d}P}/_{\mathrm{d}V} = 0$, with P being given by the product $P = i \cdot V$. Inserting Eq. (2) results into an transcendental equation in V that does not have an analytical solution and needs to be solved numerically. However, some approximate analytical solutions can be found in the literature.

2.1 Without Lambert's W function

Already in 1981, Singal derived in Ref. [6] approximate analytical expressions for V_{mpp}, i_{mpp} and P_{mpp}. In his derivation, Singal did not make use of Lambert's W function. Instead, he noted that, for most solar cells, $V_{\mathrm{oc}} >> V_{\mathrm{t}}$, which allowed him to take a series of approximations that converted the transcendental problem into

an analytically solvable equation. The proposed expressions for the maximum-power point were

$$V_{\mathrm{mpp}} = V_{\mathrm{oc}} \left[1 - \frac{1}{v} \log(1 + f(v)) + \frac{1}{v} \log \left(1 + \frac{2 i_{\mathrm{sc}} R}{V_{\mathrm{oc}}} \frac{v f(v)}{(1 + f(v))^2} \right) \right.$$

$$\left. - \frac{i_{\mathrm{sc}} R}{V_{\mathrm{oc}}} \frac{f(v)}{1 + f(v)} + \left(\frac{i_{\mathrm{sc}} R}{V_{\mathrm{oc}}} \right)^2 \frac{2 v f(v)}{(1 + f(v))^3} \right], \quad (3)$$

$$i_{\mathrm{mpp}} = i_{\mathrm{sc}} \left[1 - \frac{1}{1 + f(v)} - \frac{2 i_{\mathrm{sc}} R}{V_{\mathrm{oc}}} \frac{v f(v)}{(1 + f(v))^3} \right], \quad (4)$$

where $v = {}^{V_{\mathrm{oc}}}/_{V_{\mathrm{t}}}$ and $f(v) = v - \log(v)$. The corresponding expression for P_{mpp} is obtained by multiplying Eqs. (3) and (4).

2.2 With Lambert's W function

Sanchez and Strandberg showed in Ref. [8] that approximating Lambert's W function by its argument in the derivation of V_{mpp} allowed for an approximate analytical solution of the transcendental problem. The obtained expression was

$$V_{\mathrm{mpp}} = i_{\mathrm{sc}} R + V_{\mathrm{t}} \left(\mathrm{W} \left[\exp \left[1 + \frac{V_{\mathrm{oc}}}{V_{\mathrm{t}}} - 2 \frac{i_{\mathrm{sc}} R}{V_{\mathrm{t}}} \right] \right] - 1 \right). \quad (5)$$

From Eq. (2), it is possible to calculate the maximum-power point current, i_{mpp}, and power, P_{mpp}, by inserting Eq. (5) into Eq. (2) and then calculating the product $i_{\mathrm{mpp}} \cdot V_{\mathrm{mpp}}$. The authors in Ref. [8] also proposed two approximate expressions for these quantities,

$$i_{\mathrm{mpp}} = i_{\mathrm{sc}} \left(1 - \frac{1}{\mathrm{W}\left[\alpha(R)\right]} \right), \quad (6)$$

$$P_{\mathrm{mpp}} = i_{\mathrm{sc}}^2 R \left(1 - \frac{1}{\mathrm{W}\left[\alpha(R)\right]} \right) + i_{\mathrm{sc}} V_{\mathrm{t}} \left(\mathrm{W}\left[\alpha(R)\right] - 2 + \frac{1}{\mathrm{W}\left[\alpha(R)\right]} \right), \quad (7)$$

where $\alpha(R)$ equals the argument of Lambert's W function in Eq. (5).

2.3 The ideality factor

Foreseeing its usability in the comparison with our experiments, it is worth dedicating a section to the ideality factor, n. At the beginning of this section, we introduced the recombination term of the diode equation as $i_0 \exp\left[{}^{V}/_{V_\mathrm{t}}\right]$. This is true only for solar cells that follow the ideal diode equation, which assumes that all recombination occurs in the cell bulk through band-to-band transitions or through Shockley-Read-Hall (SRH) recombination. Real cells experience other types of recombination and, also, in different areas of the device [10]. In order to account for these, we need to introduce an ideality factor, n, in the exponent as $qV_\mathrm{t} \to qnV_\mathrm{t} = nkT$. The ideality factor is then a measure of how ideal the cell in question is [10].

The ideality factor of a cell may be extracted from the experimental data by fitting the obtained $I-V$ characteristics to Shockley's diode equation. Let us instead propose an alternative method that requires less computational power. From Eq. (1), we can solve for nV_t and obtain

$$nV_\mathrm{t} = \frac{V + iR - V_\mathrm{oc}}{\log\left(1 - \frac{i}{i_\mathrm{sc}}\right)}. \tag{8}$$

Here, we have also approximated i_G by i_sc and made use of $i_0 = i_\mathrm{sc}/\exp\left({}^{V_\mathrm{oc}}/_{V_\mathrm{t}}\right)$. Eq. (8) is only defined in the real axis within the interval $0 < i < i_\mathrm{sc}$, i.e., for all points in the $I - V$ curve except V_oc and i_sc. Assuming that the ideality factor is constant throughout the $I - V$ characteristic, we can evaluate Eq. (8) at the maximum-power point and express n as

$$n = \frac{q}{kT}\frac{V_\mathrm{mpp} + i_\mathrm{mpp}R - V_\mathrm{oc}}{\log\left(1 - \frac{i_\mathrm{mpp}}{i_\mathrm{sc}}\right)}. \tag{9}$$

All the physical quantities appearing in Eq. (9) can be extracted from the measurements, which allows for the determination of n at different temperatures.

In Ref. [12], Townsend proposed a method for estimating the performance of coupled photovoltaic systems. To this end, he compared various models that could be potential candidates. It is worth mentioning that Townsend arrived at Eq. (9) when obtaining a solution for what he denoted the "Lumped, 1 Mechanism with 4 Parameters" model [12].

3 Experimental Method

To compare the analytical expression with experimental data, 18 compensated p-type mc-Si solar cells were studied. The cells were fabricated from three different

ingots with different bulk resistivities, ρ, and different cell architectures. The cells can be divided into three groups: (a) $\rho = 0.5\ \Omega \cdot \mathrm{cm}$, Passivated Emitter Rear Cells (PERC), (b) $\rho = 1.3\ \Omega \cdot \mathrm{cm}$, PERC, and (c) $\rho = 1.3\ \Omega \cdot \mathrm{cm}$, Aluminum Back Surface Field (Al-BSF) cells. Each group contains six cells from various brick positions, numbered from 001-060, with position 001 at the bottom of the brick and position 060 at the top. The measurements were performed using a NeonSee$^{\mathrm{TM}}$ AAA Sun simulator, enabling acquisition of the $I - V$ characteristics of the cells, as well as the series resistance, at various temperatures ranging from 293 K to 343 K. The cell temperature was controlled using a built-in water heater.

4 Numerical Method

We denote with the label "exp", the experimental values of V_{mpp}, i_{mpp} and P_{mpp}. The experimental values of V_{oc}, i_{sc} and R are used as inputs to evaluate Eqs. (5), (6) and (7) to calculate V_{mpp}, i_{mpp} and P_{mpp} at multiple temperatures. We denote these with the label "mod". Singal's model, i.e., Eqs. (3), (4) and the corresponding P_{mpp}, will be labeled "S". As all the expressions presented in sections 2.1 and 2.2 result from approximations, it may also be of interest to compare the experiments with the value of V_{mpp}, i_{mpp} and P_{mpp} that we can obtain directly from Eq. (2). To do so, we calculate values of V_{mpp} by finding numerically the voltage that maximizes $P = Vi$, with i being given by Eq. (2). In order to do this, we first make use of experimental values of V_{oc}, i_{sc} and R and insert them in Eq. (2). We then make use of an auxiliary function, $f(V) = -Vi$, and find the voltage that minimizes it. We denote by $V_{\mathrm{mpp}}^{\mathrm{num}}$, the values of V_{mpp} obtained in this way. The corresponding i_{mpp} and P_{mpp} are also denoted by the label "num".

4.1 Simultaneous determination of the ideality factor and the series resistance

Before we compare with the experiments, we need to address the way R is obtained from the experimental $I - V$ characteristics. In our case, the NeonSee$^{\mathrm{TM}}$ AAA Sun simulator software estimates the value of the series resistance from the $I - V$ characteristics by computing the negative reciprocal of the slope at $V = V_{\mathrm{oc}}$. As noted in, e.g., Ref. [12], this method overestimates the value of R. This can be analytically shown from Eq. (1) by taking the derivative of i with respect to V,

evaluating at $V = V_{\rm oc}$ and solving for R. We obtain

$$R = -\frac{1}{\left.\frac{\partial i}{\partial V}\right|_{V=V_{\rm oc}}} - \frac{1}{\frac{qi_0}{nkT}\exp\left[\frac{qV_{\rm oc}}{nkT}\right]} = R_0 - \frac{nkT}{qi_{\rm sc}}, \tag{10}$$

where we have introduced R_0 as the estimate of the R that the software gives and again made use of the identity $i_0 = i_{\rm sc}/\exp\left({}^{V_{\rm oc}}/_{nV_{\rm t}}\right)$. From Eq. (10), we note that R is always going to be smaller than the given estimate, R_0 [12].

In order to being able to compare with the experiments, we need to not only accurately estimate R but also n. A straightforward method would be to extract these parameters from the measured $I-V$ characteristics by, e.g., least-square fitting the data points to Eq. (1). Alternatively, we can note from Eqs. (9) and (10) that we have $n(R)$ and $R(n)$, respectively. Solving the system of equations in closed-form yields

$$n = \frac{q}{kT}\frac{i_{\rm sc}}{i_{\rm mpp}}\frac{i_{\rm mpp}R_0 + V_{\rm mpp} - V_{\rm oc}}{\left(1 + \frac{i_{\rm sc}}{i_{\rm mpp}}\log\left[1 - \frac{i_{\rm mpp}}{i_{\rm sc}}\right]\right)}, \tag{11}$$

$$R = -\frac{V_{\rm mpp} - V_{\rm oc} - i_{\rm sc}R_0\log\left[1 - \frac{i_{\rm mpp}}{i_{\rm sc}}\right]}{i_{\rm mpp} + i_{\rm sc}\log\left[1 - \frac{i_{\rm mpp}}{i_{\rm sc}}\right]}, \tag{12}$$

which again requires less computational power.

As a final note, it is worth pointing out that the NeonSee$^{\rm TM}$ AAA sun simulator software has been updated since these measurements were obtained and now the "Variable Intensity Method" is used to extract the series resistance from the $I-V$ curves [13].

5 Numerical Results and Discussion

In Figs. 1, 2 and 3, we display $V_{\rm mpp}$, $i_{\rm mpp}$, and $P_{\rm mpp}$, respectively, as a function of the cell temperature. The values correspond to the cell in brick position 012 of group (a). In all three figures, the experimental values of the corresponding parameters are represented with blue crosses. The values corresponding to the numerical model are represented with continuous black lines. The "mod" parameters, i.e., Eqs. (5), (6) and (7), are represented with continuous gray lines. Finally, Singal's model, i.e.,

Eqs. (3) and (4), is represented with dashed red lines. In all three figures, it is assumed an ideality factor of 1 in both the numerical and the analytical models.

Starting with Fig. 1, we see that the values of $V_{\mathrm{mpp}}^{\mathrm{num}}$ and both the approximate analytical models overlap well, but all three models appear to underestimate $V_{\mathrm{mpp}}^{\mathrm{exp}}$ by 3.5%, on average. As for Fig. 2, we we see that the numerical and the analytical models overlap well, but overestimate the experimental values of i_{mpp}. Since there is a good agreement between the "num", "mod" and "S" V_{mpp} and i_{mpp} values, we also find a good agreement between $P_{\mathrm{mpp}}^{\mathrm{mod}}$, $P_{\mathrm{mpp}}^{\mathrm{S}}$ and $P_{\mathrm{mpp}}^{\mathrm{num}}$, as we can see in Fig. 3. All three methods appear however to underestimate the experimental values.

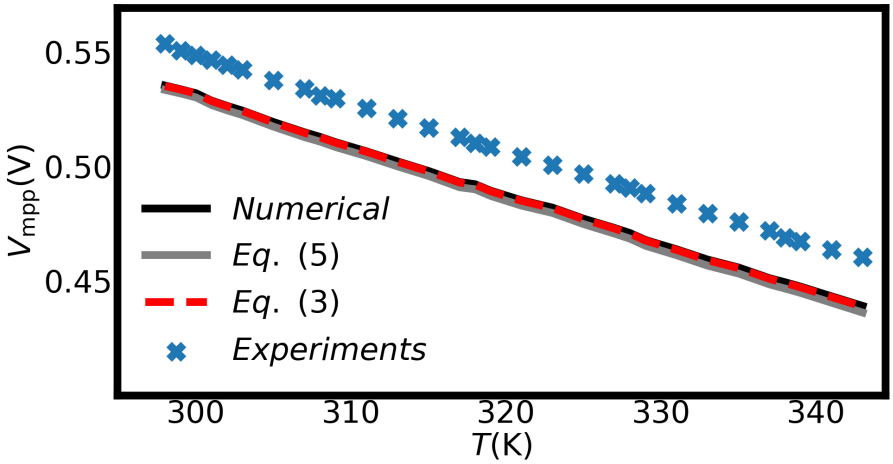

Figure 1: V_{mpp} as a function of the temperature for the cell from brick position 012 in group (a). The experimental values are represented with blue crosses. The numerical model, corresponding to $V_{\mathrm{mpp}}^{\mathrm{num}}$ in section 4, is represented by continuous black lines. The analytical models, corresponding to Eqs. (3) and (5), are represented by dashed red and continuous gray lines, respectively.

5.1 The effect of the ideality factor

Understandingly, we may find discrepancies between the experiments and both analytical models, as the latter result from approximations of the numerical model. But one would expect the numerical model to accurately describe the experiments as it is derived from the (modified) diode equation, Eq. (1).

One possible reason for the mismatch between the models and the experiments is the ideality factor of the measured cells. To compute Figs. 1, 2 and 3, we have

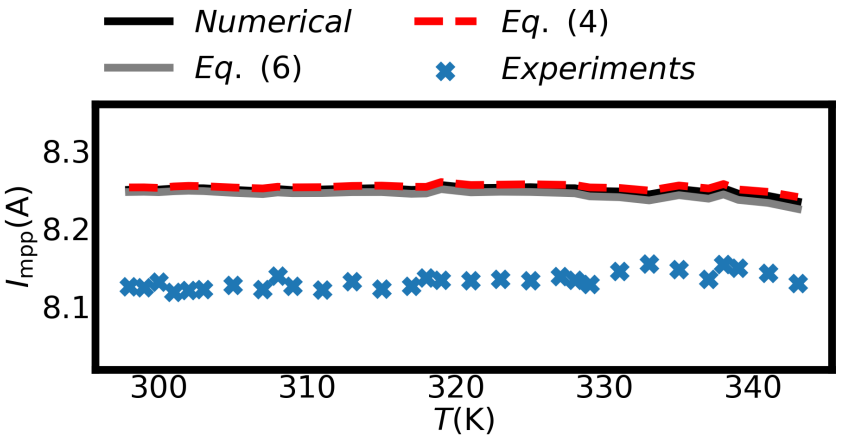

Figure 2: i_{mpp} as a function of the temperature for the cell in position 012 in group (a).

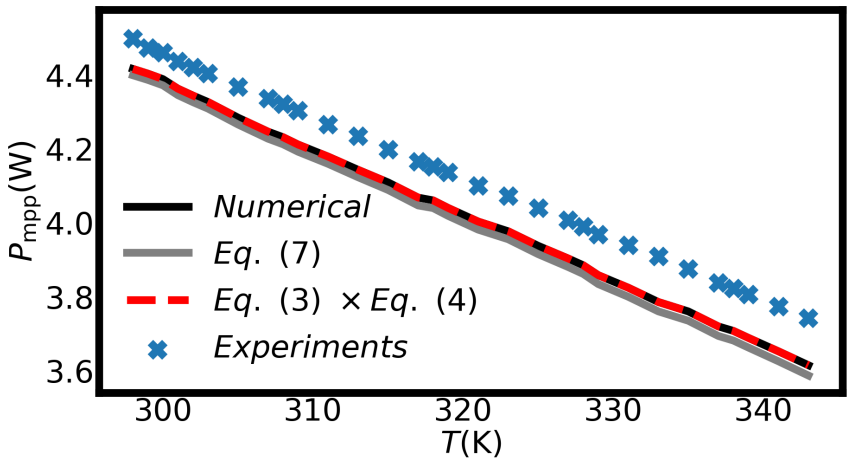

Figure 3: P_{mpp} as a function of the temperature for the cell from brick position 012 in group (a).

assumed $n = 1$ which, as noted in section 2.3, is only true for solar cells that follow the ideal diode equation. Indeed, the measured cells do not behave like ideal diodes. To see this, we display in Fig. 4 the $I - V$ characteristics corresponding to the cell from brick position 005 of group (c) at $T = 298$ K (black dots), as well as three simulated cases where the ideality factor was obtained using different methods: (i, in blue) by fitting the experimental $I - V$ curve to Shockley's diode equation (Eq. (1)

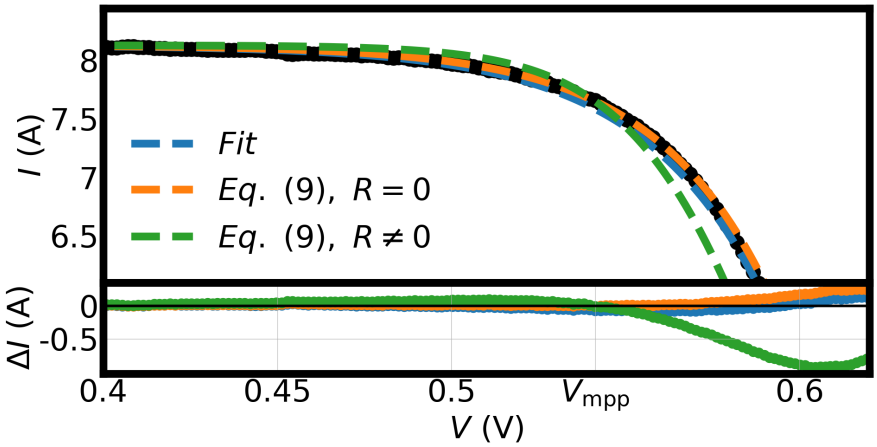

Figure 4: $I-V$ characteristics corresponding to cell from brick position 005 of group (c) at $T = 298$ K. The experimental values are represented with black dots. The dashed blue line is obtained by evaluating Shockley's single diode equation (Eq. (1) with $R = 0$) with the measured voltages and an ideality factor obtained from a least-square fit. The orange dashed line is also obtained from the single diode equation but evaluated with an ideality factor obtained from Eq. (9), setting $R = 0$. Finally, the green dashed line is obtained by evaluating Eq. (2) with the measured voltages and an ideality factor obtained from Eq. (9) with the measured values of the series resistance, R_0. At the bottom, we display a residual plot.

with $R = 0$) and extracting n from the fit, (ii, in orange) by evaluating Eq. (9) with $R = 0$ and the experimental values of $V_{\rm oc}$, $i_{\rm sc}$, $V_{\rm mpp}$ and $i_{\rm mpp}$ corresponding to the displayed $I-V$ curve and (iii, in green) by evaluating Eq. (9) with $R = R_0$ (the series resistance value provided by the Sun simulator software) and the experimental values of $V_{\rm oc}$, $i_{\rm sc}$, $V_{\rm mpp}$ and $i_{\rm mpp}$. At the bottom of Fig. 4, we display the corresponding residual plot, i.e., a plot of the difference between the models and the obtained experimental values. The obtained ideality factor is different from one in all three represented cases; 1.37 and 1.32 for methods (i) and (ii), respectively and 0.80 for method (iii).

In Fig. 5, we display the relative discrepancy between the experimental values of $V_{\rm mpp}$ (dots) and $P_{\rm mpp}$ (crosses) and the corresponding values obtained from the analytical models for the cells in group (a) at $T = 298$ K. The "mod" parameters (Ref. [8]) are represented with the color blue and the "S" parameters (Ref. [6]), with the color red. Here, we have introduced the ideality factor of the corresponding cells calculated with Eq. (9) and the measured value of the series resistance, R_0 (method

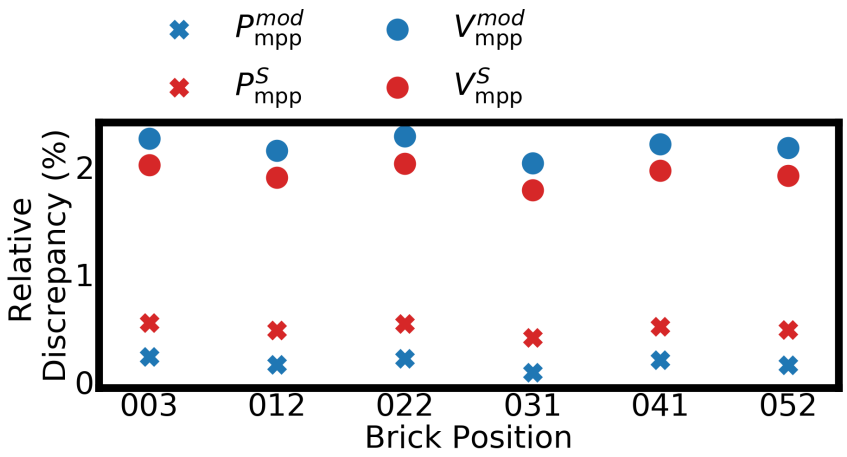

Figure 5: Relative discrepancy between the experimental and the modeled values of $V_{\rm mpp}$ (dots) and $P_{\rm mpp}$ (crosses) for all cells in group (a) and at $T = 298$ K. The Ref. [8] points correspond to the "mod" parameters, i.e., Eqs. (5) and (7). Ref. [6] points correspond to the "S" parameters; Eqs. (3) and $P^{\rm S}_{\rm mpp}$ given by Eqs. (3) $\times$ Eqs. (4). All expressions are evaluated at the series resistance provided by the Sun simulator software, R_0, and at $n(R_0)$ with n being given by Eq. (9).

(iii) above). In the case of $V_{\rm mpp}$, accounting for the ideality factor of the cells reduces the relative discrepancy between the experiments and both the numerical and the analytical models by approximately 50%. From Fig. 5, we see that both Eq. (7) and Singal's expression predict the experimental values of $P_{\rm mpp}$ for all brick positions with a relative error below 0.5% for all cells in all three groups.

5.2 Extraction of n and R

Even though we obtain a reasonable relative discrepancy with the experiments when comparing the $P_{\rm mpp}$ values, the results for $V_{\rm mpp}$ are not ideal. We can reduce the relative discrepancy between the models and the experiments by extracting R and n directly from the $I - V$ curves. As noted in section 4.1, this may be done by fitting the obtained $I - V$ characteristics to Eq. (2) or by making use of Eqs. (11) and (12). The results of this procedure are displayed in Figs. 6 and 7, where we show the relative discrepancy between the experimental values of $V_{\rm mpp}$ and $P_{\rm mpp}$ and the corresponding values obtained from the analytical models for the cells in groups (b) and (c). As it can be seen from the figures, making use of Eqs. (11) and (12) to extract n and R results in a more accurate estimation.

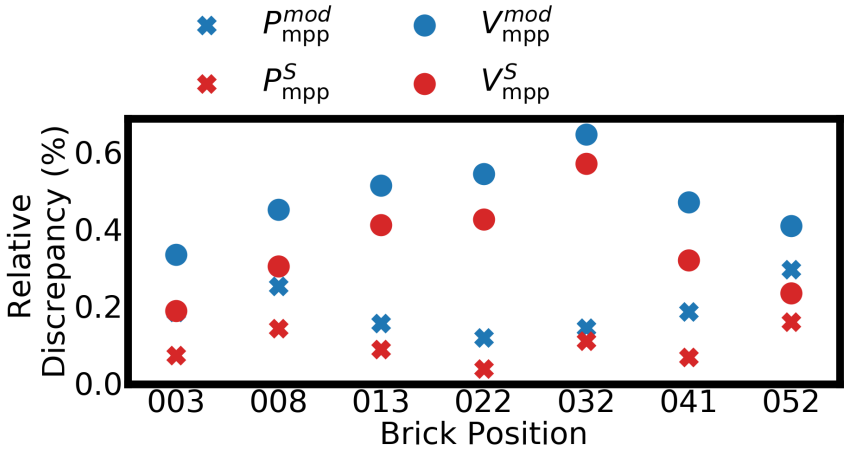

Figure 6: Relative discrepancy between the experimental and the modeled values of $V_{\rm mpp}$ (dots) and $P_{\rm mpp}$ (crosses) for all cells in group (b) and at $T = 298$ K. Here and also in Fig. 7, we have obtained n and R from Eqs. (11) and (12), respectively.

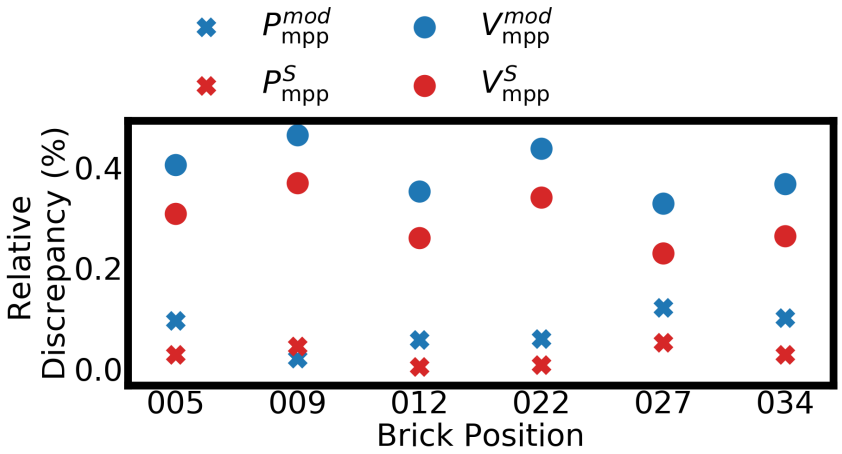

Figure 7: Relative discrepancy between the experimental and the modeled values of $V_{\rm mpp}$ (dots) and $P_{\rm mpp}$ (crosses) for all cells in group (c) and at $T = 298$ K.

Regarding the accuracy of the analytical models, we see from the figures that both models predict similar values when provided with the same input. We can therefore regard them as equally capable to predict experimental values. The main improvement that Eqs. (5), (6) and (7) may present compared to Singal's model is a simplification of the mathematical expressions.

6 Conclusion

In this work, we have tested the usability of a model for the maximum-power point, previously derived in Ref. [8], with mc-Si solar cells. To this end, we studied 18 compensated p-type mc-Si cells at multiple temperatures. To allow a comparison with the experiments we have also developed an analytical method, based on the works of Townsend in Ref. [12], that allows for the simultaneous extraction of n and R from the $I - V$ curves. We have shown that, when provided with the right input, the analytical model is able to predict experimental data with low relative discrepancy. We have also compared this new model to two already existing models; one numerical and one analytical, previously derived by Singal in Ref. [6]. Both analytical models are very similar in accuracy. The main difference between the two lies in the simplicity of the mathematical expressions. Overall, we may conclude that the model presented in Ref. [8] accurately predicts the experimental values of V_{mpp} and P_{mpp} and can be successfully applied to mc-Si solar cells.

7 Acknowledgments

A.S.G. would like to thank Martin Maier from NeonSee$^{\mathrm{TM}}$ for providing valuable information and details regarding the software employed in the Sun simulator.

References

[1] A. Khanna et al. "A fill factor loss analysis method for silicon wafer solar cells". In: *IEEE Journal of Photovoltaics* 3.4 (2013), pp. 1170–1177.

[2] A. Sergeev and K. Sablon. "Exact solution, endoreversible thermodynamics, and kinetics of the generalized Shockley-Queisser model". In: *Physical Review Applied* 10.6 (2018), p. 064001.

[3] R. M. Corless et al. "On the Lambert W function". In: *Advances in Computational Mathematics* 5.1 (1996), pp. 329–359.

[4] T. C. Banwell and A. Jayakumar. “Exact analytical solution for current flow through diode with series resistance”. In: *Electronics letters* 36.4 (2000), pp. 291–292.

[5] A. Jain and A. Kapoor. “Exact analytical solutions of the parameters of real solar cells using Lambert W-function”. In: *Solar Energy Materials and Solar Cells* 81.2 (2004), pp. 269–277.

[6] C. M. Singal. “Analytical expression for the series-resistance-dependent maximum power point and curve factor for solar cells”. In: *Solar Cells* 3.2 (1981), pp. 163–177.

[7] M. A. Green. “Accurate expressions for solar cell fill factors including series and shunt resistances”. In: *Applied physics letters* 108.8 (2016), p. 081111.

[8] A. S. Garcia and R. Strandberg. “Analytical Modeling of the Maximum-Power Point with Series Resistance”. In: *To be published.* ().

[9] W. Shockley and H. J. Queisser. “Detailed balance limit of efficiency of p-n junction solar cells”. In: *Journal of Applied Physics* 32.3 (1961), pp. 510–519.

[10] J. Nelson. *The Physics of Solar Cells*. World Scientific Publishing Company, 2003.

[11] A. Cuevas. “The recombination parameter J0”. In: *Energy Procedia* 55 (2014), pp. 53–62.

[12] T. U. Townsend. “A method for estimating the long-term performance of direct-coupled photovoltaic systems”. PhD thesis. 1989.

[13] M. Maier. *NeonSee*. Personal communication. June 8, 2021.

Appendix F

The Recombination Parameter γ: Modeling and Comments